OAK RIDGE NATIONAL LABORATORY
operated by
UNION CARBIDE CORPORATION
NUCLEAR DIVISION
for the
U.S. ATOMIC ENERGY COMMISSION

ORNL - TM - 1829
NASA CR-72151

BRAYTON-CYCLE RADIOISOTOPE HEAT-SOURCE DESIGN STUDY PHASE II (PRELIMINARY DESIGN) REPORT

R. A. Robinson
T. G. Chapman
S. T. Ewing
A. J. Miller
J. P. Nichols

These evaluation studies at ORNL were supported by the National Aeronautics and Space Administration, Lewis Research Center, under an Interagency Agreement with the Atomic Energy Commission - C-64217-A.

ORNL-TM-1829
NASA CR-72151

Contract No. W-7405-eng-26

BRAYTON-CYCLE RADIOISOTOPE HEAT-SOURCE DESIGN STUDY
PHASE II (PRELIMINARY DESIGN) REPORT

R. A. Robinson
T. G. Chapman
S. T. Ewing
A. J. Miller
J. P. Nichols

These evaluation studies at ORNL were supported by the National Aeronautics and Space Administration, Lewis Research Center, under an Interagency Agreement with the Atomic Energy Commission — C-64217-A.

AUGUST 1967

OAK RIDGE NATIONAL LABORATORY
Oak Ridge, Tennessee
operated by
UNION CARBIDE CORPORATION
for the
U.S. ATOMIC ENERGY COMMISSION

CONTENTS

BRAYTON-CYCLE RADIOISOTOPE HEAT-SOURCE DESIGN STUDY

PHASE II (PRELIMINARY DESIGN) REPORT

R. A. Robinson S. T. Ewing
T. G. Chapman A. J. Miller
J. P. Nichols

Abstract

A preliminary design was prepared for a 25-kw(th) $^{238}PuO_2$ heat source that can be coupled with a Brayton-cycle power-conversion system for use in space. Primary containment is provided by multilayered fuel capsules, with tantalum-based alloy T-111 as the principal stress-bearing layer and platinum as the outer corrosion-resistant layer. The multipurpose mission module specified by NASA is used as the vehicle configuration for integration studies. The assembly of fuel capsules is contained within a single reentry body for protection against reentry heating and subsequent impact in the event of a mission abort. The fuel capsule complies with the design criterion of no more than 1% creep in five years of service. The safety guideline that the radioisotope fuel can be contained within the fuel capsules for a period of ten half-lives of ^{238}Pu or longer is a goal toward which the capsule design is directed. The weight of the heat-source system, including the reentry body, fuel, heat exchanger, shield, etc., is 2670 lb. Preliminary designs are described of facilities for fueling and assembling capsules, shipment of capsules to launch site, and handling at the launch site. Since the heat-source design is based partly on near-future materials technology and on extrapolation from present aerodynamic data, identification is made of areas where further investigations will have to be carried out to test the validity of the design.

1. INTRODUCTION

In July 1965, the Oak Ridge National Laboratory started work on design concepts for a 25-kw radioisotope heat source that could be coupled to a Brayton-cycle power-generating system to provide electric power for use in space applications. The study was done for the National Aeronautics and Space Administration, Lewis Research Center, under Interagency

Agreement C-64217-A, and valuable assistance was provided for the study by L. I. Shure of NASA–Lewis Research Center, who had NASA technical responsibility.

The overall objectives of the study were to

1. provide the NASA–Lewis Research Center with one or more preliminary designs of the radioisotope heat source, and
2. identify research and development problems that require solution prior to undertaking the detailed design of such a heat source.

Safety guidelines and the ground rule that the concepts should be limited to what could be achieved with current or near-future technology were the most important factors influencing the designs.

The work was divided into two phases: the conceptual design (phase I), which was completed and reported[1] in December 1966, and the preliminary design (phase II), which is the subject of this report.

In phase I, various heat source concepts were evolved, critical problems were identified, the feasibility of their solution was evaluated, and estimates were made of the weights and physical dimensions of the various concepts. These studies evaluated a shielded model in an unidentified 15-ft-diam manned vehicle. Fuel forms of ^{238}Pu, ^{147}Pm, and ^{244}Cm were considered, and many capsule designs and heat transfer methods were studied. An uncontrolled reentry vehicle for emergency return of the capsules was assumed for all designs. The lift-off weights of the various concepts ranged from 3,000 to 26,000 lb. Considerable portions of the justification and basis for features subsequently incorporated into the phase II design are presented only in the phase I report (e.g., basis for choice of materials, discussion of pressure-temperature history of capsules, capsule strength requirements, criticality hazards).

The most promising concept of the phase I work from the standpoint of weight and feasibility was selected for the phase II work; and a more detailed preliminary design was prepared for a specific mission concept. For the phase II study, the heat source was assumed to be required to provide power to a manned laboratory in a near-earth orbit. The source was assumed to be contained in a multipurpose mission module positioned between an Apollo command and service module and a second multipurpose

module, as illustrated in Fig. 1.1. The radiation shield was designed to reduce the exposure to 25 rads per year based on the projected man-hours to be spent in each module. The fuel was assumed to be $^{238}PuO_2$ contained in a plane array of fuel capsules radiating their heat to Brayton-cycle heat exchangers. To effect emergency heat rejection in orbit, the source was pivoted so that it radiated to space.

Some of the performance and design criteria for the heat source in phase II were different from those in phase I because of changes in the proposed Brayton-cycle equipment, the need to relate the shielding requirements to a specific mission, and some reassessment of material performance requirements. A schematic diagram of the radioisotope-fueled Brayton-cycle power system is shown in Fig. 1.2, and the operating conditions specified by the NASA-Lewis Research Center for use in the phase II study are given in Table 1.1.

The primary concern in the conceptual designs and the preliminary design for the $^{238}PuO_2$ system was to insure that the radioisotope fuel would remain contained within the fuel capsules under all credible conditions. Weight and volume considerations were kept secondary to safety in evolving the designs. The major safety guidelines used in the design

Table 1.1. Brayton-Cycle Specifications (Phase II)

Working fluid	Helium-xenon (mol. wt, 83.8)
Shaft power, kw	6.8
Turbine inlet temperature, °R	1960
Turbine inlet pressure, psia	26.3
Compressor inlet temperature, °R	540
Compressor inlet pressure, psia	13.8
Pressure drop in heat-source heat exchanger, %	3
Recuperator effectiveness	0.90
Weight flow, lb/sec	0.96
Nominal thermal input (at end of 1 year), kw	25

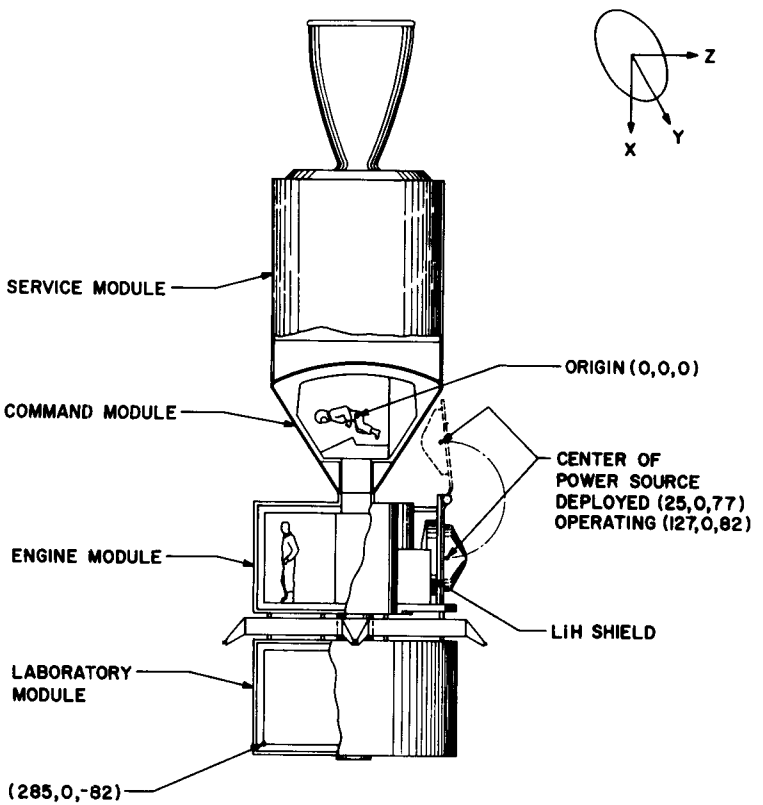

Fig. 1.1. Orientation of Isotopic Power Source in Multipurpose Mission Module Concept.

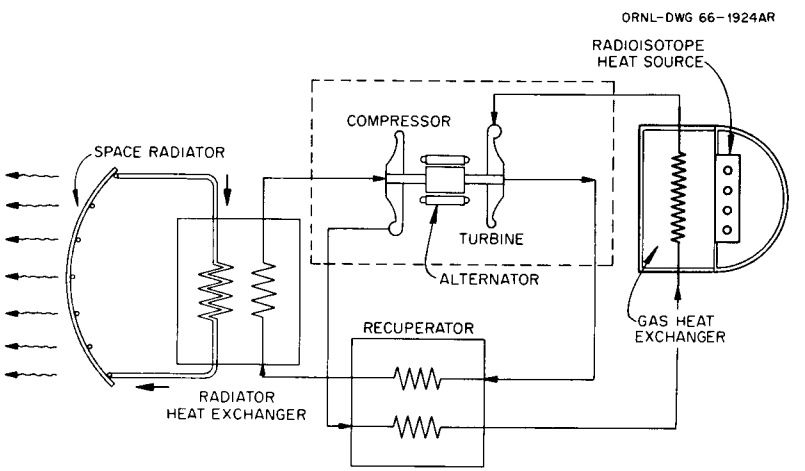

Fig. 1.2. Schematic Diagram of Radioisotope Brayton-Cycle Power-Conversion System.

studies were the following:

1. The maximum surface temperature of the fuel capsules at any time during the prelaunch, launch, and orbital phases of the mission must not exceed 2000°F, even if the Brayton-cycle system is inoperative.
2. The system must be designed so that heat can be transferred to either of two completely independent Brayton-cycle systems, including two completely independent heat exchangers.
3. The system design is directed toward containment of the radioisotope within the capsules for a period of time equal to ten half-lives or more of the radioisotope under all credible conditions. (Loss or containment due to sabotage or catastrophic explosions of fuels in orbit were not considered.)
4. The radioisotope fuel must remain contained within the fuel capsules in the event of a launch-pad fire or other emergencies during launch and orbital injection.
5. The radioisotope fuel must remain contained within the capsules during and after an uncontrolled reentry from space.
6. Burial with subsequent loss of containment must be avoided.
7. The assembly of a critical mass of the ^{238}Pu fuel form must be prevented under all credible conditions.

These goals can be approached in only a limited fashion in conceptual and preliminary design studies. In the case of $^{238}PuO_2$, complete containment of the radioisotope fuel for a time equal to ten fuel half-lives requires a containment lifetime of approximately 875 years. It is impractical to expect that in the near future there will be sufficient understanding of long-term materials behavior to prove that a particular capsule will remain intact for centuries. However, the use of a ten half-lives containment guideline as a goal toward which the capsule design is directed is very useful because the central design problem then becomes one of evaluating and coping with long-term stress effects within the limits of the best available data and methods of extrapolation. Since the relatively short-term mission operational requirements are less stringent, they are secondary in importance. This approach can be

expected to lead to conservative capsule designs from a structural-integrity standpoint and, in turn, should lead to a safer heat source design.

In the phase II capsule design, the operational criterion for the primary (stress-bearing) fuel capsules was that they not undergo more than 1% creep in five years. This requirement is more typical of the usual engineering specification, and a design can be proved by reasonably short-term experiments. However, the 5-year 1% strain criterion was established only after the phase I work had indicated that this limitation would result in a capsule design which would have sufficient structural strength to withstand the stresses caused by the buildup of helium pressure from the decay of the $^{238}PuO_2$ fuel for times approaching ten half-lives at the expected temperatures. This prediction of the potential lifetime of the capsule was supported by more detailed calculations during the phase II work.

The NASA–Lewis Research Center did not put any restrictions on the designs with respect to weight or volume, since it was recognized that safety, not size, is the paramount problem in the design of radioisotope heat sources. It was recognized, however, that if safety considerations were equal, light and compact heat-source designs were preferable. The NASA–Lewis Research Center did specify that the designs should adhere as closely as possible to current or expected near-future technology with regard to materials, methods of fabrication, and launch operation capabilities.

The radioisotope fuel requirements for the phase II heat source were based on an operating life of 1 year, and the rate of heat output at the end of the 1-year operational period would be 25 kw. It was assumed that in a normal mission the radioisotope fuel would be returned to earth in a separate ferry vehicle, returned by controlled deorbiting and impact in a selected area, or injected into a long-lived orbit. Since it would be possible for an accident to occur during launch or after some period in orbit that would result in random reentry of the heat source, the design was more strongly influenced by abnormal mission conditions than by the normal mission mode.

2. SUMMARY

A preliminary design was prepared for a nominal 25-kw(th) $^{238}PuO_2$ heat source that can be coupled with a Brayton-cycle power-conversion system for use in space. The design was based on the premise that the radioisotope heat source would be used aboard a manned spacecraft, and the appropriate shielding and safety considerations were included for this type of application. The characteristics of the design are summarized in Table 2.1, and the weight breakdown is summarized in Table 2.2. Figure 2.1 is an exploded view of the design.

The choice of $^{238}PuO_2$ as the radioisotope fuel for the heat source was made as a result of the phase I conceptual design study,[1] which indicated that plutonium would give a lighter system weight than would be obtained by using $^{244}Cm_2O_3$ or $^{147}Pm_2O_3$ in this type of application. The differences in heat-source system weights estimated in the phase I work depended greatly on the design concept; however, a comparison of the lightest weight concepts for each fuel (Table 2.3) shows a significant advantage for ^{238}Pu because of its lighter shielding requirements.

The general design approach of incorporating all the fuel capsules into a single passive emergency-reentry body that is essentially independent of the heat exchanger, shield, and other parts of the Brayton-cycle system was also an outgrowth of the phase I analysis. The phase I work indicated that the single reentry body offered the most flexibility in solving many of the safety problems associated with a radioisotope system.

In the phase II design the $^{238}PuO_2$ fuel, in microsphere form, is contained in 156 multilayered fuel capsules, which are approximately 6 in. long and 1 1/2 in. in diameter (shown in cross section in Fig. 2.2). The inner layer, which is an annular tungsten cup that holds the fuel, is contained within a stress-bearing envelope of tantalum-base alloy T-111, which, in turn, is contained within a corrosion-protection envelope of platinum or Pt—20% Rh. A diffusion-barrier layer of thoria is used between the platinum and the T-111 alloy, and a coating of iron titanate is used on the platinum to increase its emissivity to about 0.8 for heat transfer purposes.

Table 2.1. Summary of Phase II Radioisotope Heat-Source Design Characteristics

Component or System	Design Characteristics
Fuel	$^{238}PuO_2$ microspheres
Fuel capsule	Not to exceed 1% creep in 5 years at 2000°F Individual capsule burial temperature limited to 2000°F Complete containment of helium Maximum operating temperature of 2000°F Air and seawater corrosion protection Up to five years normal operating life
Shielding	Dose rate not to exceed 20 rads per year β-γ and 5 rads per year neutron Occupancy model for three-man crew Sleep: 7.5 hr/man·day Personal (meals, etc.): 3.5 hr/man·day Exercise: 1.0 hr/man·day Laboratory checkout: 10 min/3 hr·crew-day Apollo checkout: 10 min/3 hr·crew-day Scheduled maintenance: 48 min/crew-day Laboratory: 32.5 hr/crew-day
Heat transfer	Radiant transfer for all modes One active and one redundant Brayton-cycle heat exchanger Separate launch-pad-cooling heat exchanger Direct (radiant) transfer to space in emergency cooling mode
Reentry body	Single heat-source reentry body Intact reentry Inherent (nonactive) stabilization Low frontal loading at impact to prevent burial Launch-abort ejection system
Power conversion	Electrical power output, 5–6 kw System efficiency, 23% (including 5000 Btu/hr heat loss) Working fluid, helium-xenon (average molecular weight, 83.8) Inlet temperature to heat source, 1089°F Inlet temperature to turbine, 1500°F Turbine inlet pressure, 26.3 psia Maximum allowable heat transfer pressure drop, 3%

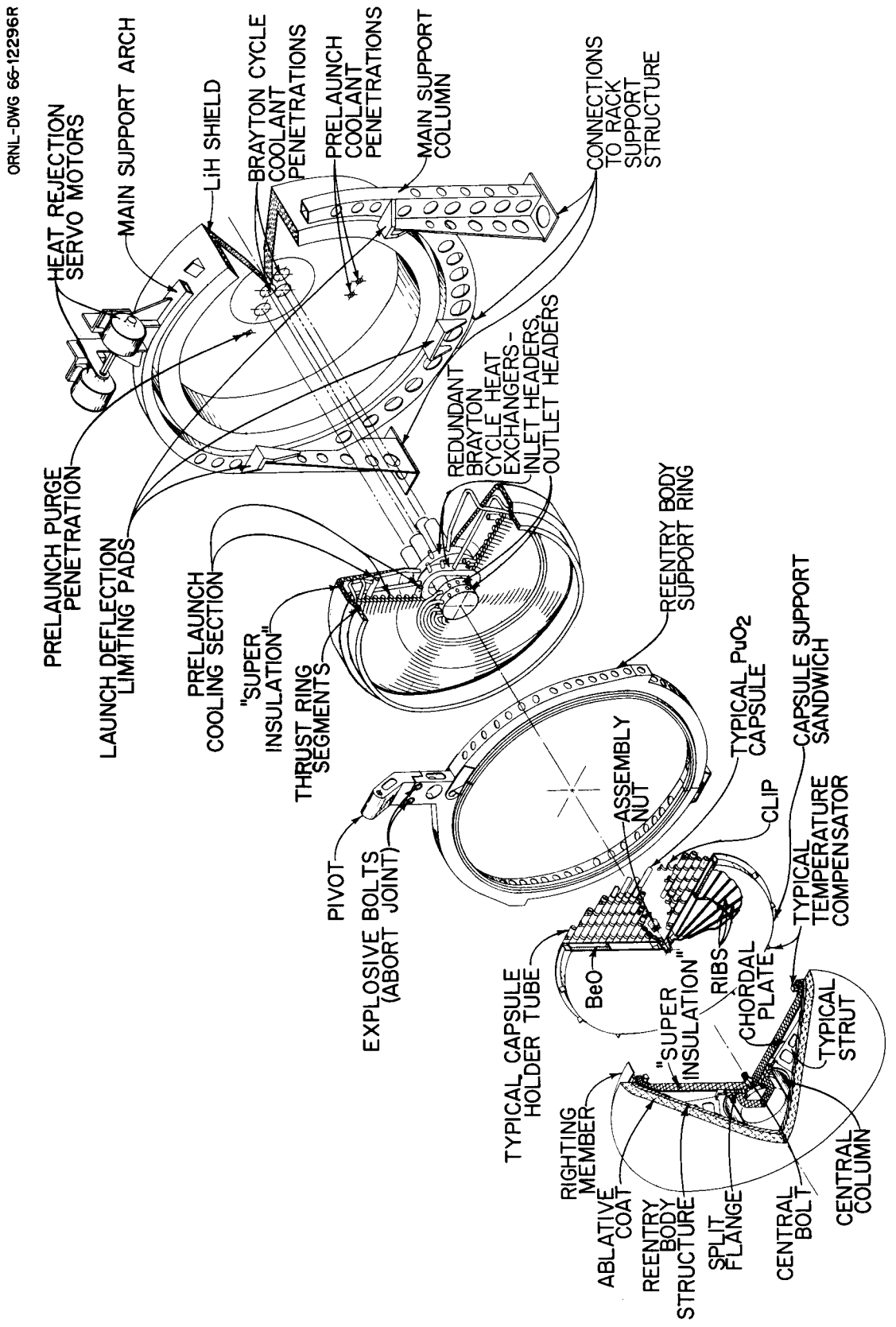

Fig. 2.1. Isotopic Brayton-Cycle Heat Source.

Table 2.2. Radioisotope Heat Source Component Weights

Specific weight: 110 lb/kw(th)

Component	Weight (lb)
Reentry body (including fuel)	1300
Abort rockets and support ring	120
Heat exchanger	390
Shield	660
Structure	150
Servos	50
Total	2670

Table 2.3. Phase I Fuel Versus Weight Comparison for Minimum-Weight Concepts

Fuel	Reentry Body Weight (lb)	Heat Source System Weight (lb)
$^{238}PuO_2$	2300	3200
$^{147}Pm_2O_3$	1390	4940
$^{244}Cm_2O_3$	650	7400

One of the major structural design requirements for the phase II capsule is that it not exceed 1% creep in 5 years when its initial surface temperature is 2000°F. As in the phase I design, the capsule is designed to have a potential life equivalent to at least ten fuel half-lives while maintaining complete containment of the fuel and the helium generated by alpha decay. It was found that the 5-year 1% strain criterion was consistent with the long-term containment-safety guideline for the temperature conditions expected in this application. Since both the amount of strain and the ultimate life of the capsule depend on the temperature history, the phase II design limits the surface heat flux of the individual

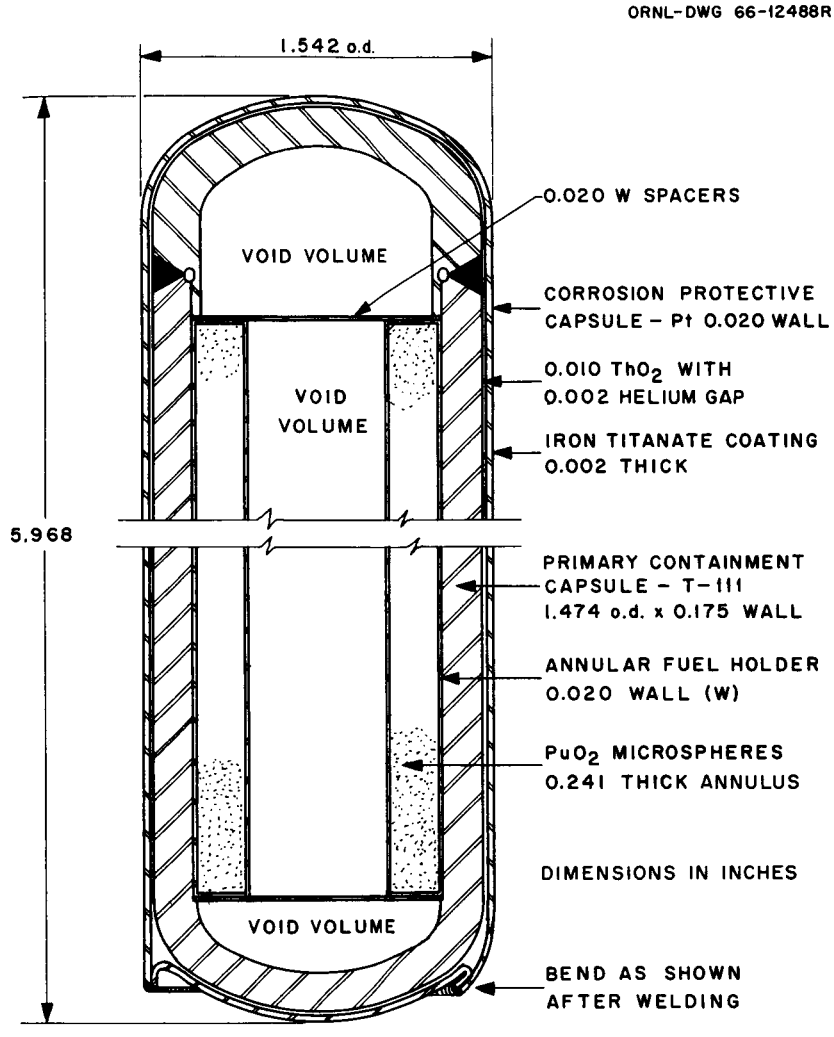

Fig. 2.2. Conceptual Design of the ^{238}Pu-Fueled Capsule; 156 Capsules Required for 24.5-kw(th) End-of-Life Power.

capsules to a value which assures that the surface temperature of the capsule will not exceed 2000°F during normal operation or in the event a single capsule is buried in dry sand. An incremental method was used to design the fuel capsule that was developed in the phase I work for treating the creep-behavior problem created by varying stress and varying temperature. In addition, a more nearly analytical solution to the problem was obtained and applied to the phase II capsule design. This solution indicated that the capsule as designed will not reach 1% creep until 13.8 years after encapsulation of the fuel and will not rupture due solely to internal pressure for over 890 years.

Since the time periods of interest in the capsule design are quite long compared with the experimental creep data available for the T-111 alloy, it was necessary to make long extrapolations in time of the mechanical property data. In order to obtain some indication of the reliability of long extrapolations, a comparison was made of the results predicted by extrapolating short-term data with longer term experimental results for Cb–1% Zr, Hastelloy N, and type 304 stainless steel. The results indicate that extrapolations of at least a factor 10 in time, and possibly longer, give results for these alloys that are accurate within the limits of normal heat-to-heat variations and experimental error.

The multipurpose mission module[2] specified by NASA was used as the vehicle configuration for integration studies. The permissible dose rate for the crew and the occupancy model are given in Table 2.1. The gamma contribution from the $^{238}PuO_2$ fuel (1.2 ppm ^{236}Pu) is insignificant compared with the neutron dose rate. To reduce the contribution from (α,n) neutrons, the oxygen in the $^{238}PuO_2$ fuel compound is depleted in the isotope ^{18}O by a factor of 10 below its normal abundance. Further reduction in the ^{18}O content will not significantly reduce the neutron output of the present-day fuel because of (α,n) reactions with trace amounts of other impurities. There are 0.214 neutrons produced per original source neutron by subcritical multiplication in the phase II source array. The total neutron source strength (including neutron multiplication) is calculated to be 9200 ± 3000 neutrons/sec per gram of ^{238}Pu.

A 4-in.-thick shield of LiH is required to reduce the time- and volume-averaged dose rate in the three modules of the multipurpose mission module spacecraft to 5 rads per year from neutrons and 20 rads per year from gamma radiation. The shield (illustrated in Fig. 1.1 of Sect. 1) is needed only in the direction of the manned compartments, since the dose rate at 1 m from the unshielded side of the source array is only about 100 mrem/hr.

The components that make up the heat-source system (shown in Fig. 2.1) are the reentry protective shell, fuel plate, reentry body support ring, heat exchanger assembly, main support structure, and LiH shield. The system is arranged so that the fuel block and reentry shell are assembled as a separate unit that can be rapidly disengaged from the rest of the

system in the event of a mission abort. The use of a single reentry body to contain all the fuel capsules offers several advantages. All the radioisotope fuel is kept in one place in the event of a random reentry from orbit, and the terminal velocity can be kept low enough to prevent burial and capsule deformation on impact. With an optimum mass of moderator and heavy-metal reflection, a critical configuration of fuel could be achieved only by rupture, release, and reassembly of fuel from the capsules. The reentry body, including the fuel plate, weighs 1300 lb and has a diameter of 5.5 ft. The calculated impact velocity is 250 fps, and enough of the impact force can be absorbed in the reentry protective shell and fuel plate to prevent significant deformation of the fuel capsules.

The fuel capsules are contained in Cb—1% Zr tubes attached to the surface of the fuel plate. Heat is transmitted, principally by radiation, from the surface of the capsules to the tubular holders and then to the working-fluid heat exchanger. All surfaces involved in the radiant transfer of heat are coated with iron titanate to improve their emissivity. The heat exchanger is designed for a helium-xenon gas-mixture working fluid with an effective molecular weight of 83.8. The heat exchanger assembly consists of both active and redundant exchangers arranged in the form of involute tubes in a planar disk geometry. The disk is the same diameter as the fuel block and, in the operating position, is located about 5 in. from the tubular capsule holders. The matching geometry of the fuel plate and heat exchanger (planar disks) enhances radiant heat transfer, and the average operating temperature of the fuel capsules will be approximately 1750°F. A hot-spot calculation indicates that a few of the capsules near the heat-exchanger outlet header may run at approximately 2050°F, which is slightly above the design goal of 2000°F. In addition to the active and redundant exchangers, the heat-exchanger assembly also contains a third exchanger through which liquid coolant is circulated during launch-pad operations to keep the fuel plate below its normal operating temperature.

An alternate heat exchanger design, based on the use of pure argon as the working fluid, will fit within the space required for the helium-xenon design. This alternate exchanger will also meet the design criteria of not exceeding a pressure drop of 3%.

Linde Superinsulation, a multifoil type of insulation, surrounds the heat exchanger–fuel block cavity. Since the fuel plate and its reentry protection shell are separable from the heat exchanger and other parts of the Brayton-cycle system, a labyrinth seal arrangement is used to form the joint between the two halves of the insulated volume. Allowances were made in the fuel capsule design for a 10% heat loss through the insulation; however, the calculated loss is less than 5%. In addition to its main function of preventing heat loss, the insulation is also used to partially support the fuel plate and heat exchanger and to keep them centered. Since this action is accomplished without penetrations through the insulation, this design feature is largely responsible for the low system heat loss.

Safety devices are included in the system design to protect the integrity of the capsules in the event of malfunction or mission abort and in periods when the Brayton-cycle equipment is inoperative. While the launch vehicle is on the pad, the heat source cannot be deployed for cooling, since it is enclosed within the Saturn LEM adaptor (SLA) section between the Apollo service module and the S-IVB stage. The previously mentioned third heat exchanger, which is connected to an external coolant loop, keeps the fuel plate temperature under control during the launch-pad checkout period. At lift-off, this launch-pad heat exchanger is disconnected from the coolant supply and only the heat capacity of the system is available to control the rate of rise of the fuel capsule temperatures. A heat capacity sufficient to keep the capsules below the maximum operating temperature of 2000°F for about 30 min after disconnecting the launch-pad heat exchanger is provided in the form of 100 lb of BeO located in the fuel block. It is assumed that within 30 min after launch the SLA can be deployed, and the fuel plate in its reentry body can be rotated to reject its heat to space until the Brayton-cycle equipment is put into operation. With 100 lb of BeO, up to 1 hr can elapse without external cooling before the temperature of the capsules reaches a level close to the melting point of the platinum cladding on the capsules. The design of the fuel plate allows enough space to contain up to 300 lb of BeO if needed for a mission requiring a longer heat-storage capability.

An abort rocket system is included in the design to provide a means of ejecting the fuel plate within its protective reentry shell in the

event of a launch-pad fire or a mission abort after lift-off but prior to achieving orbit. The abort rockets are attached to a structural ring which, in turn, is attached to the reentry-body support ring. They are designed to eject the reentry body a horizontal distance of about 200 ft from the side of the launch vehicle.

After the SLA has been deployed and orbit has been achieved, the abort rocket ring is separated from the reentry-body support ring by explosive cord and allowed to drift off into space. If, during the course of the mission, the Brayton-cycle equipment becomes inoperative, the reentry body can be rotated through 180° so that the hot surface of the fuel block is facing toward space rather than at the heat exchangers. This rotation will normally be accomplished by two low-torque servo motors located at the reentry-body support-ring pivot point (Fig. 2.1). If the motor system fails, the BeO heat sink will provide from 30 to 60 min to deploy the heat source to its emergency cooling position manually. If the manual efforts fail, the reentry body with the fuel plate can be separated from the spacecraft by means of an explosive cord that will split the support ring around its circumference.[3,4] Hexanitrostilbene is specified for the explosive cord because there has been considerable practical experience with this material, and NASA experiments have indicated that it can reliably be expected to detonate properly even after exposure to a space environment for two years.

The reentry body was designed with a large projected area in order to achieve a low ballistic coefficient (~79) and correspondingly low terminal velocity and frontal loading. The shell is covered with a 2 1/2-in.-thick ablative coating to provide complete protection against reentry heating. The blunted-cone shape was chosen because of its inherent stability in the forward direction. To guard against the remote possibility of the reentry body stabilizing in the wrong direction, a righting member was placed on the rear surface to tip the body over to the forward direction. The high ratio of spin inertia to tumbling inertia (1.86) of the design will minimize the tendency for the body to oscillate during reentry while enhancing the tendency for it to spin stabilize.

A facility for fueling and assembling the individual fuel capsules consists of a bank of seven lightly shielded cells (~2 ft of concrete) equipped with master-slave manipulators. Two of the cells are for receiving and shipping, and the other five are for capsule assembly operations. The equilibrium temperature in air of a fully fueled capsule will be approximately 1000°F, so all operations up through the assembly of the outer platinum cladding will be carried out in an inert atmosphere to prevent oxygen contamination of the refractory metals used in the capsule construction. After the outer platinum cladding is sealed, the individual fuel capsules can be handled in air without difficulty. Shipment of the capsules to the launch site will be made in water-shielded casks that meet all ICC regulations for shipment of radioactive materials. Four individual shipments of 6 kw(th) each are proposed to make up each heat source.

Loading of the individual capsules into the fuel block can be carried out manually at the launch site. The fuel plate in its reentry body can be installed aboard the launch vehicle prior to fueling, and the reentry body can be pivoted outward slightly to expose the ends of the tubular capsule holders. Individual groups of capsules corresponding to the number going into each tubular holder will be transported in small shields to the level of the Brayton-cycle equipment and slid individually, using a specially adapted tool, into the tubular holder. After each holder is filled it will be capped, sealed, and crimped to hold the capsules in place. The dose rate at 1 m from the unshielded fully fueled heat source will be only 100 mrem/hr, and it is expected that the entire fueling can be carried out without exceeding dose limits to members of the fueling team.

Identification is made of those fields of research and some of the detailed research and development problems where further investigations will have to be carried out in order to test the validity of the design. The problems are mainly in the fields of high-temperature materials and aerodynamics because compliance of the design with the safety ground rule for containment of fuel under all credible conditions is based partly on utilization of what is judged to be near-future materials technology and on extrapolations from present aerodynamic data.

3. CAPSULE DESIGN

3.1. Phase II Fuel Selection

In the phase I study,[1] several forms of ^{147}Pm, ^{244}Cm, and ^{238}Pu fuel were investigated. Based on the results of this study, $^{238}PuO_2$ microspheres were selected as the fuel to be considered in the phase II preliminary design. Some of the significant properties of $^{238}PuO_2$ are listed in Table 3.1. These values are based on the most recent information from Mound Laboratory[5-7] and, in some instances, vary slightly from the values given in the previous report (Ref. 1, p. 14).

The recommended value from Mound Laboratory[5] for the specific power of the compound in the present-day microspheres is 2.6 ± 0.1 w/cm^3 based on a packing fraction of approximately 56%. The required volume of fuel corresponding to this value would fit into the phase II capsule as designed; however, the fuel would be dispersed throughout the capsule volume (except for the end caps) instead of being in the annular configuration. The center-line temperature of the dispersed fuel arrangement would be substantially higher than the design value (outer surface temperature limitation of 2000°F), but it would still be well below the design criterion of limiting the maximum fuel temperature to 200°F or more below the melting point.

At the present time, the Oak Ridge National Laboratory is developing the "sol-gel" technique for preparing microspheres with a controlled particle size distribution. Plutonium oxide microspheres with an 80% packing fraction have been prepared[8] and, as indicated in Table 3.1, this value was used in the phase II capsule design.

In order to provide a minimum of 5 kw(e) at the end of a 1-year mission, a total of 24.5 kw(th) is required for the initial fueling. This value is based on

1. a Brayton-cycle total system efficiency of 23%,
2. a two-month lag period between the loading and fabricating of the capsules and spacecraft launching,
3. a 10% excess wattage factor for heat losses through system insulation.

Table 3.1. Data Sheet for $^{238}PuO_2$ as a Brayton-Cycle Heat Source

General properties[a]	
Half-life, y	87.5
Density, g/cm^3	11.4
Specific power of compound, w/g	0.406
Power of compound, w/cm^3	
Maximum	4.63
ORNL design value	3.7[b]
Melting point, °C	2240
Thermal conductivity at 1200°C, w/cm·°C	
Maximum	0.0235
ORNL design value	0.0135[b]
Requirements	
Total thermal power to provide 5 kw(e) at end of 1-year mission, kw	24.5[c]
Initial fuel activity, curies	740,000
Total fuel weight, lb	133

[a]Based on 80% ^{238}Pu–20% ^{239}Pu and other impurities.

[b]Based on 80% packing fraction with 1 atm helium occupying the void volume.

[c]Includes 2-month lag between load and launch and 10% excess wattage for heat losses through insulation.

The calculated heat losses for the phase II system show that the 10% excess wattage factor used at the start of the phase II design was slightly higher than necessary.

3.2. Phase II Capsule Design

3.2.1. Criteria

After considering the initial safety guidelines and the essential design criteria established in the phase I study, the phase II capsule design was based on the following:*

*The calculational method for choosing the best relationship between the number of capsules, wall thickness, and void volume is described in detail in the phase I report.

1. The capsules would be multilayered cylinders with ellipsoidal end caps. (For structural purposes, the hemispherical end cap configuration used in the phase I study was replaced by the ellipsoidal configuration.)

a. Primary (stress-bearing) capsule material — For stress bearing to withstand internal pressure buildup and reentry earth impact, a tantalum-based alloy, T-111,[9] would be used.

b. Fuel holder material — Tungsten (20-mil wall) would be used for the annular fuel holder inside the primary capsule, since there is a possible compatibility problem between the PuO_2 and the tantalum-base alloy of the primary capsule.

c. Outer (corrosion-protection) capsule material — Platinum would be used to provide protection under corrosive conditions such as high-temperature oxidation, earth burial, and immersion in seawater. A wall thickness of 20 mils was judged to be sufficient to provide protection from the various corrosive atmospheres at temperatures up to 2000°F.

d. Barrier coating between primary and outer capsule — A 10-mil coating of ThO_2 would be used on the outside of the primary capsule to prevent possible interaction and diffusion of the platinum with the primary capsule material.

e. Exterior capsule coating — Since platinum has a low emissivity (~0.2), a 2-mil coating of iron titanate would be required to raise the emissivity value to approximately 0.8 for heat transfer in the Brayton-cycle heat exchanger system.

2. The length-to-diameter ratio of the primary capsule would be 4. The choice of this L/D ratio was based mainly on available impact data obtained from tests on similarly shaped capsules in connection with AEC isotopic power safety evaluation programs.

3. The primary capsule wall thickness would be no less than 0.060 in. and no more than 0.250 in. This maximum thickness is assumed to be the limit for which existing remote-welding facilities can obtain a full-penetration structurally satisfactory welded joint.

4. The maximum capsule surface temperature would be 2000°F under normal operating conditions and for burial in case abort or accident conditions resulted in burial of a single capsule.

5. Creep would not exceed 1% in 5 years. This criterion is based on the assumption that the layers which constitute the fuel capsule will still be able to perform their respective functions at the time 1% creep has occurred in the primary capsule wall.

6. No critical array of fuel could be formed under any credible conditions.

3.2.2. Design

The phase II capsule design provides for a time to 1% creep of 5 years under normal operating conditions. As will be described later in this section, this creep criterion limits the allowable rate of stress increase in the capsule walls (from helium production) to a value that will not exceed the ultimate tensile strength of the capsule in a time period equal to ten half-lives of the $^{238}PuO_2$ fuel. This creep criterion would allow possible extension of mission life if a change were desirable. Brayton-cycle specifications provide a 1-year mission life; but with ^{238}Pu as the fuel, mission life could easily be extended to 5 years without exceeding the capability of the fuel to provide adequate heat.

During the phase I study, a method was developed for calculating an allowable stress-rate versus time curve for the primary capsule material. This method was applied in the phase II design to generate two curves for $^{238}PuO_2$ encapsulated in T-111: the time to reach 1% creep and the time to rupture versus the allowable stress rate, as shown in Figs. 3.1 and 3.2, respectively. Only T-111 data were used for determining these curves; however, if future data prove T-222 to be the superior alloy, this material can be substituted in future designs. Both curves utilize an initial capsule material temperature, T_0, of 2000°F and reflect a continually decreasing temperature due to decay of the ^{238}Pu fuel.

As shown in Fig. 3.1, the allowable stress rate for a time to 1% creep of 5 years is 0.14 psi/hr (represented by the dot on the curve). To obtain the best capsule design within this allowable stress rate, a

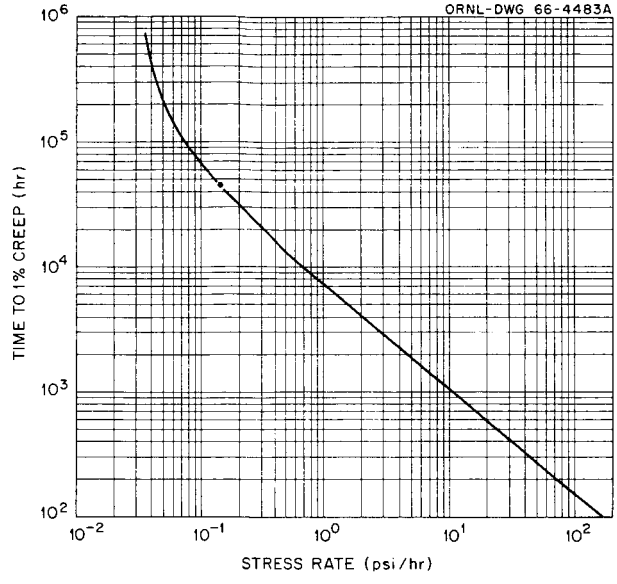

Fig. 3.1. 1% Creep Stress-Rate Envelope for T-111 Capsule Containing ^{238}Pu; T_0 = 2000°F.

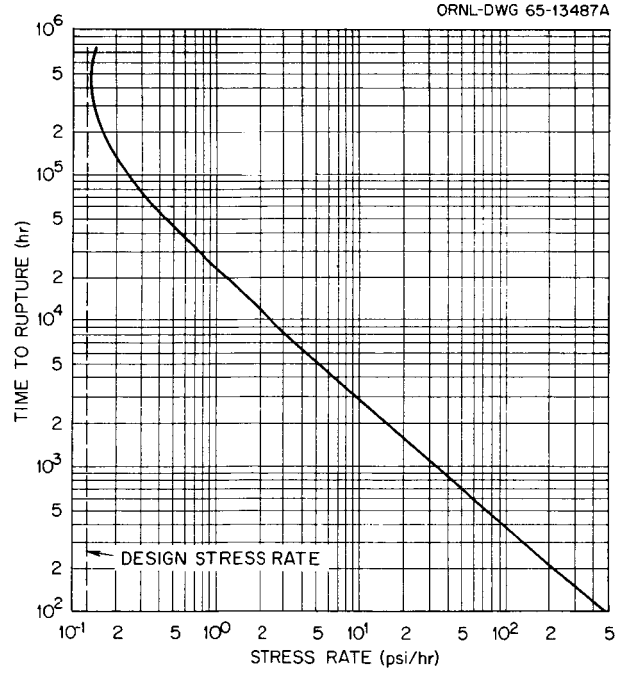

Fig. 3.2. Rupture Stress-Rate Envelope for T-111 Capsule Containing ^{238}Pu; T_0 = 2000°F.

computer program was developed to vary the capsule inside diameter and the allowable pressure rate (and thus change the wall thickness) to give the combination of variables that would result in the minimum total volume of capsules and the combination for the minimum total weight of capsules for each pressure rate considered. Figure 3.3 shows the results of this analysis and compares the minimum weights and volumes required for various rates of increase in internal pressure. These values are based on the thicknesses of the other capsule layers remaining constant, as previously described, and no values are included that give capsules whose surface temperature would exceed the 2000°F burial limitation. The dotted portions of the curves in the figure show where capsule wall thickness fails to meet specifications (0.06 in. < T < 0.250 in.) by being too thick for the higher allowable pressure rates and too thin for the lower allowable pressure rates.

The minimum-weight capsule design occurs at a pressure rate slightly under 0.01 psi/hr and requires only about 550 lb for capsules and fuel.

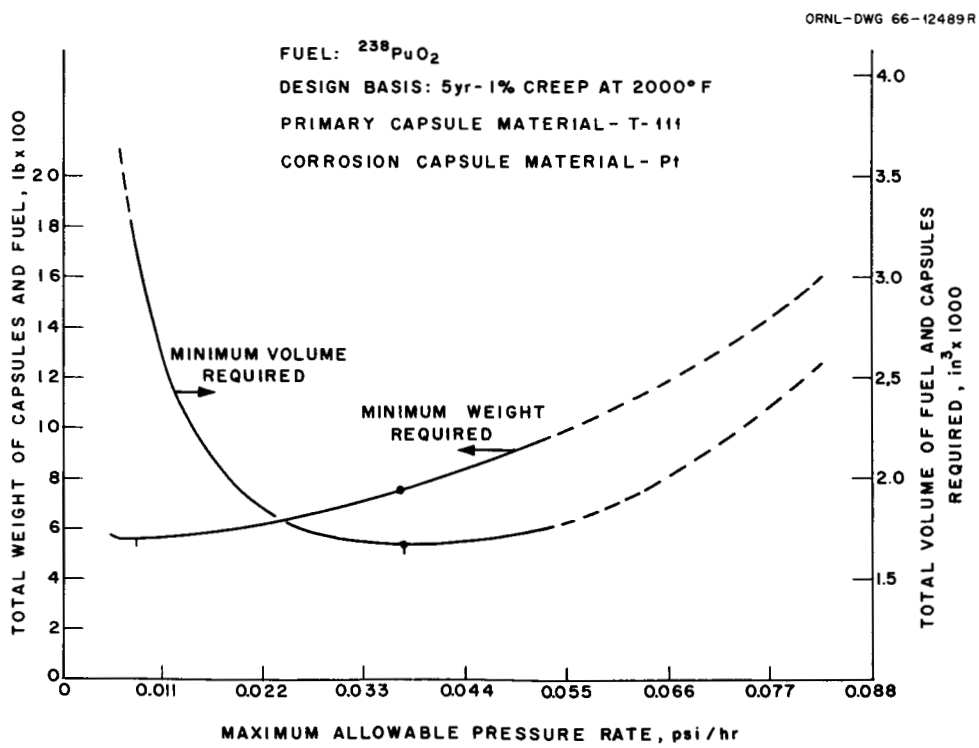

Fig. 3.3. Minimum Capsule and Fuel Weights and Volumes Required for Various Rates of Increase in Internal Pressure.

The volume of approximately 3300 in.^{3} required for this design is, however, very high and would result in a large and heavy system that would more than offset the slightly lower total weight for the fueled capsules.

The best design was determined to be the one that required the minimum volume. In this case the minimum-volume design had an initial internal pressure buildup rate of 0.037 psi/hr and required a total weight of 698 lb for the unshielded fuel and capsules. This total weight is only about 25% higher than the minimum-weight design, but the 1660-in.^{3} volume represents a reduction of 50% in total volume when compared with that of the minimum-weight capsule design.

The phase II ^{238}Pu capsule design developed in this study is shown in Fig. 2.2. The fuel, in microsphere form, is contained in the tungsten holder, which has an annulus thickness of 241 mils. The T-111 primary capsule is 175 mils thick and has the specified length-to-diameter ratio of 4. With this design, 156 capsules, each containing 157 w of ^{238}Pu fuel, will be needed to provide the required 24.5 kw(th) for initial loading. Table 3.2 lists the capsule design characteristics.

Table 3.2. Phase II $^{238}PuO_2$ Capsule Design

Capsule layer thicknesses, in.	
Tungsten inner fuel annulus liner	0.020
$^{238}PuO_2$ fuel	0.241
Tungsten outer fuel annulus liner	0.020
T-111 primary containment wall	0.175
ThO_2 diffusion barrier	0.010
Helium-filled gas gap	0.002
Platinum corrosion barrier	0.020
Iron titanate coating	0.002
Tungsten fuel spacer	0.020
Capsule dimensions, in.	
Inside diameter	1.124
Outside diameter	1.542
Fueled length	4.132
Overall length	5.968
Data for 156 capsules	
Volume, in.^{3}	1660
Weight, lb	698
Thermal power, kw	24.5

3.2.3. Thermal Profile of Phase II Capsule Design

Under normal conditions, the capsule reaches its highest temperature immediately after the primary capsule container is welded. This weld will be produced by a remotely operated electron-beam welder under vacuum and, after final closure of the primary capsule, the void volumes in the capsule and the fuel will be under a 10^{-4} to 10^{-5} torr vacuum. This condition is expected to result in an internal heat problem for about two weeks until the decay of the fuel has generated enough helium to reach one atmosphere. To determine the maximum internal temperature that will be experienced while the inside of the capsule is in a vacuum and the capsules are within the cell bank, an analysis was made for three progressive cases: (1) fuel with bare primary capsule as outer covering, (2) case 1 with a ThO_2 coating applied, and (3) case 2 encapsulated in platinum with an iron titanate coating applied.

The most severe case was the fuel in the uncoated primary capsules because the unclad capsule has the lowest emissivity value. In this case the maximum internal temperature of a capsule is approximately 2835°F and the surface temperature is about 1700°F in an argon atmosphere. These temperatures are well below the melting point of the fuel and capsule materials. During some of the capsule assembly operations, cooling blocks can be utilized to lower the temperatures; however, inert atmosphere cells will be required when handling the unclad fueled primary capsules to insure that the structural properties of the T-111 alloy are not altered by oxygen pickup.

During normal operation in the Brayton-cycle system, the maximum surface temperature is limited to 2000°F, but helium will occupy the void volumes in the capsule and this will result in a much lower temperature drop across the fuel layer. Figure 3.4 shows a thermal profile of the phase II capsule design with a surface temperature of 2000°F. Because of the relatively large surface areas and the low total heat output per capsule (157 w), the temperature drop across each of the protective layers is very small, except for the drop across the fuel itself, which is 75°F. The maximum temperature in the fuel is not expected to exceed 2090.5°F, and the calculated average helium temperature is 2053°F.

ORNL-DWG 66-12550R

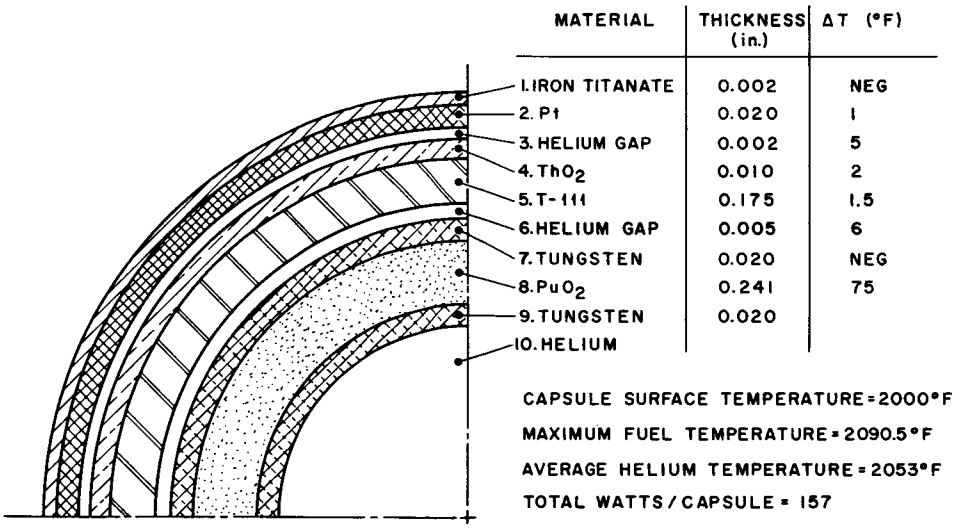

Fig. 3.4. Thermal Profile of $^{238}PuO_2$ Capsule.

3.2.4. Phase II Capsule Life Under Long-Term Stress

With an initial average helium temperature of 2053°F, the long-term temperature-pressure history of the capsule for ten half-lives is shown in Fig. 3.5. The void volume-to-fuel volume ratio for this capsule is 1.26, and the maximum pressure in the capsule (~14,500 psi) occurs at about 130 years, which is approximately 1.5 times the fuel half-life. This pressure condition could occur only in the event of an accident or an abort that resulted in burial of a capsule in loose dry sand. If a capsule were lost and remained on the surface of the ground, the capsule initial surface temperature would be only approximately 1150°F, and the maximum pressure would not exceed 11,000 psi.

In predicting the behavior of the capsule over a long period of time under conditions of constantly changing stress and temperature, creep was assumed to be the dominant mode of failure until the capsule material reached a temperature that was approximately one-third its absolute melting temperature. In the present case (a T-111 capsule containing ^{238}Pu with an initial temperature of 2000°F), this temperature point occurs at

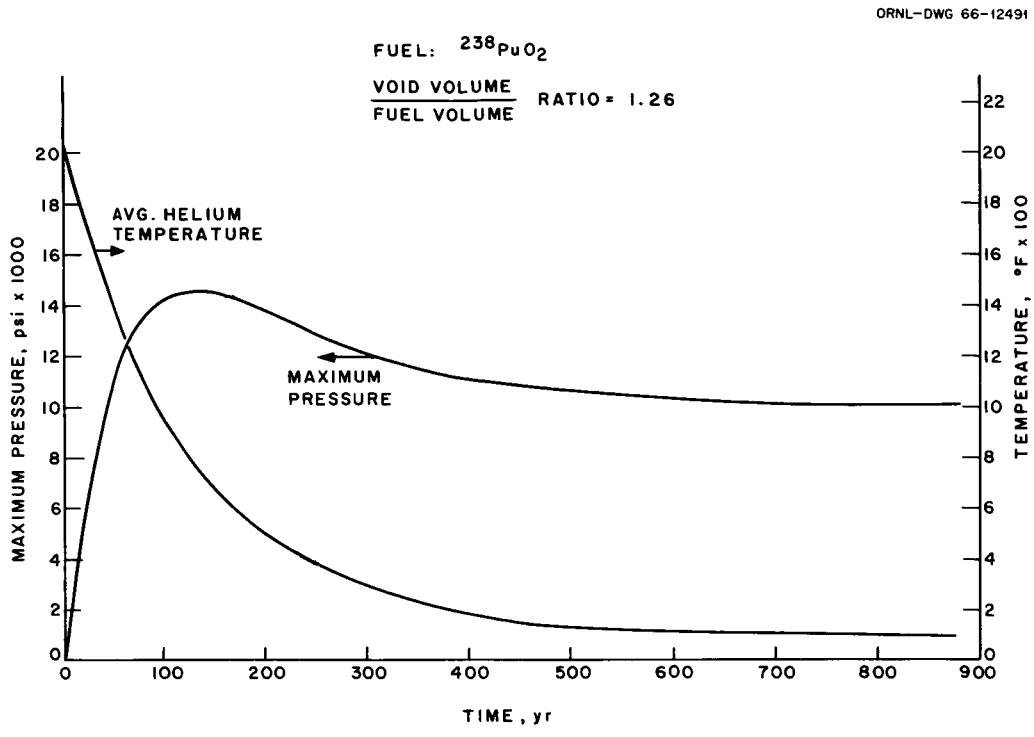

Fig. 3.5. Long-Term Temperature-Pressure History of Capsule.

about 54 years. After this time, the ability of a capsule to withstand rupture due to internal pressure is based on its tensile strength.

Figure 3.2 (above) is a plot of the stress rate for creep rupture versus time for T-111 alloy initially at 2000°F and containing ^{238}Pu fuel. As shown on this figure, the minimum initial rate of stress increase that will cause creep rupture occurs at 54 years, which is approximately the time to reach one-third the absolute melting point for the T-111 alloy (m.p., ~4400°F). The vertical dotted line in the figure is the initial stress rate, 0.14 psi/hr, which satisfies the 5-year 1% creep limitation. Since the 0.14 psi/hr design value is below the minimum value for creep rupture, the capsules are expected to pass through the entire creep-temperature range without failure. The total creep is estimated to be less than 5%. The peak pressure in the capsule does not occur for about 130 years (Fig. 3.5) and the time between the limitation for creep rupture (54 years) and the time to reach peak pressure (130 years) could be the limiting factor on the capsule design. During these 76 years, capsule

rupture life is determined by the elastic limit of the material; ultimate tensile-strength data were used to evaluate the structural integrity of the capsule. For a conservative estimate, the peak pressure for this time period (14,500 psi) was coupled with the highest temperature occurring during this time (the temperature at the point where creep ceases to be a dominant factor). The ultimate strength for recrystallized T-111 alloy at one-third the melting point is 85,000 psi, and this stress corresponds to an internal pressure of 22,300 psia in the phase II capsule. As noted previously, the maximum internal pressure experienced by the phase II capsule is only 14,500 psia, corresponding to a hoop stress of 55,250 psi. The data shown later in Table 3.7 for yield and ultimate strength indicate that at the lower temperatures the yield strength is very nearly the same as the ultimate strength, and therefore significant yielding is not expected.

It was recognized during phase I work that the calculated stress-rate curves might be conservative because they are based on the assumption that the rate-of-stress increase with time is constant. Since in an actual capsule the rate-of-stress increase will decrease with time because the amount of radioactive fuel is decreasing, the actual closeness of the 5-year 1% creep line to the creep-rupture line (shown in Fig. 3.2) is probably conservative. An improved method of capsule analysis that is more exact and rigorous was developed late in phase II and was used to check the results of the previous calculations (see Sect. 3.4). This improved method confirmed that the analysis is conservative, especially in the time to 1% creep.

3.2.5. Impact Analysis

The preceding analysis of the long-term containment integrity of the fuel capsules is based on a right-circular-cylinder capsule with ellipsoidal end caps. If the capsules are significantly deformed upon impact, the stresses resulting from the internal pressure may be much larger than those calculated for cylindrical geometry, and the capsule may fail. Therefore, the design for long-term containment must be adequate to prevent significant distortion of the capsules in the event of random

reentry of the heat source from space and impact on a hard surface (e.g., rock).

Sandia Corporation has been engaged in impacting capsules of various sizes and shapes at different velocities as part of SNAP-system safety evaluation activities for the USAEC. This work is providing a better understanding of how high-velocity impact forces are distributed and absorbed. At the present time, however, there is no rigorous analytical technique for calculating the results of a high-velocity impact on the shape of a capsule, and each design must be verified by experiment. Total force calculations combined with the yield-strength properties of materials can serve to indicate whether a capsule has a reasonable chance of surviving a specified impact, and this type of calculation was used to check[10] the phase II capsule design.

For the calculation model a 1500-lb blunted-cone body impacting at a terminal velocity of 300 fps and coming to rest in a distance of 1 ft was assumed. (It should be noted that the conditions assumed for the model are somewhat more stringent than the design finally arrived at in the phase II work — an impact velocity of approximately 260 fps and a reentry body weight of 1300 lb.) It was assumed that the 1-ft stopping distance was all taken up by deformation of the cone rather than by deformation of the ground. Under these conditions, the total impact force was calculated to be 4.2×10^6 lb, of which only 4.4×10^5 lb was absorbed by crushing the blunted cone back a distance of 1 ft. The remaining 3.76×10^6 lb was assumed to be transmitted through the reentry body structure to the fuel plate and into the capsules. If the force is distributed evenly in the 156 capsules, each capsule must absorb approximately 24,000 lb by permanent and/or elastic deformation. If it is assumed that the capsules are at 2000°F at impact, the yield strength of T-111 alloy is 40,000 psi. For the phase II capsule design (Fig. 2.2), 70,000 lb of force applied along the side is required to equal the 40,000-psi yield stress of T-111 alloy. Therefore no permanent deformation of the T-111 alloy should occur if the impact forces are applied perpendicular to the longitudinal axis of the capsule. If the impact force is applied on the ends of the capsule, the end caps may be deformed to form a flat spot 0.5 in. in diameter.

This evaluation of the impact behavior of the fuel capsules in the reentry body assembly is conservative from the standpoint that no credit is taken for energy absorption in the ground, by rebound, by deformation of the fuel-plate support struts, and by deformation of the fuel plate and tube holders. While it is recognized that in an actual impact, shock waves may travel throughout the structure and produce higher-than-average stresses in some parts of the assembly, the results of the total force evaluation indicate that is is not unreasonable, for the purpose of a preliminary design, to expect that the phase II capsules can survive the impact conditions postulated for the heat source without significant deformation.

3.3. Effect of Strain and Temperature Criteria

Six specific concepts were studied in phase II to determine the effects that varying the design criteria would have on capsule weight and volume requirements.

Concept 1 was based on an allowable stress rate that results in a total of 1% creep during the time the capsule is in the creep temperature range (54 years). This results in a minimum safety factor of 3.5 with respect to both the ultimate tensile strength and the creep strength of the capsule for the 875-year containment period. The equilibrium surface temperature of a single capsule buried in dry sand was not to exceed 2000°F.

Concept 2 was based on providing for a safety factor of about 1.5 with respect to the ultimate strength and creep strength of the capsule for ten half-life containment. No burial or creep limitations were imposed on the capsule design.

Concept 3 was identical to concept 2 expect that a 2000°F burial temperature limitation was imposed for single capsule burial.

Concept 4 was based on the limitation of 1% creep in 5 years. There was no burial temperature limitation on capsule design.

Concept 5 was identical to concept 4 except that a 2000°F burial temperature limitation was imposed for single capsule burial (phase II design)

Concept 6 was based on the use of a vented capsule. No allowances were provided for stress or burial temperature limitations. The fuel center-line temperature was the main determining factor for number of capsules required in the heat source. A packing fraction of 80% of theoretical density was assumed.

To determine the best capsule design to satisfy the allowable stress criteria for each concept, calculations were made by computer analysis. The effects of varying fuel loading, capsule diameter, primary capsule wall thickness, and void volume-to-fuel volume ratio were determined by varying the capsule inside diameter and allowable pressure rate but keeping the allowable stress constant. In each case, the combination of variables that gave the minimum total volume of capsules was selected as the best design, since the phase I work had shown that this would give the minimum system reentry body diameter and the lowest total system weight.

The results of these calculations for each concept are given in Table 3.3. As indicated, the required weights and volumes increased as the safety factor for long-term containment increased. Concepts 4 and 5 have only a 5-year 1% creep stress criterion; however, as noted in Section 3.2.4, this also results in a capsule design for a 2000°F start-of-life temperature in which the maximum internal pressure ever experienced by the capsule does not result in a stress that exceeds the ultimate strength of the T-111 alloy. Concepts 2 and 3 have a minimum safety factor of 1.5 for ten half-lives containment, and concept 1 has a safety factor of 3.5. Imposition of the 2000°F burial temperature limitation on a single capsule is shown to result in a very small increase in total weights and volumes required (comparison of concepts 2 and 3, 4 and 5); however, the maximum allowable size of an individual capsule is greatly reduced, and this results in an appreciable increase in the number of capsules required.

3.4. A General Method for Design and Analysis of Alpha-Emitting Radioisotope Fuel Capsules

In capsules containing alpha-emitting radioisotopes for use in space power packages, it is desirable to provide maximum power per unit of

Table 3.3. Phase II Capsule Designs for Various Concepts[a]

	Concept	Total Weight Required (lb)	Total Volume Required ($in.^3$)	Number of Capsules Required	Capsule Dimensions (in.)			
					ID	Primary OD	Total OD	Total Length
1.	1% creep in 54 years; safety factor of 3.5 on rupture stress; 2000°F burial temperature limit	1490	4960	85	2.125	2.625	2.693	10.564
2.	Safety factor of 1.5 on rupture stress; no burial temperature limit	750	1870	60	1.625	2.125	2.193	8.568
3.	Same as concept 2 with 2000°F burial temperature limit	775	1900	144	1.187	1.586	1.654	6.412
4.	5-year 1% creep limit; no burial temperature limit	640	1630	45	1.750	2.236	2.304	9.012
5.	5-year 1% creep limit; 2000°F burial temperature limit	698	1660	156	1.125	1.475	1.542	5.968
6.	Vented capsule; 80% packing	205	505	6	2.750	2.950	3.018	11.868

[a]Based on minimum-volume design and utilizing 24.5 kw(th) ^{238}Pu fuel.

weight, volume, or projected area within the constraints imposed by the need to maintain capsule integrity during normal operation and in the event of accidental conditions. Because of the continuous generation of helium gas, together with decay of the thermal power, these capsules are characterized by time-dependent stress and temperature. Because of very high initial temperatures, creep is an important consideration in the design.

The general approach to capsule design in this study has been toward the fuel capsules that remain intact for a period equal to ten or more half-lives. A limiting design condition was also imposed which requires that a capsule maintain its structural integrity in the event that, after reentry, it becomes separated from the reentry body, is buried in earth, and is never found. When this condition is applied to ^{238}Pu fuel, it requires that resistance to creep be provided for a time that exceeds the practical duration of creep experiments. If the capsule has an initial operating temperature of 2000°F and the temperature difference decays in transient equilibrium with the thermal power, creep is an important consideration for a period of about 54 years until the temperature decreases below one-third the absolute melting temperature.

In phase I studies[1] an approximate method was developed for analyzing the long-term creep problem and designing a capsule for maximum power per unit of weight or volume. In this method, a function relating creep life to stress and temperature was determined by making a polynomial fit of creep data with the Larson-Miller parameter. The allowable stress rate to avoid failure at each time-temperature point in the history of the capsule was then calculated by a graphical and incremental process involving a simple formula that may be derived by assuming linear accumulation of partial creep lives. Capsules were then designed which had the property that their maximum (initial) stress rate was equal to the minimum stress rate that would avoid failure at any time in the life of the capsule. Capsules with maximum power per unit of weight or volume were chosen by a graphical and parametric analysis of the acceptable capsules. This method was also used to select a reference capsule for the phase II $^{238}PuO_2$ heat-source system.

Concurrent with the phase II design study, an improved method was developed for analysis of creep life and optimization of fuel capsules. In this method, creep life is calculated by solving an integral equation that can, theoretically, accommodate a precise description of stress and temperature as a function of time. This analytical formulation of the creep problem permits an analytical capsule optimization procedure in which Lagrange multipliers are used. A phenomenological creep-life function generated by fitting both ultimate strength and creep data is used that is applicable over a wider domain and is more amenable to extrapolation than the previous polynomial fit of creep data.

The following sections cover the development of the new creep model, elements of a computer program (CAPSUL) for calculating optimum capsule dimensions, an analysis of creep data that pertain to the phase II design, and a reanalysis of the optimum design and predicted lifetimes of $^{238}PuO_2$ capsules. A report by Nichols and Winkler[11] gives a more complete substantiation of the new method of creep analysis and details of the computer program.

3.4.1. Mathematical Model

A phenomenological model of creep was developed with the use of a common theory,[12] for which it is assumed that the fractional creep life for a given stress and temperature is independent of other fractions of life under different conditions and that these fractions may be accumulated linearly. Stated mathematically,

$$1 = \int_0^{\Theta} \frac{dt}{\theta[\sigma(t),\ T(t)]}\ , \tag{1}$$

where

$\theta[\sigma,T]$ = life to a prescribed strain or rupture for given stress, σ, and temperature, T,

t = time since application of load,

σ = resultant life to prescribed strain or rupture for time-varying stress and temperature.

Equation (1) requires knowledge of the creep life as a function of stress and temperature. Larson and Miller[13] have shown that for a variety of metals the creep life at a given stress is related to the absolute temperature by an equation that may be derived from the Arrhenius rate law:

$$T \log K\theta = \text{constant} ,$$

where the constant is the Larson-Miller parameter.

As the temperature increases and therefore the stress for a given finite life decreases, the creep strain becomes a progressively larger fraction of the total strain, and the fractional strain from elastic and "instantaneous" plastic flow becomes progressively more negligible. At high temperatures the logarithm of the applied stress for many materials[13,14] is a linear function of the Larson-Miller parameter. It was assumed that the creep component of stress, σ_c, has this form for all temperatures; that is,

$$\log \frac{\sigma_c}{\alpha} = -mT \log K\theta . \tag{2}$$

At temperatures below about one-third the absolute melting temperature, the applied stress generally becomes more nearly constant in the Larson-Miller parameter because of the increasing importance of elastic and instantaneous plastic strain. This behavior, as well as the behavior at high temperatures, is accommodated by a resultant stress function of the following form:

$$\frac{1}{\sigma^{\gamma}} = \frac{1}{\sigma_u^{\gamma}} \frac{1}{\sigma_c^{\gamma}} , \tag{3}$$

where

σ = resultant nominal uniaxial stress,

σ_u = ultimate strength at room temperature,

α, m, K, γ = constants to be determined by a least-squares fit of Eq. (3) by using a known value of σ_u and an experimentally determined set $\{\sigma, T, \theta\}$.

A general equation for creep life for time-dependent stress and temperature is obtained by substituting Eqs. (2) and (3) into Eq. (1) and making provisions for individual safety factors on ultimate strength, S_u, and creep strength, S_c:

$$1 = K \int_0^{\Theta} \left\{ \frac{S_c^{\gamma} \sigma_u^{\gamma} \sigma^{\gamma}(t)}{\alpha^{\gamma} [\sigma_u^{\gamma} - S_u^{\gamma} \sigma^{\gamma}(t)]} \right\}^{1/\gamma m \Gamma(t)} dt \, . \tag{4}$$

In principle, the integral in Eq. (4) can be evaluated numerically for any time behavior of stress and temperature. For radioisotope fuel capsules, the integral was chosen to neglect the effect of strain on the volume of the capsule and end effects, since the capsules will have a length-to-diameter ratio greater than 2. The stress is considered to be the maximum nominal tensile stress (the circumferential stress at the inner wall of the capsule):

$$\sigma(t) = \frac{P(t)}{E} \left(\frac{r_4^2 + \mu r_3^2}{r_4^2 - r_3^2} \right), \tag{5}$$

where

P = pressure in the capsule,

E = weld efficiency,

r_4 = outer radius of primary container,

r_3 = inner radius of primary container,

μ = a multiplier equal to one for maximum tensile stress and zero for maximum shear stress.

The time-dependent pressure is calculated from the ideal gas law since the helium gas is well above the critical point. The volume of gas is the void volume at the center of the capsule plus any additional void in the fuel region. The moles of gas are those present initially plus those formed by decay of the radioisotope. Temperatures are calculated by assuming that the heat flux is in transient equilibrium with the power in capsules containing long-lived radioisotopes.

Equation (4) reduces to one previously derived by Kennedy[15] under conditions of high constant temperature and constant stress rate, $\dot{\sigma}$. Kennedy, and later McCoy,[16,17] verified that this equation is valid for several materials (including types 304 and 309 stainless steels, T-111 and T-222 alloys, and Cb-1% Zr alloy) by comparing creep-rupture lives obtained at high constant temperatures and constant stress with those obtained at the same temperature but constant stress rate. These data serve, indirectly, to validate the use of Eqs. (1) and (2).

The adequacy of the model can be tested for other materials and at lower temperatures by performing experiments in which stress and temperature are known functions of time and evaluating the integral in Eq. (4) either analytically or numerically.

3.4.2. Computer Program

CAPSUL is a Fortran program for the IBM 360/75 computer for calculating optimum dimensions of alpha-emitting radioisotope fuel capsules exposed to varying stress and temperature. The capsules (Fig. 3.6) are right cylinders with multilayered walls and elliptical end caps. Independent variables are RO, the inside radius of the capsule; X(2), the thickness of the fuel layer; and X(4), the thickness of the primary container wall.

The program has five main routines. LSTSQ determines constants in an equation for rupture life (or life to a prescribed strain) as a function of stress and temperature by a least-squares fit of creep and ultimate strength data. Once the constants are determined, LSTSQ is normally bypassed for calculations with the same material and design life criteria. The routine MAX uses a numerical Lagrange multiplier formulation to find a maximum of one of three thermal power functions (thermal power per unit projected area of a flat array of capsules, per unit volume of a rectangular parallelepiped that encloses a capsule and its auxiliary structural material, or per unit weight of capsule) subject to a time-integrated stress-temperature constraint that is dictated by a prescribed rupture or strain life. A subroutine, RZERO, calculates the allowable inside radius as a function of thermal power if it is

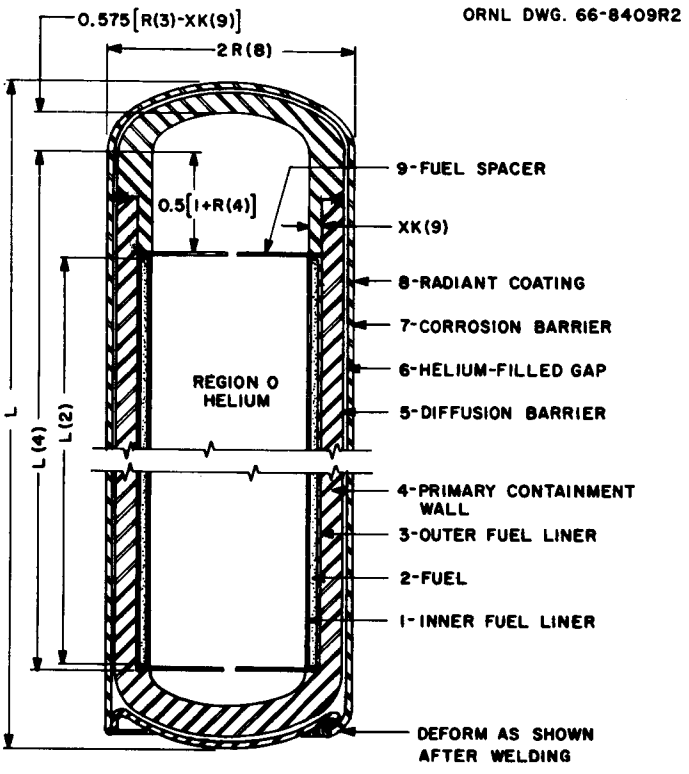

Fig. 3.6. Fuel Capsule Reference Design for CAPSUL Program Calculations.

required that the capsule surface temperature not exceed a given value if the capsule is buried in an infinite medium of earth. The routine LIMIT examines the dimensions of the optimized capsules for adherence to limits dictated by engineering considerations. If the wall thickness or radius of the capsule is too small or too large, the appropriate dimension is fixed at its nearest limit, and MAX or the routine DF is used to determine the maximum power function in the remaining variable(s). The routine DF calculates a single remaining variable to satisfy the stress-temperature constraint. The routine THETA calculates the rupture life or life to a prescribed strain of a capsule with specified dimensions and is used to determine the life of capsules that have been optimized on the basis of another criterion. The routine THETA also calculates safety factors for a fixed value of life.

3.4.3. Analysis of Creep Data for T-111 and T-222 Alloys

Creep data for the alloys T-111 and T-222 (Tables 3.4 through 3.7) were fitted by least squares with the new CAPSUL program. Best fits of the pertinent creep data for these alloys are shown in Figs. 3.7 and 3.8. The master Larson-Miller functions for 1% strain in T-111 and T-222 alloys recrystallized for 1 hr at 3000°F have greater slope and smaller Larson-Miller constants than the function for 1% strain in T-111 alloy stress

Table 3.4. Creep Data[a] and Fitted Constants for Alloy T-111 (Ta–8% W–2% Hf)

Temperature (°R)	Stress (psi)	Time to Creep Criterion (hr) and Values of Fitted Constants	
		1% Strain	Rupture
2660	35,000	0.54	8.6
	30,000	0.98	23.7
	25,000	2.4	65.6
	22,500	3.2	101.5
	20,000	8.4	485.0
	17,500	9.8	975.1
	15,000	16.0	1737.3
3060	18,000		5.45
	15,000	0.35	19.2
	12,500	2.0	25.1
	12,500	2.7	27.2
	10,000	17.2	168.5
	7,500	30.5	
3460	13,900	0.024	0.62
	10,000	0.25	2.90
	7,000	1.52	22.6
	4,500	1.0	177.0
	3,500	10.6	493.2
Fitted constants			
σ_u		145,000	150,000
α		8,091,800	8,449,500
K		1.3379×10^{13}	6.6296×10^{12}
m		0.000067844	0.000062914
γ		1.0	1.0

[a]Material stress relieved for 1 hr at 2000°F (Ref. 18).

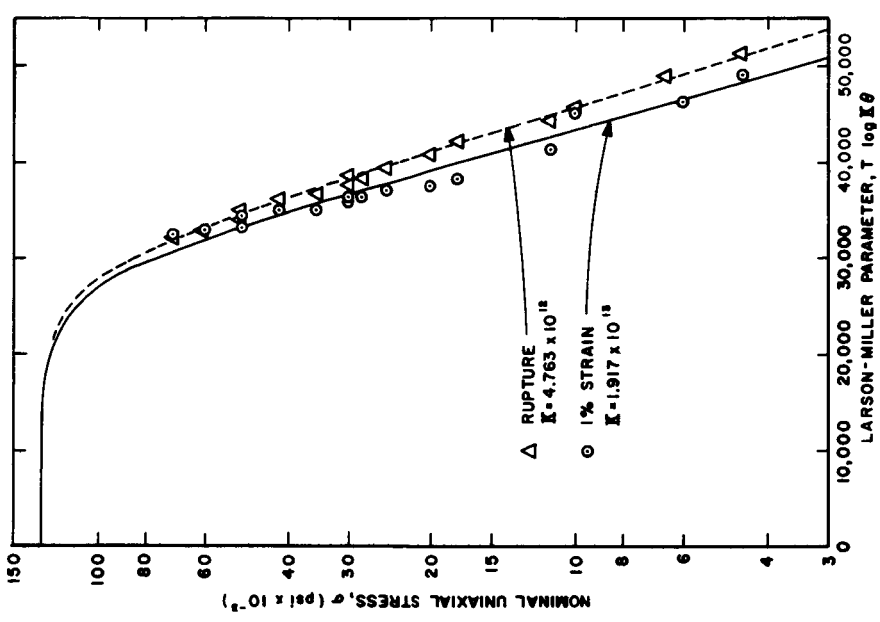

Fig. 3.8. Master Larson-Miller Plot for 1% Creep and Rupture in T-222 Alloy. Heat annealed 2 hr at 2400°F and tested at $2260 \leq T \leq 3460$, $\theta \leq 1443$ hr.

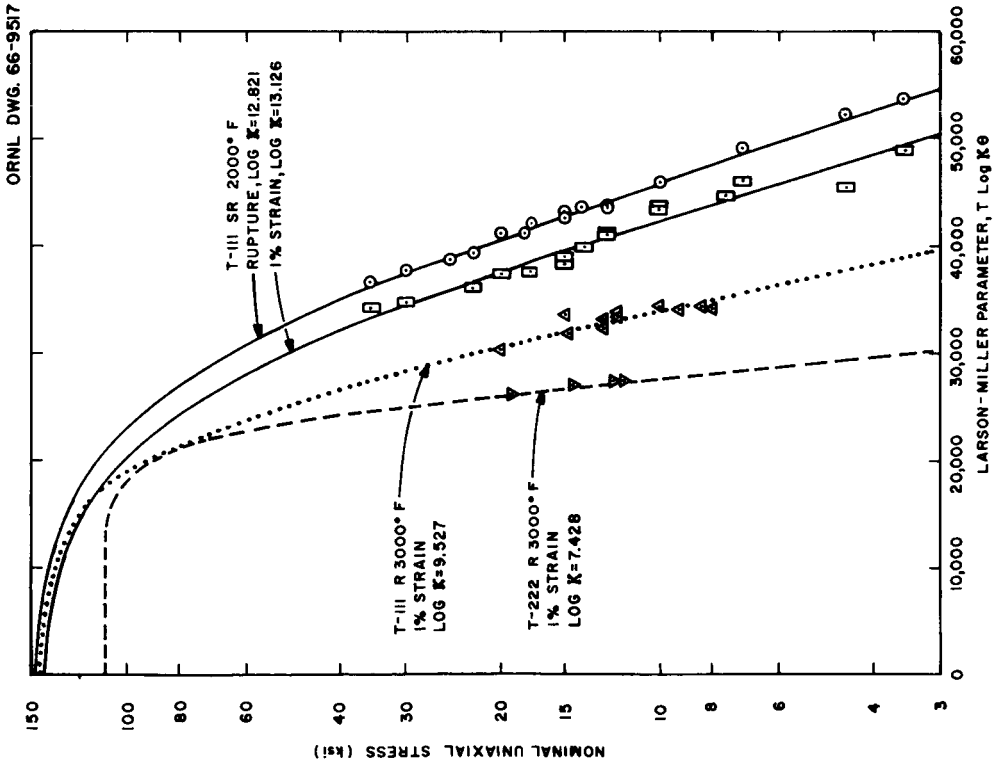

Fig. 3.7. Master Larson-Miller Plots for T-111 and T-222 Alloy Obtained by Least-Squares Fit of Creep Data. Heat treatment consisted of stress relief for 1 hr at 2000°F or recrystallization for 1 hr at 3000°F.

Table 3.5. Creep Data[a] and Fitted Constants for Alloy T-222 (Ta–9.5% W–2.5% Hf)

Temperature (°R)	Stress (psi)	Time to Creep Criterion (hr) and Values of Fitted Constants	
		1% Strain	Rupture
2260	70,000	12.5	42.5
	60,000	21.8	83.05
	50,000	93.0	561.4
2460	50,000	1.7	17.7
	42,000	9.2	102.4
	35,000	9.5	187.6
	30,000	29.0	1052.5
	28,000	30.0	780.5
2660	30,000	1.6	35.05
	25,000	5.0	161.2
	20,000	7.5	541.2
	17,500	12.0	1443.0
3060	11,300	1.7	69.0
3460	10,000	0.62	3.9
	6,500	1.3	30.1
	4,500	8.0	142.7
Fitted constants			
σ_u		130,000	130,000
α		1.236×10^{7}	9.535×10^{6}
K		1.917×10^{13}	4.763×10^{12}
m		7.107×10^{-5}	6.503×10^{-5}
γ		2.0	2.0

[a]Material annealed 2 hr at 2400°F (Ref. 18).

relieved for 1 hr at 2000°F. This difference may be due to the difference in heat treatment, but it is more likely that the functions for recrystallized material are distorted because there are relatively few data points in a narrow stress range.

The effects of stress on the 1% strain life at constant temperatures of 2000 and 2200°F as predicted by the "best-fit" functions for T-111 alloy stress relieved at 2000°F, T-111 alloy recrystallized at 3000°F, and T-222 alloy recrystallized at 3000°F are shown on Fig. 3.9. Also

Table 3.6. Creep Data and Fitted Constants for Alloys T-111 and T-222

Temperature (°R)	Stress (psi)	Time to Creep Criterion (hr) and Values of Fitted Constants		
		T-111,[a] 1% Strain	T-222,[a] 1% Strain	T-222,[b] Rupture
2460	20,000	670		
2516	19,200		925	
2580	12,000	3300		
2660	12,000	1140	600	
	12,000		700	
	8,000	2000		
2860	40,000			2.15, 2.55
	35,000			12.3, 9.95
	32,500			15.6, 26.0
	15,000	180		
	14,740	42		
	14,500		109	
	12,680	119		
	10,000	300		
2960	12,700	26		
	11,570		57	
	9,190	93		
	8,300	117		
3460	20,000			0.26
	15,000			1.11
Fitted constants				
σ_u		145,000	110,000	110,000
α		2.059×10^7	1.0035×10^{10}	4.981×10^7
K		3.3642×10^9	2.6779×10^7	8.104×10^{18}
m		0.000096554	0.00021536	0.00005246
γ		1.0	1.0	1.0

[a] Materials recrystallized 1 hr at 3000°F (Refs. 19–21).

[b] T-222 reduced 90% and recrystallized 1 hr at 3000°F (Ref. 22).

Table 3.7. Yield and Ultimate-Strength Data for Alloys T-111 and T-222

Temperature (°R)	T-111[a]			T-222[b]	
	0.2% Yield Stress (psi)	Ultimate Stress (psi)	Time to Rupture (hr)	Ultimate Stress (psi)	Time to Rupture (hr)
460				115,000	~0.1
535	144,800	150,000	0.03		
860	121,600	124,000	0.013	90,000	~0.1
1260	111,600	114,800	0.012	85,000	~0.1
1660				85,000	~0.1
2060				85,000	~0.1
2460	67,500	92,100	0.027	75,000	0.1
2660	52,200	67,100	0.067		
2860	38,600	42,400	0.093	59,000	0.1
3160	21,000	25,000	0.25		
3260				27,500	0.1
3460	14,100	16,300	0.17		
3960	10,900	11,300	0.14		

[a]T-111 alloy cold rolled 90% and stress relieved 1 hr at 2000°F; strain rate 0.05 in./in./min (Ref. 17).

[b]T-222 alloy reduced 90% and recrystallized 1 hr at 3000°F (Refs. 22 and 23).

data points are shown that were measured for these materials at 2200°F. The predicted properties of the recrystallized materials appear to have longer life to 1% creep at high stress values and shorter life to 1% creep at low stress values than the stress-relieved T-111 alloy. The general effect of lower 1% strain life for the recrystallized materials at low stress values is not unexpected, since recrystallization is known to cause greater ductility and lower yield strength but significantly greater strain at rupture. Most of the effect shown, however, is believed to be due to distortion induced by few data points in a narrow range.

It is observed that the function obtained for the stress-relieved T-111 alloy, although based on short-term data, provides a fairly good fit of the longer term data at 2200°F for the recrystallized materials.

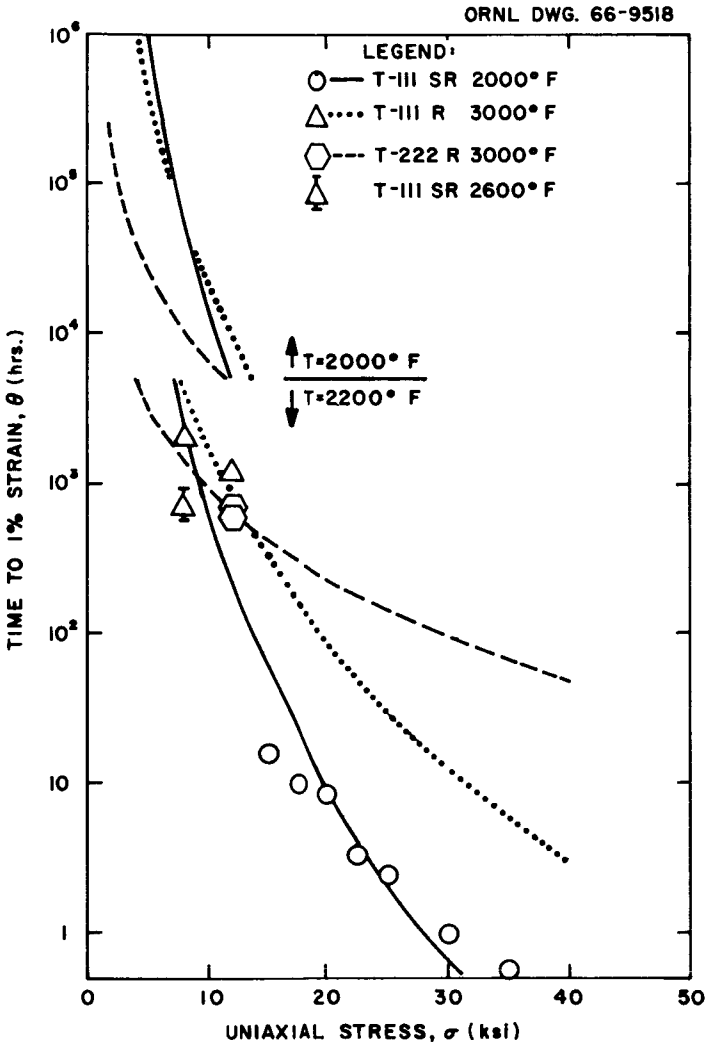

Fig. 3.9. Effects of Stress on Time to 1% Strain as Predicted by Least-Squares Fits of Creep Data. Experimental data at 2200°F are shown for comparison.

It is also observed that the recrystallized and stress-relieved T-111 functions predict the same stress (8300 psi) for a 5-year life to 1% strain at 2000°F.

The best fit of the 1% strain data for stress-relieved T-111 is shown again in Fig. 3.10, together with the 1% strain data for recrystallized T-111 and T-222 alloys plotted by using the same Larson-Miller constant. This plot tends to indicate that the recrystallized T-111 and T-222 alloys have about 40% greater creep strength than stress-relieved T-111 alloy.

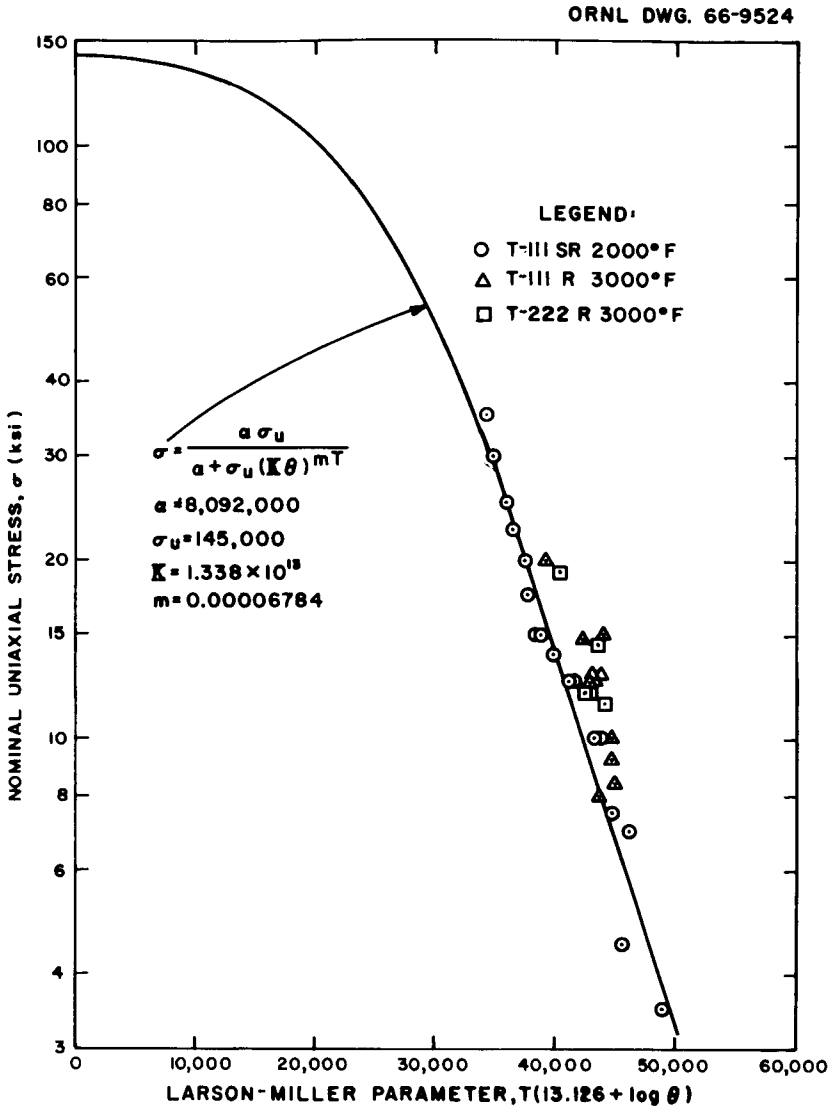

Fig. 3.10. Master Larson-Miller Plot for 1% Strain in T-111 Alloy Stress Relieved 1 hr at 2000°F. Creep data for T-111 and T-222 recrystallized 1 hr at 3000°F are plotted for the same Larson-Miller constant for comparison.

The best fit of the rupture data for stress-relieved T-111 is shown in Fig. 3.11, together with short-term creep data for T-222 (Table 3.6) and ultimate-strength data for T-111 and T-222 (Table 3.7); all data are plotted for the same Larson-Miller constant. The ultimate-strength data fit the predicted function surprisingly well, since ultimate-strength tests are made with a constant imposed strain rate rather than the

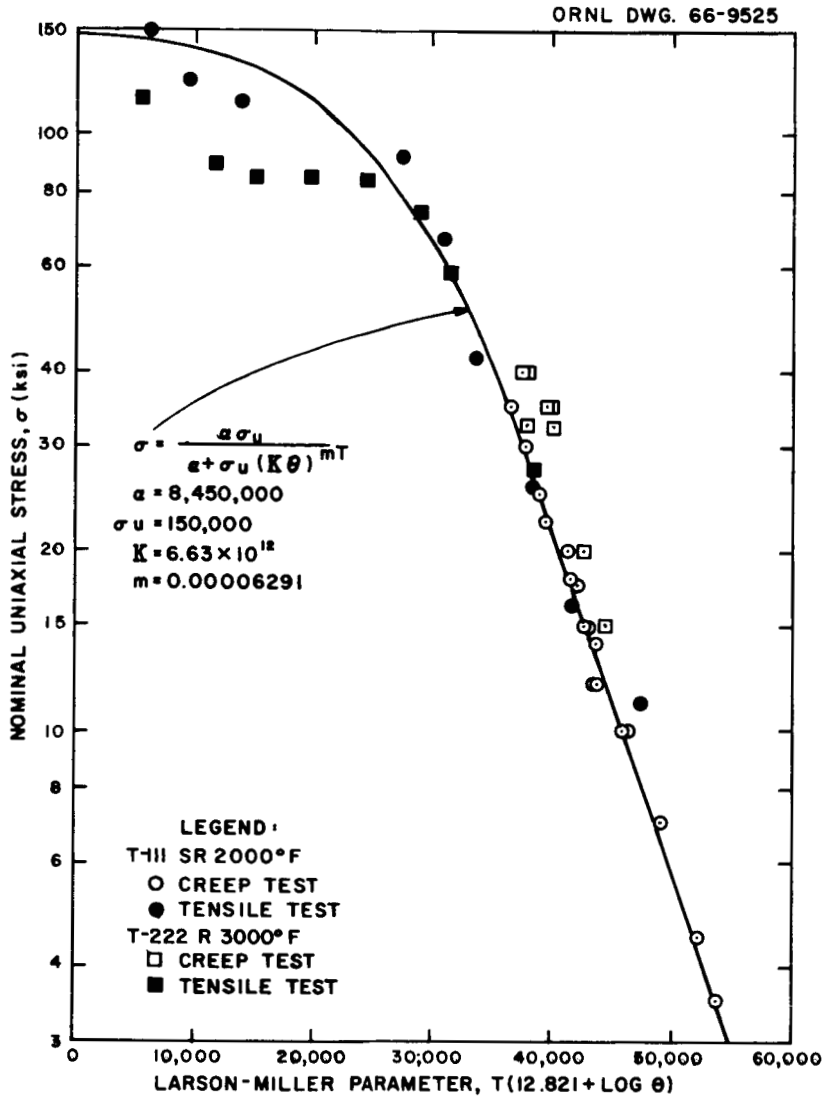

Fig. 3.11. Master Larson-Miller Plot for Rupture of T-111 Alloy Stress Relieved 1 hr at 2000°F. Tensile strength data for T-111 and T-222 and creep data for T-222 are plotted for the same Larson-Miller constant for comparison.

"natural" rate at constant stress. The more ductile recrystallized T-222 appears stronger in creep but has lower tensile strength.

Data corresponding to the mechanical strength properties of T-222 annealed at 2400°F (Table 3.5, Fig. 3.8) were used for reevaluation of the phase II design. This material appears, on the basis of this correlation, to be more creep resistant than the stress-relieved T-111 and comparable in 1% creep strength to the recrystallized T-111 on which the phase II design was based. Data for both 1% strain and rupture are available and,

since the data cover a sufficiently wide range of the variables, a good fit of the stress-temperature creep-life equation is expected.

A parametric comparison of the best-fit equation for 1% creep in T-222 annealed at 2400°F with the equation for 1% creep in stress-relieved T-111 and data for 1% creep in recrystallized T-111 and T-222 are shown in Fig. 3.12. Both equations, although they are derived from relatively short-time (<93 hr) data, provide a relatively good fit of the longer term data for the recrystallized materials. The annealed T-222 has appreciably greater 1% creep strength than the stress-relieved T-111.

A parametric plot of the best-fit creep-rupture equation obtained by combining the data for stress-relieved T-111 and T-222 annealed at

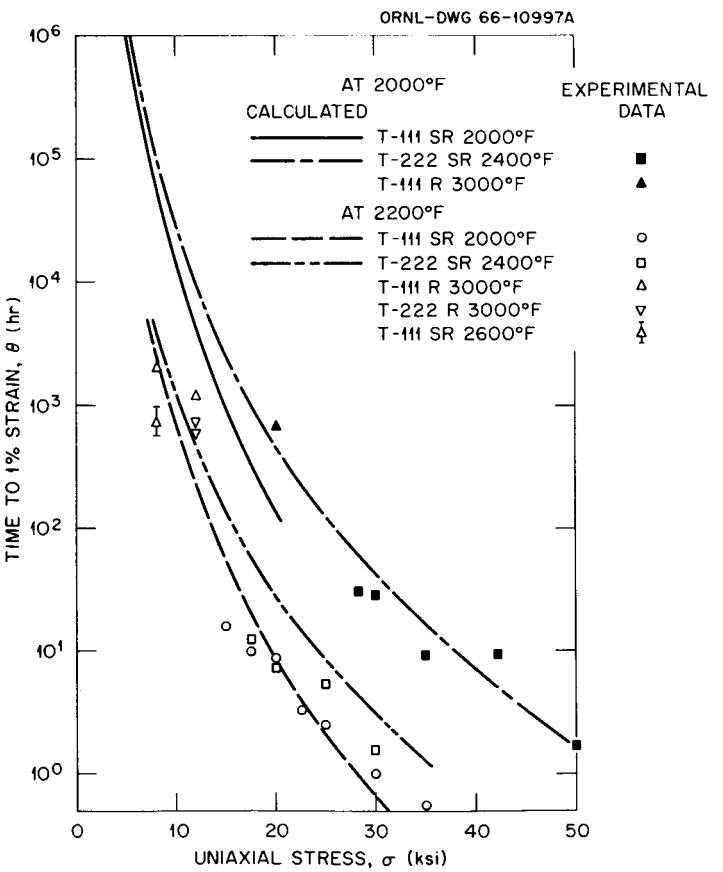

Fig. 3.12. Parametric Plots of the Derived 1% Creep Functions for the Alloys T-111 and T-222. Experimental data points shown for comparison.

2400°F is shown in Fig. 3.13. The data points for annealed T-222 generally fall above the curves; this indicates that it is more resistant to creep rupture than the stress-relieved T-111.

3.4.4. Analysis of the Predictability of Creep Data

The analysis in the previous section tends to indicate that the new model may be adequate for long-term extrapolation of the creep life for T-111 or T-222 when additional, more definitive creep data become available. Since there are relatively few data for these alloys at present, additional confirmation of the model was sought by analyzing the more abundant data for three commercial alloys (type 304 stainless steel, Hastelloy N, and Cb–1% Zr), which are believed to bracket T-111 and T-222

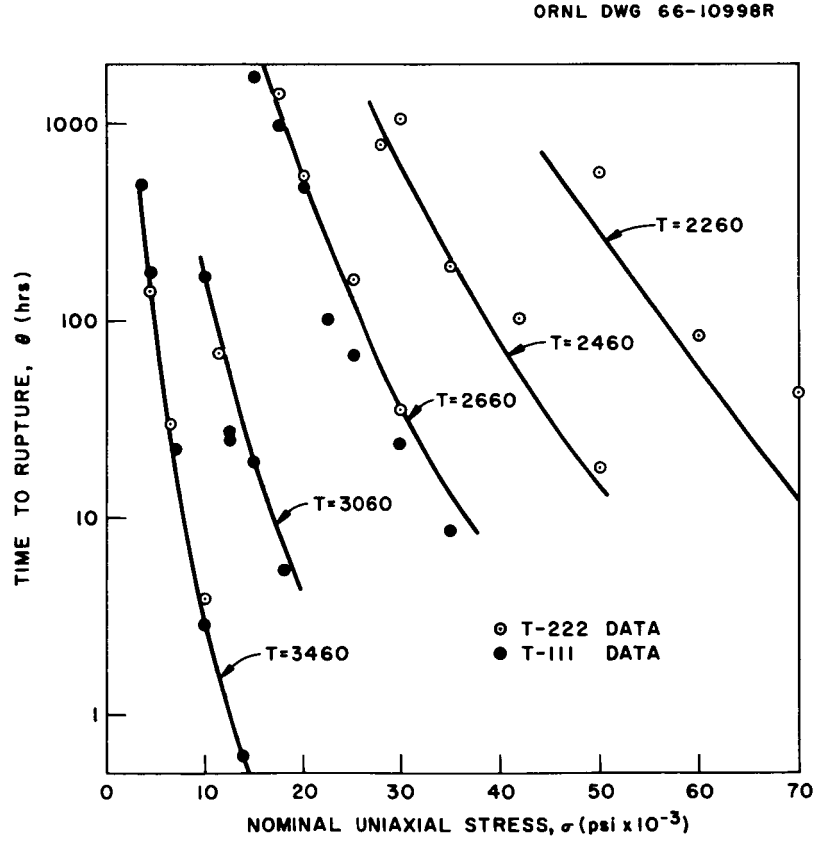

Fig. 3.13. A Parametric Plot of the Derived Creep Rupture Function for Combined T-111, T-222 Data.

in terms of long-term predictability. Best-fit equations (Figs. 3.14 through 3.16) for these commercial alloys were calculated with long-term data[24–28] from many heats of each alloy.

The accuracy of the model for extrapolation of creep life in the three commercial alloys was determined (Table 3.8) by making fits of constant stress and temperature creep data with a rupture life less than a selected time, using these fitted functions to predict the stress as a function of temperature to cause rupture at a greater time, and comparing the predicted stress with the actual average stress that caused failure at the greater time. The accuracy of the extrapolation, expressed in terms of the maximum relative error (or bias) in the predicted stress as a function of temperature, is then compared with the standard error (error at 67% confidence level, since the distribution of stress data is approximately Gaussian) in relative stress caused by the normal scatter of data about the predicted best-fit function. The model is then

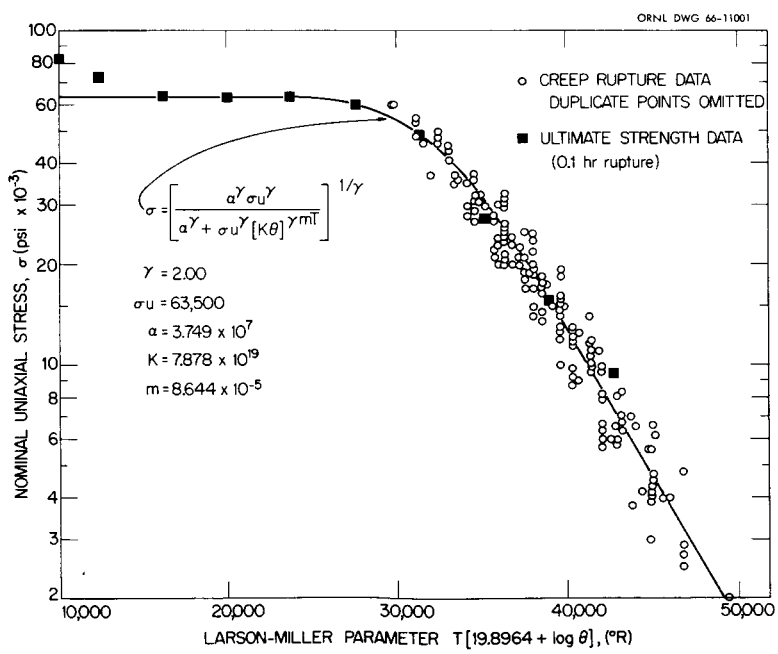

Fig. 3.14. Master Larson-Miller Plot for Creep Rupture in Type 304 Stainless Steel. Data from 18 heats, 189 data points, at $1360 \leq T \leq 2160$, $10 \leq \theta \leq 100{,}000$.

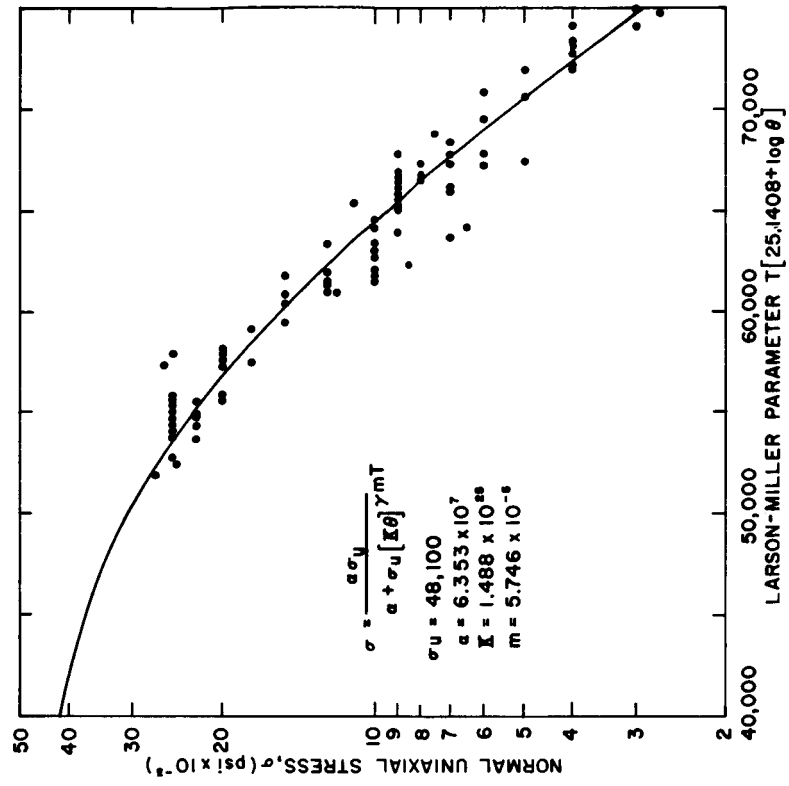

Fig. 3.16. Master Larson-Miller Plot for Creep Rupture in Cb-1% Zr. Data from 25 heats at $2060 \leq T \leq 2660$, $\theta \leq 1733$ hr.

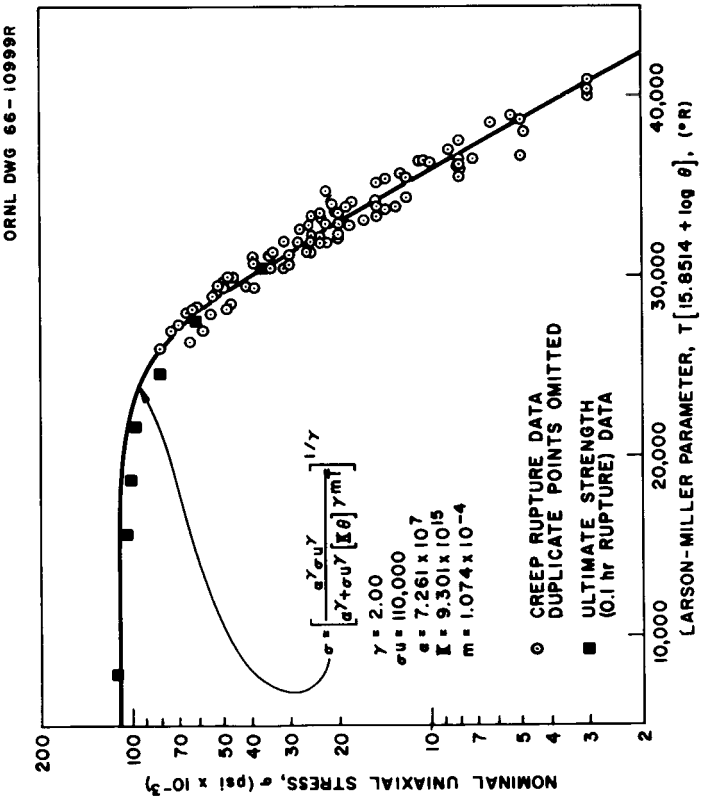

Fig. 3.15. Master Larson-Miller Plot for Creep Rupture in Hastelloy N. Data from 5 heats; 93 data points, at $1560 \leq T \leq 2260$. $\theta \leq 14{,}400$ hr.

Table 3.8. Statistics and Predictability of Creep-Rupture Data for Several Alloys

Material, Number of Heats, and Temperature Domain (°F)	Number of Data Points	Maximum Lifetime in Data (hr)	Life To Be Predicted (hr)	Relative Standard Error in Stress	Maximum Absolute Relative Bias in Predicted Stress
Type 304 stainless steel, 18 heats, $900 \leq T \leq 1700$	15	10	100,000	0.03	-1.0
	63	100	100,000	0.13	-0.10
	123	1,000	100,000	0.14	-0.09
	173	10,000	100,000	0.16	-0.05
	189	100,000	100,000	0.17	0.0
Hastelloy N, 5 heats, $1100 \leq T \leq 1800$	26	100	10,000	0.16	0.2
	40	200	10,000	0.16	0.08
	55	500	10,000	0.17	-0.04
	69	1,000	10,000	0.16	-0.02
	81	2,000	10,000	0.16	0.008
	93	15,000	10,000	0.16	0.0
Cb-1% Zr, 25 heats, $1600 \leq T \leq 2200$	49	80	1,500	0.09	0.25
	66	150	1,500	0.10	0.07
	83	300	1,500	0.12	-0.04
	92	750	1,500	0.13	0.05
	104	1,800	1,500	0.14	0.0
T-222 alloy, 1 heat, $1800 \leq T \leq 3000$	16	1,440	500,000	0.051	
T-222 + T-111 alloy, 2 heats, $1800 \leq T \leq 3000$	33	1,740	500,000	0.072	

known to provide for adequate extrapolation of creep within the time range such that the bias in the predicted stress is small compared with the standard error.

In Table 3.8 the first column gives the material, number of heats, and temperature range of the creep data that were analyzed. The next two columns give the values of the selected times and the corresponding number of data points (with rupture life less than the selected time) for which best-fit functions were evaluated. The fourth column presents the values of rupture life for which stress as a function of temperature was predicted by the model. The fifth column cites the standard error in relative stress for each of the best-fit functions. The last column gives the maximum bias in the predicted stress defined as the ratio of the maximum difference between the predicted and mean measured stress to the mean measured stress within the temperature range of the experiments. The last two rows of Table 3.8 compare the relative standard error in the stress for the functions that were fitted to T-111 and T-222 data. The relative

standard error in stress is lower for these alloys than for the commercial alloys because the number of heats and data points is small.

Two very striking, but tenuous, conclusions may be based on the data given in Table 3.8:

1. It appears that for a large number of metals, probably including many of the refractory alloys, the present creep model can provide a fit of creep data such that the standard error in stress will not exceed 15 to 17%. Knowledge of the statistics of the fit will permit the choice of a design stress for a predetermined confidence level (e.g., a stress safety factor of 2 would provide a probability of failure of about 0.001).

2. In each of the commercial alloys analyzed, the bias in predicted stress for a long-time extrapolation becomes small by using only 100- to 200-hr creep data. For these alloys the creep data for periods of time greater than 100 to 200 hr is superfluous. The data seem to suggest that if creep data are available that span two to three decades in time (1 to 200 hr, for example), a fitted function can be determined that will permit extremely long extrapolations in time, with the error of the extrapolation being less than the normal scatter in moderate-time creep-rupture data. For this conclusion it is assumed, of course, that the long-term environment is the same as the test environment.

3.4.5. Design and Analysis of $^{238}PuO_2$ Capsules by the New Method

The CAPSUL program was used to generate dimensions for $^{238}PuO_2$ capsules having maximum power per unit volume of a rectangular parallelepiped that encloses a capsule and the auxiliary spacing and uses structural materials that are dictated by the phase II reentry body design. These calculations were made for a stress safety factor of 1.0, since sufficient data are not available to select a statistically significant safety factor and the actual structural material may be stronger than the annealed T-222 used for reference.

In Table 3.9 optimum designs for various burial temperature and creep criteria are compared with the present phase II capsule design (designed by the method developed in phase I studies on the basis of 1% creep in 5 years and an initial surface temperature of 2000°F). The new optimum designs for both 1% creep in 5 years and rupture after ten half-lives of

Table 3.9. Phase II Capsule Compared with Capsules[a] Having Maximum Power-to-Volume Ratio for Various Burial Temperatures and Creep Criteria

	Phase II Capsule Design	Optimum Designs[b]							
Initial burial temperature,[c] °F	2000[d]	1800	1800	2000	2000	2200	2200	2500	2500
Strain criterion	1%	1%	Rupture	1%	Rupture	1%	Rupture	1%	Rupture
Life to strain criterion, years	5	5	890	5	890	5	890	5	890
Dimensions, in.									
Void volume diameter	0.562	0.0522	0.3904	0.225	0.589	0.561	0.965	1.076	1.960
Fuel thickness	0.241	0.406	0.278	0.355	0.245	0.272	0.194	0.199	0.121
T-111 wall	0.175	0.0564	0.115	0.109	0.160	0.151	0.183	0.253	0.203
Outside diameter	1.542	1.125	1.325	1.300	1.548	1.553	1.866	2.128	2.755
Length	5.968	4.500	5.299	5.202	6.191	6.214	7.464	8.511	11.020
Specific power									
Per area,[e] Btu/hr·in.^{2}	51.0	64.2	55.9	63.4	54.5	60.0	51.0	51.7	40.8
Per volume,[f] Btu/hr·in.^{3}	30.6	51.4	38.6	44.5	32.6	35.8	25.6	23.0	14.2
Per weight, Btu/hr·lb	119.8	231.1	159.7	181.1	132.0	145.4	111.1	92.7	80.0
Totals for 24.5 kw (thermal)									
Number of capsules	156	215	183	167	140	127	105	81	63
Weight, lb	698	362	523	462	633	575	752	901	1045
Volume,[f] in.^{3}	2730	1630	2170	1880	2560	2340	3260	3640	5900

[a]For all capsules: X(1) = X(3) = 0.020 in. tungsten, X(5) = 0.010 in. ThO_2, X(6) = 0.002 in. helium, X(7) = 0.020 in. platinum, X(8) = 0.002 in. iron titanate, X(9) = 0.020 in. tungsten, XK(9) = 0.040 in. T-111. Refer to Fig. 3.6 for nomenclature definition.

[b]Optimized to provide minimum volume and to meet only the strain criterion shown. Designs (other than phase II) based on 1% strain do not necessarily avoid rupture in ten half-lives.

[c]It is assumed that capsule becomes immersed in an infinite medium of conductivity 0.2 Btu/hr·(ft/°F).

[d]Medium conductivity of 0.176 Btu/hr·(ft/°F) assumed for this case.

[e]Projected area per capsule = $4R_8(L/D)(R_8 + 0.1094)$; R_8 = outside radius; L/D = outside length/diameter.

[f]Circumscribed volume per capsule = $8R_8(L/D)(R_8 + 0.1094)(R_8 + 0.0625)$.

the ^{238}Pu with an initial surface temperature of 2000°F result in 24.5-kw(th) systems that have less weight and volume than the present phase II system. The optimum designs for higher temperatures (Table 3.9, Fig. 3.17) indicate that the volume and weight of a 24.5-kw(th) system with initial operating and/or burial temperature as high as 2400°F are not high enough to be completely impractical.

The CAPSUL program has been used to predict the creep life (Table 3.10) of the present phase II capsule under various hypothetical or abnormal temperature histories that might arise from a change in the normal

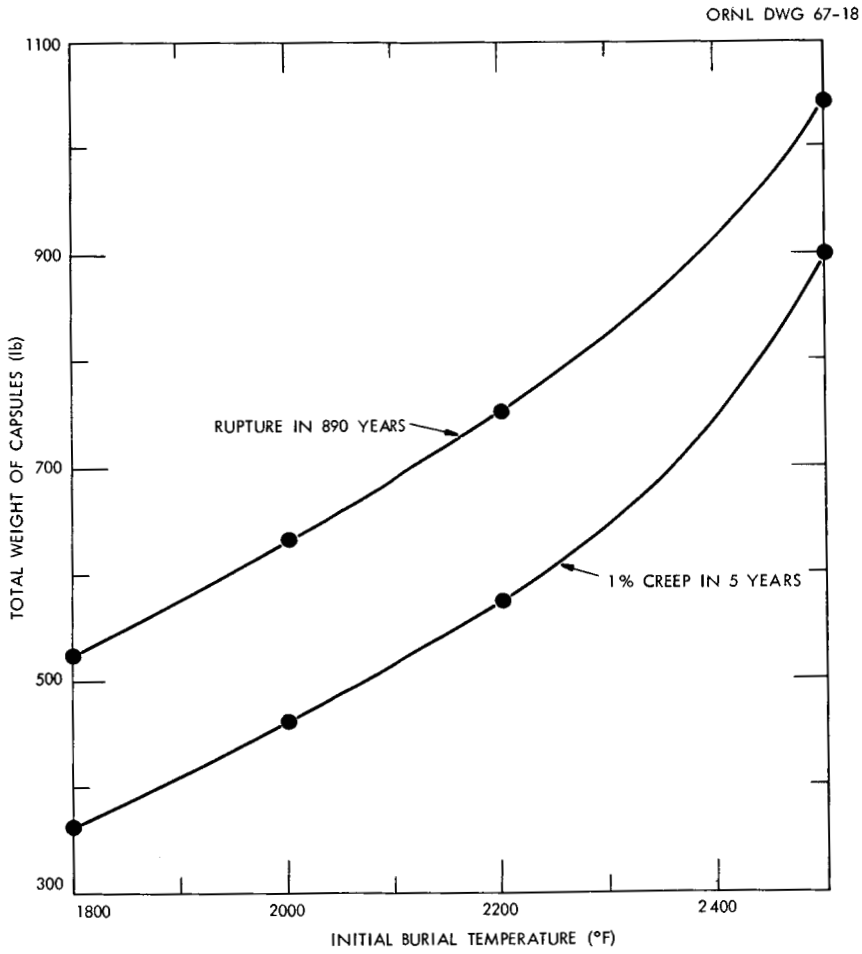

Fig. 3.17. Weight of Capsules for a Minimum Volume of 24.5-kw(th) $^{238}PuO_2$ Power Source as a Function of Initial Burial Temperature and Creep Criterion.

Table 3.10. Predicted Life to 1% Creep and Rupture for Phase II ^{238}Pu Capsules Under Various Conditions

Creep Criterion	Normal Operating Conditions		Initial Burial Temperature (°F)	Time to Creep Criterion (years)	Stress Safety Factor
	Initial Surface Temperature (°F)	Time (years)			
1% creep	2000	1.25	2000	13.7	1.0
	2200	1.25	2000	13.7	1.0
	2400	1.25	2000	13.7	1.0
	2600	1.25	2000	13.5	1.0
Rupture	2000	1.25	2000	890	1.11
	2200	1.25	2000	890	1.11
	2400	1.25	2000	890	1.11
	2600	1.25	2000	890	1.11
Rupture	2000	1.25	2500	7.2	1.0
	2000	1.25	3000	1.46	1.0
Rupture	2000	0.25	3000	1.31	1.0
	2000	0.25	3200	0.83	1.0

operating temperature, burial in a medium of exceedingly low thermal conductivity, or exposure to an insulating environment in the event of a launch-pad fire. The predicted life of the capsule to 1% strain is 13.7 years if the surface temperature during the initial 1.25-year operating period is in the range 2000 to 2600°F and the initial temperature after earth burial is 2000°F. The creep life is relatively insensitive to the temperature during the 1.25-year operating period because of the initially low helium pressure.

It is predicted that the phase II capsule has a rupture life equal to ten half-lives of the ^{238}Pu with a stress safety factor of 1.1 and undergoes a total creep of less than 5% if the surface temperature is in the range 2000 to 2600°F during the 1.25-year operating period and the initial burial temperature after operation is 2000°F. The calculation predicts that an average capsule would not rupture in an infinite time under these conditions. Considering the variation in the presently available T-111 data, the safety factor of 1.1 on 890-year rupture shown in Table 3.10

for the phase II capsule design is equivalent to a 95% reliability. While this reliability would not be considered adequate for a final design, it is thought to be adequate for a preliminary design study since the calculation method used does not take credit for the volume increase as the capsule creeps, and it is assumed that the driving force for creep is the maximum tensile stress rather than the biaxial shear stress. It is expected that longer term T-111 creep-strength data and biaxial stress data will be available to refine the capsule wall thickness requirements at the time of a final design.

If a capsule were buried in a medium with a temperature-averaged thermal conductivity of 0.13 Btu/hr·(ft/°F) after an initial operating period of 2000°F, the surface temperature would increase to 2500°F. Under these conditions, the capsule is predicted to have a total life of 7.2 years. If the medium has conductivity of 0.104 Btu/hr·(ft/°F), the initial burial temperature, total life, and life after burial are 3000°F, 1.46 years, and 0.21 year, respectively.

If it is assumed that 0.25 year after encapsulation the capsule becomes involved in a launch-pad fire such that its surface temperature is increased to 3200°F, it is predicted that the life of the capsule is 0.83 year, which is 0.58 year after immersion in the fire. This life is very long compared with the practical duration of a fire.

4. SHIELDING

Shielding and radiation calculations for the phase II $^{238}PuO_2$ heat-source system were made on the basis of dose criteria that limit the time- and volume-averaged dose rate in the three modules of a multipurpose mission module array to 5 rads per year from neutrons and 20 rads per year from gammas for the specified mission. (It was assumed that an individual astronaut would be exposed to this environment for no more than 3 months.) These criteria require a 4-in.-thick shield of LiH (weight, ~600 lb) on the inside faces of the power source. No supplementary shield is required for gamma attenuation in addition to that in the heat-source system and the walls of the modules. Sections 4.1 through 4.3 present the assumed sources of radiation, the geometrical configuration, methods of calculation, and a summary of the results.

4.1 Radiation Sources

The sources of penetrating radiation in the $^{238}PuO_2$ heat-source system include primary gamma rays from decay of the isotope and impurities, alpha-gamma interactions within the fuel, and spontaneous fission of the ^{238}Pu; secondary gamma rays from neutron capture and inelastic scattering; and neutrons from spontaneous fission, alpha-neutron reactions, and neutron-induced fission. In determining the yield of these radiations, it is assumed that the $^{238}PuO_2$ has the properties described by Stoddard and Albenesius.[29]

The yield and energy distributions of primary gamma rays from the $^{238}PuO_2$ (Table 4.1) are assumed to be those reported in phase I studies[1] for a plutonium product containing 1.2 ppm ^{236}Pu aged 1 year since separation from products of the decay chain. The dose contribution from sources of secondary gammas was determined with a multigroup transport-theory code to be negligible by comparison on the basis of calculations of the heat-source and shield system.

The total neutron source was estimated to be 9200 ± 3000 neutrons/sec per gram of pure ^{238}Pu (2600 ± 300 from spontaneous fission, 5000 ± 2500 from alpha-neutron reactions, and ~1600 from neutron-induced fission).

Table 4.1. Assumed Yield and Energy Spectrum of Primary Gamma Rays from Plutonium Dioxide[a] One Year After Purification

Photon Energy (Mev)	Yield[b] (photons/sec)
0.3	5.53×10^{11}
0.6	8.29×10^{8}
0.76	2.06×10^{10}
1.0	1.91×10^{8}
1.5	3.04×10^{8}
2.62	5.25×10^{8}
3.5	1.68×10^{7}
4.5	5.62×10^{6}
5.5	1.43×10^{6}
6.5	3.58×10^{5}

[a]Plutonium content: 80.94% ^{238}Pu, 15.26% ^{239}Pu, 2.88% ^{240}Pu, 0.79% ^{241}Pu, 0.12% ^{242}Pu, 1.2 ppm ^{236}Pu.

[b]For a 25-kw(th) source.

Approximately 15% of these neutrons will be absorbed within the reentry body. The neutron source from spontaneous fission was based on a critical analysis of literature data. Most weight was given to data reported by Hyde[30] and by Druin, Perelygin, and Khlevnikov.[31]

The neutrons from alpha-neutron reactions in $^{238}PuO_2$ were estimated by using the data published by Arnold[32,33] on the yield from ^{232}U combined with various light elements and the effect of alpha-particle energy on the yield. The estimated yields for parts per million of possible significant elemental impurities in ^{238}Pu are listed in Table 4.2. By this method the yield of neutrons from alpha-neutron reactions in $^{238}PuO_2$ containing pure natural oxygen (2040 ppm ^{18}O, 370 ppm ^{17}O, and balance ^{16}O) is 25,000 neutrons/sec per gram of ^{238}Pu; this value agrees very well with measurements of $^{238}PuO_2$ reported by Stoddard and Albenesius.[29]

In estimating the total alpha-neutron yield for the phase II shield analysis (5000 ± 2500 neutrons/sec per gram of ^{238}Pu), it was assumed

Table 4.2. Estimated Yield of (α,n) Neutrons in ^{238}Pu per ppm (by Weight) of Significant Target Elements[a]

Element	Neutron Yield [sec^{-1} (g $^{238}Pu)^{-1}$ ppm^{-1}]	Element	Neutron Yield [sec^{-1} (g $^{238}Pu)^{-1}$ ppm^{-1}]
Be	300	Cl	0.69
B	88	C	0.54
F	28	O	0.21
Li	19	K	0.15
Si	5.0	P	0.050
Na	2.0	N	<0.034
Al	1.6	Sc	0.018
Ar	1.1	S	0.013
Mg	0.80	Ti	0.011

[a]Elements are assumed to have the naturally occurring distribution of isotopes.

that the oxygen was depleted by a factor of 10 in ^{18}O and a factor of 2 in ^{17}O. The neutron yield from alpha-neutron reactions with the depleted oxygen (180 ppm ^{18}O, 200 ppm ^{17}O, and balance ^{16}O) is estimated to be 2600 neutrons/sec per gram of ^{238}Pu.

The large uncertainty in the total alpha-neutron yield is caused by the present uncertainty with respect to the concentration of minor element impurities in finished $^{238}PuO_2$ microspheres. The significant impurities in microspheres produced by the ORNL sol-gel process are expected to be calcium, sodium, and fluorine. Small-scale laboratory studies[34] indicate that these elements can be maintained at concentrations (<100 ppm of carbon and sodium; <10 ppm fluorine) such that the neutron yield will be negligible compared with the yield from the depleted oxygen.

Calculations[35] were made with a 15-group transport code and cross sections from phase I studies[1] to determine the neutron-induced fission rate in the phase II $^{238}PuO_2$ capsule array. The calculations were made in only one dimension; true dimensions of the components of the reentry body (capsules, clips, and structural, heat sink, and ablative materials) were assumed in the direction perpendicular to the plane of the capsules, but the radius of the disk was assumed to be infinite because the radius

is very large compared with the mean free path of neutrons. The calculated neutron multiplication factor of the reentry body was 0.176. The number of neutrons formed in neutron-induced fission is 0.214 per source neutron or approximately 1600 neutrons/sec per gram of ^{238}Pu.

4.2. Shield Configuration and Methods of Calculation

Figure 1.3 (Sect. 1) shows the orientation of the $^{238}PuO_2$ power source (an array of capsules on a disk perpendicular to the plane of the figure) and its reentry body with respect to the command, engine, and laboratory modules of a multipurpose mission module array.[2] The coordinate system, with its center at the center of the command module, is the same as that used by North American Aviation[36] in analyzing the shielding characteristics of the Apollo command module.

The radiation dose calculations were made by volume averaging the dose rate in each of the three modules. Point kernels for neutrons and photons were numerically integrated with respect to the area of the disk source and the volume of a module. The point kernels for gamma rays, including the attenuation by the heat source system and the walls of the modules,[2,36] were calculated by using the SDC program.[37] The neutron attenuation kernels for LiH were those presented in the phase I report[1] for the Henderson rad dose response function.

When the reentry body is deployed for heat rejection in the absence of the LiH shield, the dose rate in the command module is approximately 7 times the normal dose rate. For the calculations it was assumed that the crew will spend a proportionately larger fraction of their time in the engine and laboratory modules when the reentry body is deployed.

The unshielded reentry body is not an intensely radioactive object but compares with isotope shipping casks that are shipped within ICC regulations. The dose rate on the disk center line at a distance of 1 meter is approximately 100 mrem/hr. It will be possible to load the capsules and perform maintenance work around the reentry body on the launch pad with tolerable radiation exposure rates.

4.3. Results

Results of the dose-rate calculations in the three modules with a 4-in.-thick shield of LiH in the direction of each of the three modules are given in Table 4.3. An alternate and slightly lighter shield having 5 in. of LiH only in the direction of the command and laboratory modules was discarded on the basis that the dose rate would then be too sensitive to the occupancy of the engine module. The volume-averaged dose rates (columns 2 and 3) have not been weighted by module occupancy and can be weighted for any specified occupancy model. The time- and volume-averaged dose rates (columns 4, 5, and 6) are calculated on the basis that the percentages of total man-hours spent in the command, engine, and laboratory modules are 40, 3, and 57%, respectively. The time- and volume-averaged dose rates are not sensitive to occupancy if the engine module occupancy is less than about 5%.

Table 4.3. Radiation Dose Rates from the 24.5-kw(th) $^{238}PuO_2$ Heat Source in the Three Modules of the Multipurpose Mission Module Array

Module	Occupancy (%)	Volume-Averaged Dose Rate and Dose-Rate Range in Modules (rad/year)				Time- and Volume-Averaged Dose Rate		
		Neutrons		Gammas		Neutrons (rad/year)	Gamma (rad/year)	Total (rem/year)
		Rate	Range	Rate	Range			
Command	40	5.2	3–11	12.1[a]	7–25	2.1	4.8	30
Engine	3	10.1	4–56	50.6	23–280	0.3	1.5	5
Laboratory	57	4.6	2–16	21.9	9–74	2.6	12.5	44
Total						5.0	18.8	79

[a]This would be 15.8 rad per year if "Z" coordinate of the source were positive.

Considering the possible variations in the source-strength and shield calculations, it is estimated that the neutron dose rate calculations are accurate within a factor of 2 at a high probability level. The calculated gamma dose rates may be high by as much as a factor of 4 and low by as much as a factor of 1.5.

5. SYSTEM DESIGN

This section describes the integration of the fuel capsules into a heat source and incorporation of the source into a Brayton-cycle system in a space vehicle. The safety criteria particularly involved are those relating to

1. coolant circuit redundancy,
2. emergency heat rejection,
3. abort ejection devices,
4. reentry heating and impact protection,
5. launch-pad fire protection.

The phase II preliminary design unit (detailed in Fig. 2.1) is generally oriented toward earth-orbital missions, but it is not specifically geared to a particular mission profile. Modifications to the design would be necessary to include planetary and lunar missions; however, these could be made without altering the basic design concept.

The multipurpose mission module[2] space station (shown in Fig. 5.1) was designated by NASA to be used for phase II integration studies. This module makes use of the same launch vehicle assembly (Saturn V) as the manned lunar-landing program, except that the lunar excursion module (LEM)

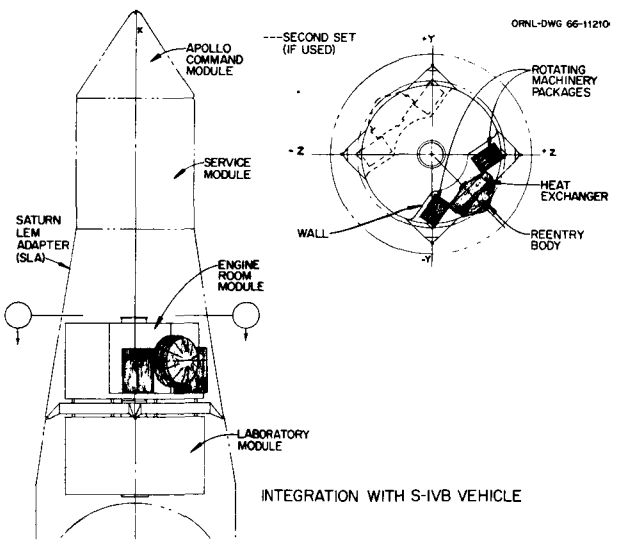

Fig. 5.1. Spacecraft for Phase II Integration Studies.

in the Saturn LEM adaptor (SLA) section between the S-IVB vehicle and the Apollo service module is replaced with two cylindrical housings (15 ft in diameter and approximately 9 ft in height). One of these is designated the engine-room module and the other the laboratory module. After orbit has been achieved, the SLA is opened, and the Appolo command module with its service module disengages, turns around, and docks with either one of the cylindrical modules (shown in Fig. 1.1).

5.1. Reentry Body

The reentry body is a separate unit (shown in Fig. 5.2) consisting of the protective shell and the fuel-plate assembly with intervening insulation. Only a minimum number of contact points functionally and structurally integrate this unit with the remainder of the associated equipment.

5.1.1. Fuel-Plate Assembly

The fuel-plate assembly is made up of two Cb–1% Zr disks. The upper disk is nominally 50 in. in diameter, and the lower disk is 46 in. in diameter. The disks are 0.156-in.-thick metal built up to 2 1/4 in. in thickness to form a light-weight strength member. The disks are separated by discontinuous radial ribs between a hub and a rim. Extending outward from the rim are temperature compensators that have 1/8-in.-thick yielding links to accommodate the 3/8-in. radial expansion that occurs when the temperature is raised from ambient to the operating level.

Orbital temperature excursions below the normal operating condition could separate the compensators from the insulation. The separation would be tolerable for short periods of time, since metal laminations in the insulation would retain their shape and the main mechanical attachment of the fuel-plate assembly to the shell is through the central bolt. Reestablishment of the normal mode of operation would result in recontact of the compensators and insulation. Rapid temperature excursions of the fuel capsules are prevented by the heat-storage capacity of pressed beryllium oxide, which is included in the fuel-plate assembly to provide a short thermal path that cannot be interrupted.

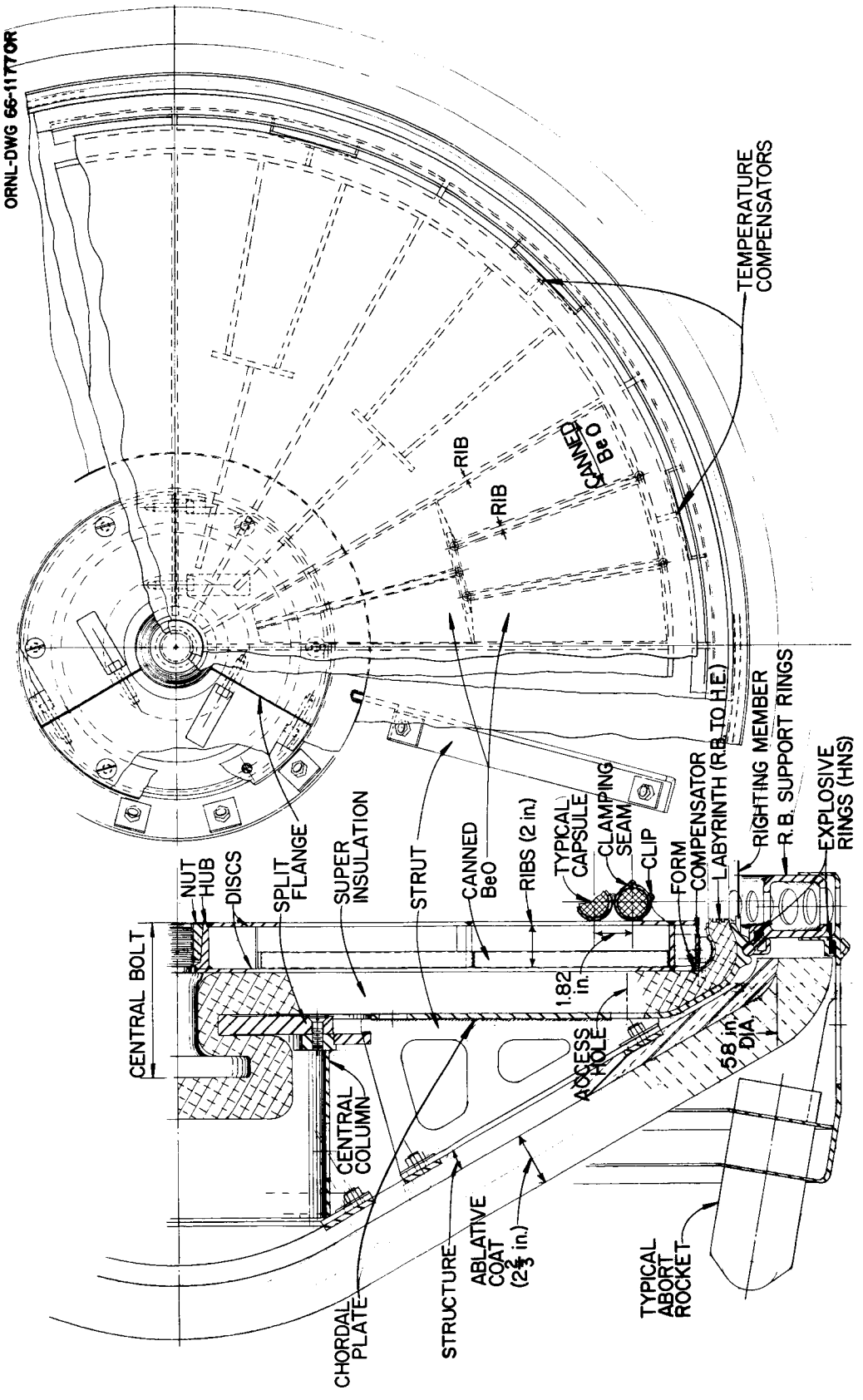

Fig. 5.2. Reentry Body Sections.

In order to attach the fuel capsules to the surface of the support plates, 1 11/16-in. nominal diameter Cb–1% Zr tubular holders are welded to 1/16-in.-thick strips of semicircular corrugated clips. These clips are fastened to the surface of the disk by plug welding in the corrugations. (Since the clips and tube wall are of equal thickness, unequal energy deposition is avoided during welding, and distortion of the holders is minimized.) This method of holding the capsules to the support plates provides a smooth bore into which the capsules can be easily inserted, and the tubes afford some protection from back-side heating during reentry. Loose-fitting fuel capsules in the tubular holders would simplify fuel loading, but the clearance would provide freedom for the capsules to vibrate independently during launch if some clamping method were not incorporated into the design. The clamping function is generated by deforming the longitudinal upset on the tubular holders by crimping. Flattening the upset reduces the tube diameter until the capsules are securely held. Long-term operation at elevated temperatures will relax the pressure on the capsules, so the platinum coatings will not be extruded. The arrangement of capsules and tubes on the 50-in. upper plate is shown in Fig. 5.3.

No fuel capsules are loaded into an 8-in.-diam central section of the tubular holders. This exclusion area corresponds to the outlet header of the heat exchangers, where ineffective heat transfer would raise capsule temperatures above the design value. Dummy capsules are included in the exclusion area, and the required 156 fuel capsules are distributed with approximate uniformity in the annular region.

Fuel-capsule insertion into the blind tubular holders is unidirectional from two adjacent quadrants when the removable part of the support ring is detached. The open ends are then capped to complete the fuel-plate assembly.

5.1.2. Reentry Protective Shell

The reentry protective shell is a 60° blunted cone with a 15-in.-radius spherical nose. The ablative protection has a uniform thickness of 2 2/3 in. and is cemented with a flexible bond to the 1-in.-thick

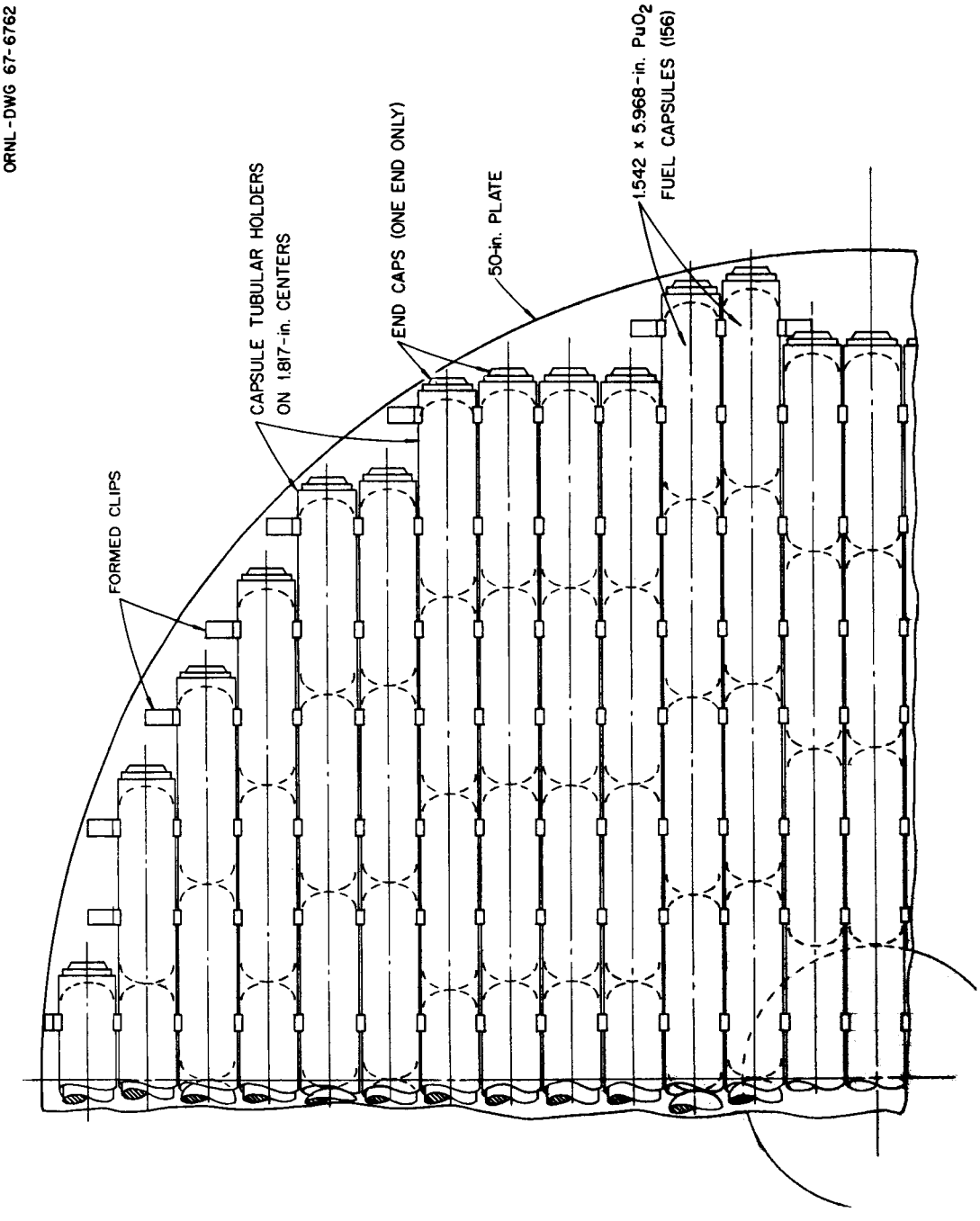

Fig. 5.3. Reentry Body Sections.

expanded or honeycombed aluminum structural member used to resist reentry forces.

Twelve 1/8-in. struts and a 1/8-in. formed chordal plate are attached to the honeycomb structure (Fig. 5.2). The formed plate controls the shape of the 2-in.-thick laminated Superinsulation and provides a bearing surface for the fuel plate through axial compression of the insulation. The chordal plate also has a peripheral torus with an external circumferential groove that mates with a tongue on the reentry body support ring to furnish the force to suspend the recovery package in place. The insulation is forced outward against the internal face of the torus by the temperature compensators on the fuel capsule support plates.

A central tubular column (1/8 in. in wall thickness, 16 in. in diameter, 8 in. in length) with a 1/2-in.-thick integral flange provides bracing for the struts from the honeycomb structure. The inner 1 in. of the 3-in. width of the integral flange mates with a split flange (3/4 in. in thickness and 4 in. in width) that is used to exert a radial load through the insulation on a 2-in.-diam bolt shank. The radial load centers the bolt in the reentry protective shell to complete this assembly.

5.1.3. Reentry Body Assembly

To join the fuel-plate assembly to the reentry protective shell, a tapered nut is threaded on the central bolt that extends through a mating hole in the support plate hub. The axial compression developed by the large bolt head and fuel-plate assembly on both faces of the insulation covering the split flange securely anchors the fuel-plate assembly to the reentry shell.

Joining the fuel-plate assembly to the shell without any penetrations in the Superinsulation adds complexity to the design, but it is necessary to prevent excessive thermal losses. The complexity arises because only compressive loads can be transmitted across the laminated insulation (shear loads would tear the laminations). The compressive stress increases heat losses through the insulation, but the 2-in. nominal thickness of alternate layers of reflective metal and separators is sufficient to keep the temperature of the reentry protective shell within tolerable limits.

5.2. Heat Exchangers

Except for the heat source, a redundant power system is required, and it is desirable that all aspects of the two conversion systems should be made as identical as possible. The duplication concept and the desire to have the disk heat exchanger oppose the heat source led to an involute tube design. The redundant heat exchangers are alternately nested together and all tubes have identical curvatures. The headers are arranged to give nearly equal tube lengths so that individual tube orificing is not needed to distribute the flow of gas in the tubes.

The involute geometry selection, with redundancy, was applied in two heat exchanger designs for two different working fluids. The designs, which can be substituted for each other, are for the specified helium-xenon mixture with a molecular weight of 83.8 and for pure argon. The overall assembly dimensions are the same; the number of tubes and the dimensions of the tubes and headers are different. (Figures 5.4 and 5.5 illustrate the differences in the two designs.) Since the two systems are operationally and physically interchangeable and both are constructed in the same manner, only the helium-xenon design is detailed in this discussion.

The involute tubes of the redundant heat exchangers are fed from 8-in.-diam headers. The tubes form a plane surface directly opposite and parallel to the disk-shaped heat source. The planes have a capsule center-line to tube center-line separation distance of 5 in. to enhance the radiant heat transfer of the capsules near the outlet headers. Since the headers are nested in a stacked arrangement, the tubes are not in a plane over a small length in the immediate vicinity of the outlet headers. The tubes double back from the periphery of the disk to the inlet headers in different but essentially parallel planes.

All headers are scrolled and have contoured flow splitters to distribute the gas flow. The tube and header junctions are also contoured to reduce inlet and exit pressure losses. [The inlet and exit pressure losses constitute about 30% of the design value ($\Delta P/P = 3\%$); the curved tube lengths contribute the remaining portion.]

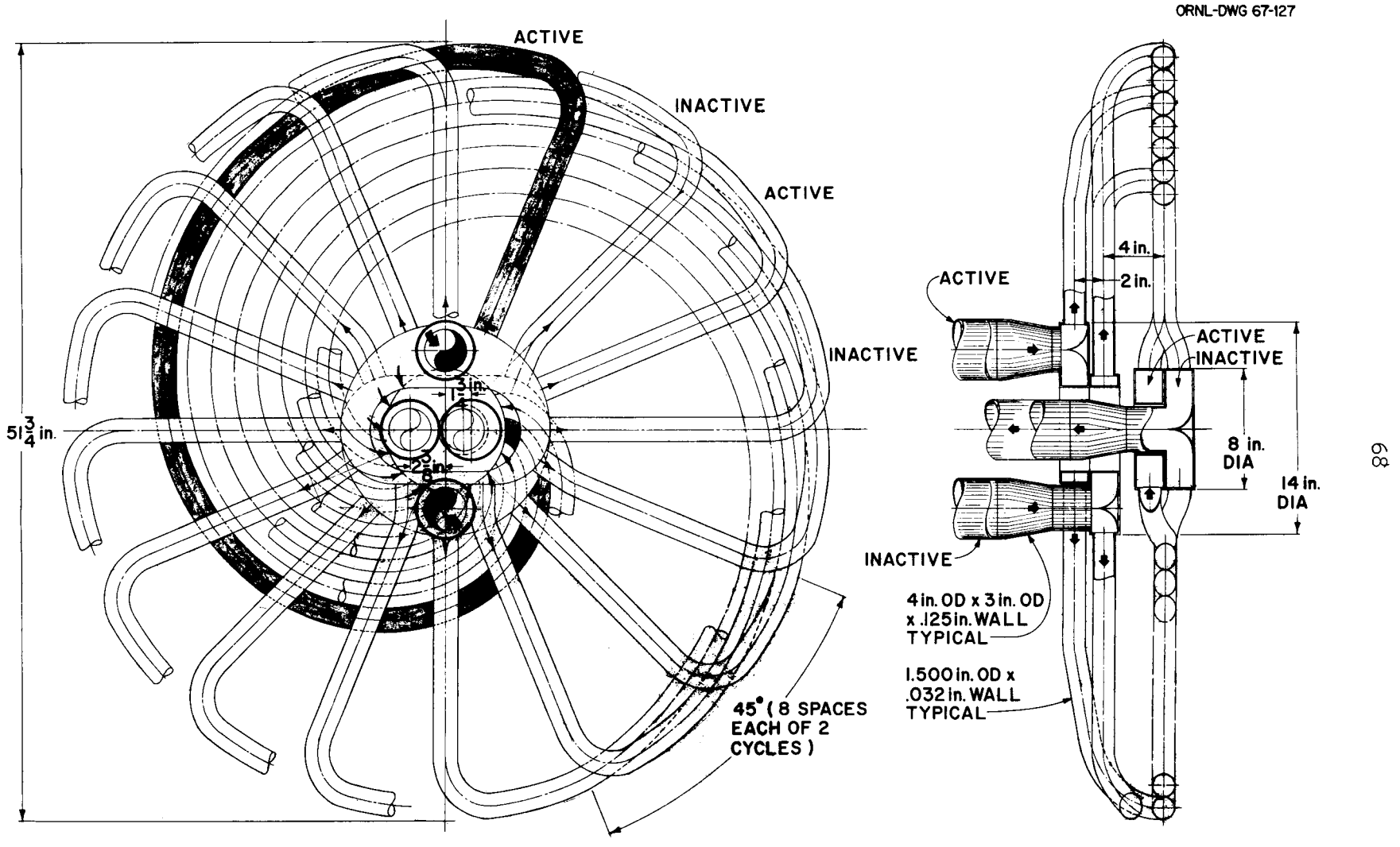

Fig. 5.4. Heat Exchanger Piping for Brayton Cycles Operating with Helium-Xenon Working Fluid.

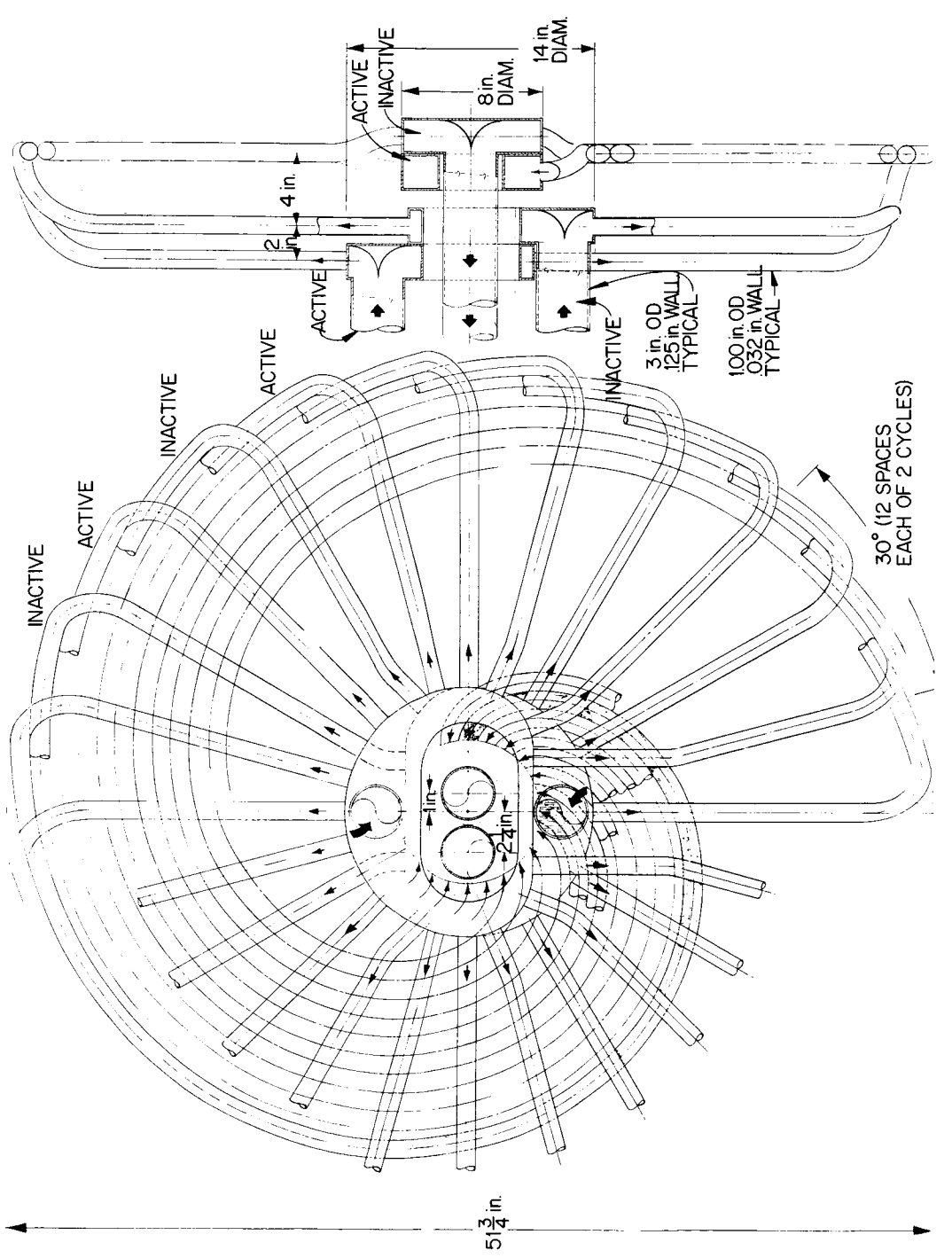

Fig. 5.5. Heat Exchanger Piping for Brayton Cycles Operating with Argon Working Fluid.

The heat exchangers are supported by a clamping force on the inlet and outlet coolant lines. The force is transmitted from the shielding container to the coolant pipes by radial compression of the Superinsulation (shown in Fig. 5.6). The container is also utilized on the cold surface; however, the hot surface has a 0.0375-in.-thick sheet metal disk and discontinuous 0.062-in.-thick ring segments to enclose the 1 in. of insulation. The ring segments are attached to U-shaped yielding links that project from the 1 1/2- by 1/2-in. radial support arms used to maintain the plane geometry. A circumferential 0.0188-in.-thick belt aids in assembly.

A prelaunch cooling section with a refrigerant as the coolant is included to remove heat from the source capsules while the launch vehicle is on the launch pad. To save space, this liquid heat exchanger is designed to nest in place above the main heat exchangers (see Fig. 5.7).

An inert-gas purge inlet has been incorporated for use on the launch pad to maintain a positive pressure inside the insulated volume formed by the heat exchangers and the reentry body. The two assemblies are not in contact, but the Superinsulation on each component forms a multiple tongue-and-groove labyrinth seal. This seal is the only uninsulated penetration into the insulated volume. The labyrinth is pervious to both the purge gas and heat. The gas can escape easily, but the heat rays would deposit their energy in the reentry-body support ring if many aligned holes were not included in the ring to keep it from intercepting the heat. The small energy deposition in the metal between adjacent holes is dissipated by conduction and reradiation to colder areas.

5.3. Shielding

A 4-in.-thick LiH nuclear radiation shield is closely associated with the heat exchanger assembly (shown in Fig. 5.6). The shield is contoured to encase the heat exchangers and fuel plate and provides approximately 2π solid-angle radiation protection. The LiH is contained in a 0.050-in.-thick stainless steel housing on the cylindrical and conical sections to transmit the shield and heat exchanger weight loads, and the cylinder (55 in. in inside diameter, 13 in. long) is attached to the main support

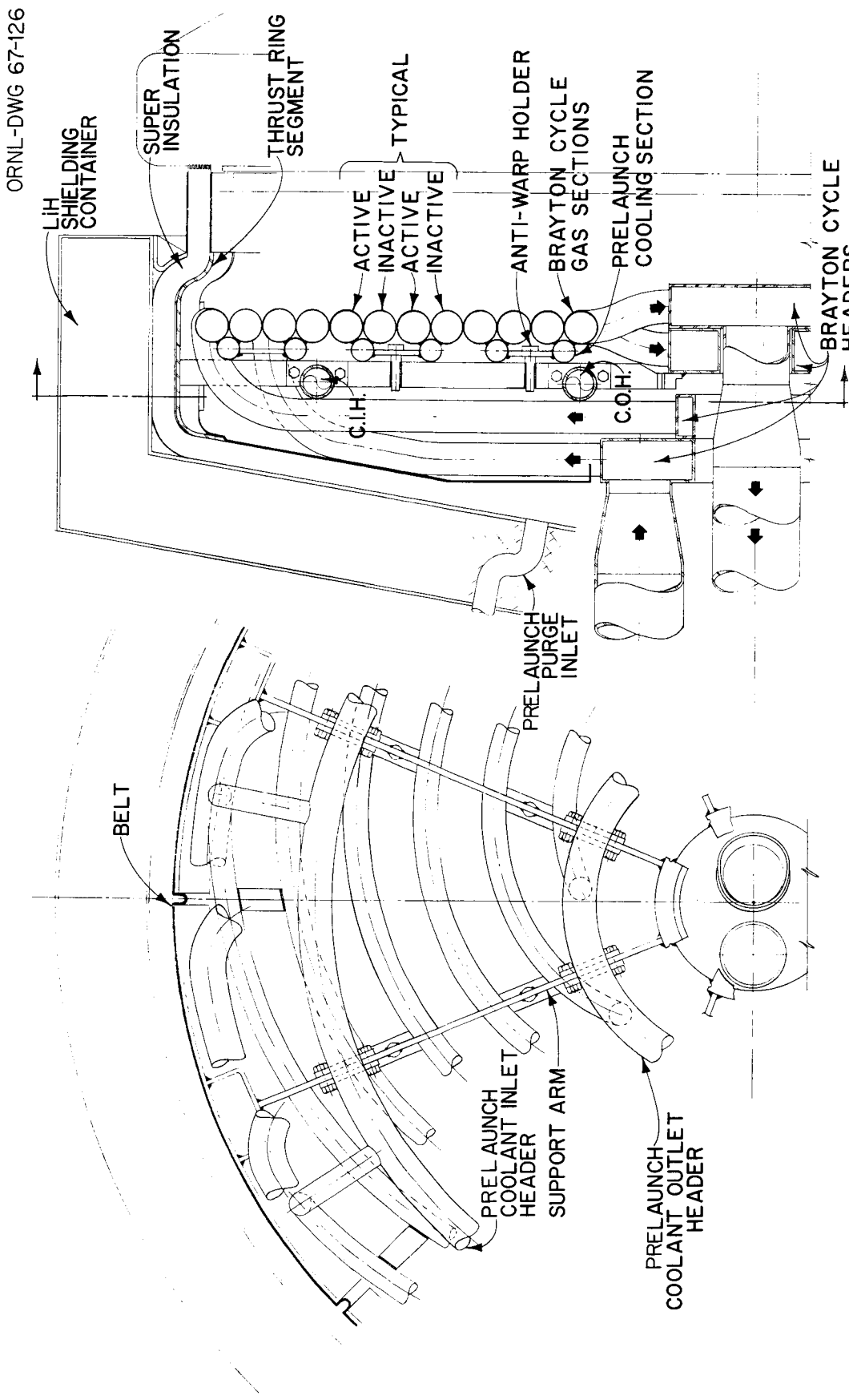

Fig. 5.6. Heat Exchanger Assembly for Use with Helium-Xenon Working Fluid.

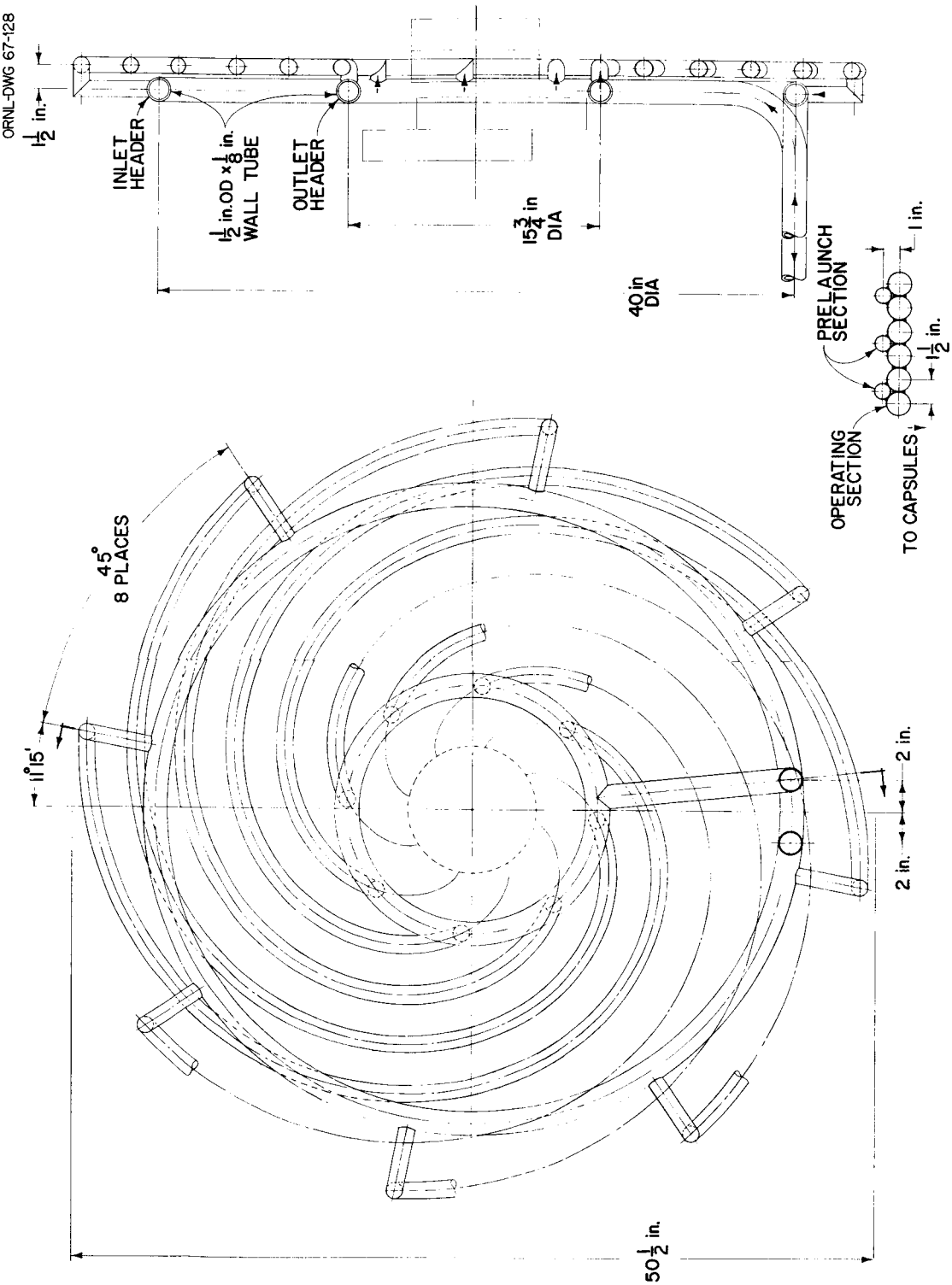

Fig. 5.7. Prelaunch Cooling Section of Heat Exchanger for Use with Helium-Xenon Working Fluid.

frame (described in Sect. 5.4.2) at the open end. The apex of the 80° cone-shaped closed end is oriented toward the engine-room module. Coolant lines and a launch-pad purge-gas inlet penetrate the cone axially. The lines then curve until they run nearly parallel to the conical surface and the rack, so there is no straight-through path for radiation streaming to the outside of the shield. Since the working fluid headers pass straight through the shield, it may be necessary to provide a 16-in.-diam 4-in.-thick piece of supplementary shielding on the engine-module bulkhead directly behind the header exit.

5.4. Vehicle Integration

Integration of the heat source into the multipurpose mission module is shown in Fig. 5.1. The power system is located in the engine-room module within the SLA, and an offset arrangement is used to conserve space. A second system (shown in phantom in Fig. 5.1) could be incorporated into the module if desired. This system would also provide complete redundancy for critical power requirements.

5.4.1. Vehicle Modification

Modifications required to the engine room of the multipurpose mission module to allow installation of the power-conversion system are shown in Fig. 5.8. The existing pressure-containment wall was rerouted more or less along a chord to provide a two-radian circular segment, external to the pressurized volume, for the equipment. The altered bulkhead of the module leaves a 2-ft minimum radial clearance around the docking port for easy maneuverability into the port from the engine room. The 2-ft minimum clearance requirement accounts for the particular shape shown.

In the circular segment, the thermal subassembly of the power supply has been positioned directly over the rack, which is the basic link holding the two cylindrical modules together. This location permits the heat source to be supported without cantilevering the unit. This arrangement was selected in order to transmit the major launch-phase loads as direct bearing loads to the rack rather than as torsion or bending loads. An

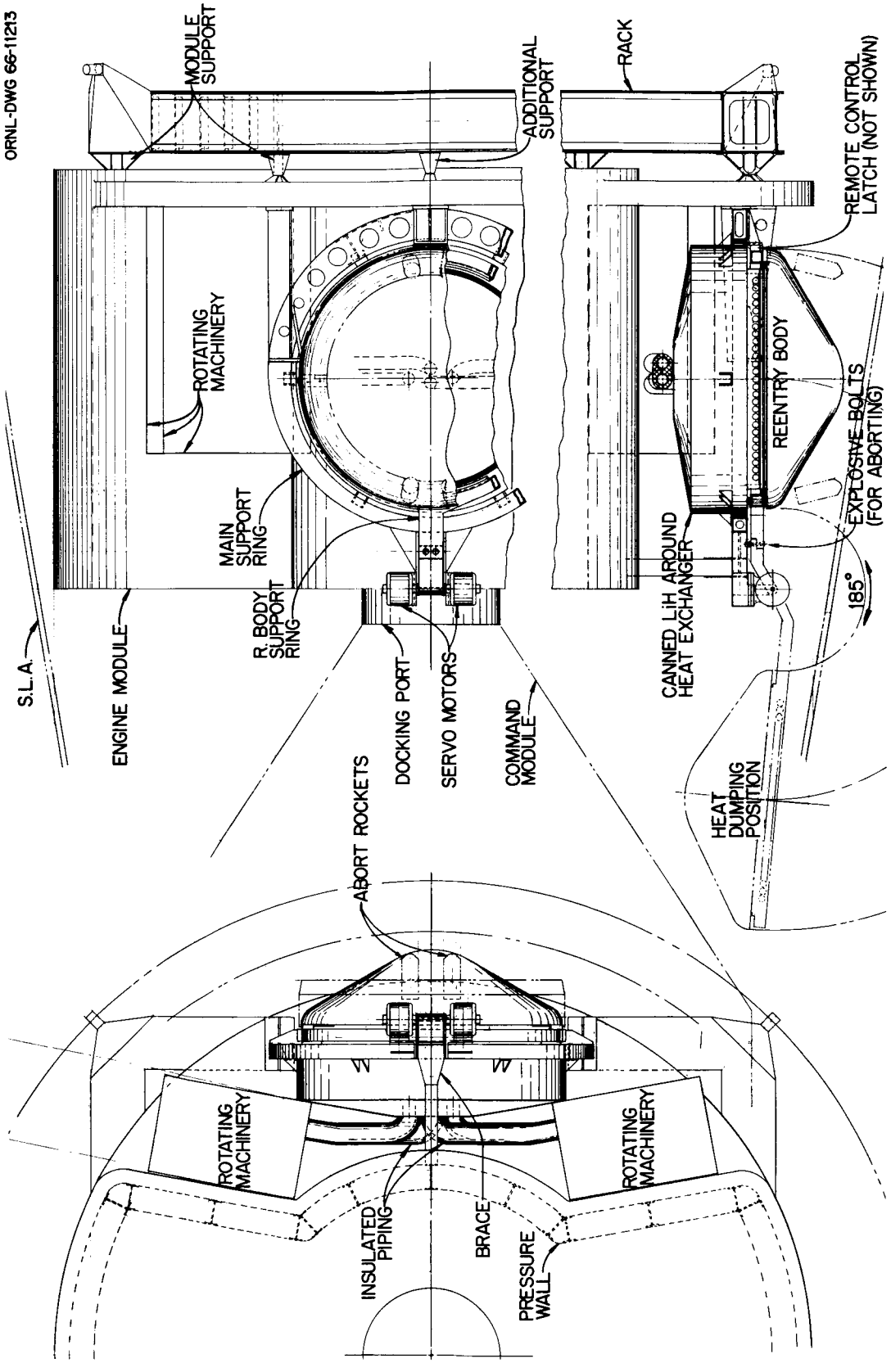

Fig. 5.8. Module Revisions for Brayton-Cycle Integration.

additional support point was added to the rack to assist the two existing points (shown in the front elevation view). The side elevation view (shown in proper perspective to the command module) shows the relationship of the SLA and the thermal source on the launch pad, as well as the proximity of the reentry body to a docked command module during an emergency requiring a heat dump in orbit after the SLA has been jettisoned.

The orbiting station consists of the modified engine module, the laboratory module, and the power supply held together by the rack framework. The modified module does not alter docking procedures at either end of the station, and there is no interference with operation of the power system from a docked vehicle.

5.4.2. Support Mechanism

The support assembly for the components is shown in Fig. 5.9. The assembly is basically two box-sectioned parts (the main support frame and the reentry-body support ring; see Fig. 2.1.) fabricated from 1/8-in. titanium sheet. The main support frame has two 6- by 4-in. rectangular columns rising from the rack load points. There is also a direct connection to the third-rack load point on the variable cross-section part of the circular arch (66 in. ID). The arch's peripheral cross-sectional variation from 6 by 4 in. to 2 by 4 in. provides a nearly constant stress distribution from the servo motors, LiH shield, and heat exchanger loads.

The servo motors have a common shaft running between them that provides support for the reentry body and its support ring. The shaft has Al_2O_3 journal bearings in the servo housings. The combination of metal shaft and oxide bearings is an antiweld joint for long-term operation in a space vacuum. Antiweld joints are mandatory because the motors are low-torque devices with only enough power to initiate the heat dumping mode in orbit. A transition to a 1-in.-square cross section between the housings produces the rotation of the reentry-body support ring. Driving the square-cross-section shaft with the servo motors rotates the weightless reentry body and support ring until the fuel capsules do not face the heat exchangers.

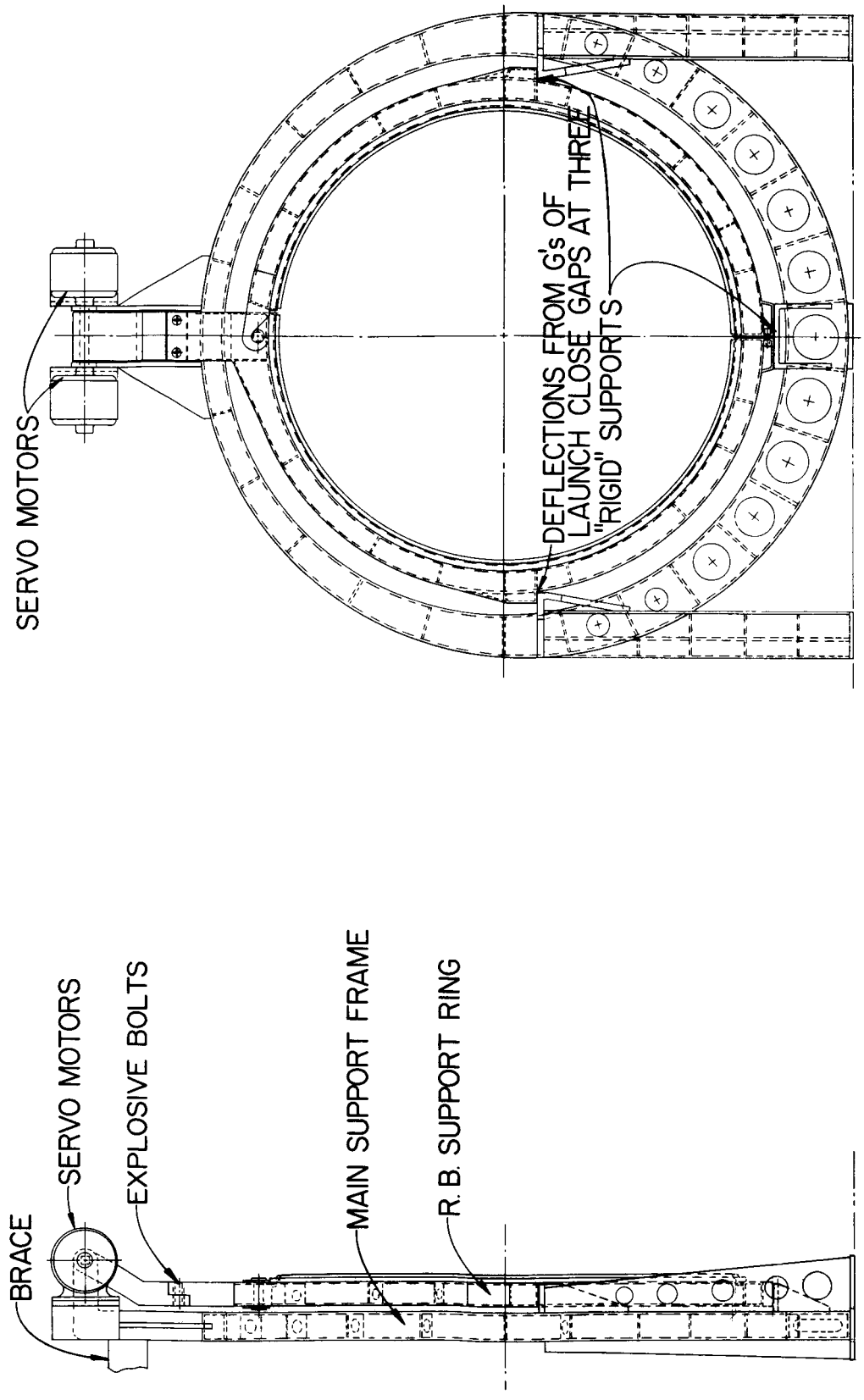

Fig. 5.9. Support Framing for Reentry Body and Heat Exchanger.

The shaft is designed to withstand only dead loads and not the dynamic launch loads of the reentry body and support ring. Provisions are included to let the launch loads deflect the upper part of the main support arch until the reentry-body support ring makes contact with three deflection-limiting pads. The clearances between the pads and the support ring are approximately 1/32 in. before the launch, and the gaps close under an additional 1-g load. The remainder of the 10-g launch load is supported through the pads to the gussets and columns directly into the rack. In orbit, the stored deflection energy will open the gaps to 1/16 in. This clearance is necessary to insure that space welding or interference does not occur between the reentry-body support ring and deflection limiting pads that would prevent pivoting the heat source into the heat-dumping mode.

A brace has been included at the servo motor location to add stability to the support mechanism. The brace is anchored to the pressure wall stanchions as a means of counterbalancing any force moments applied to the support system. A temporary latch is included in the design to prevent the reentry body from swinging like a pendulum during launch, and it will be severed when orbit is achieved.

5.4.3. Reentry-Body Attachment

The method for attaching the reentry body to its support ring is shown in Fig. 5.10. The 2- by 2-in.-square section ring has an inside diameter of 58 in. and is split. To position the reentry body, one-half the ring is rotated 20° and removed from the ring pivot boss. The reentry body is placed in the remainder of the supporting member with the ring extending through a 76-in.-diam hatch in the SLA. A temporary connection can be used to insure that the reentry body is held in place until the ring half is replaced and the ring coupling bolt is securely tightened.

The impetus to pivot the support ring through the spacecraft hatch must be supplied externally. The servo motors are not sized to provide this movement under a 1-g load; however, the hinging function of the shaft between the servo motors is utilized to permit this rotation of the support ring.

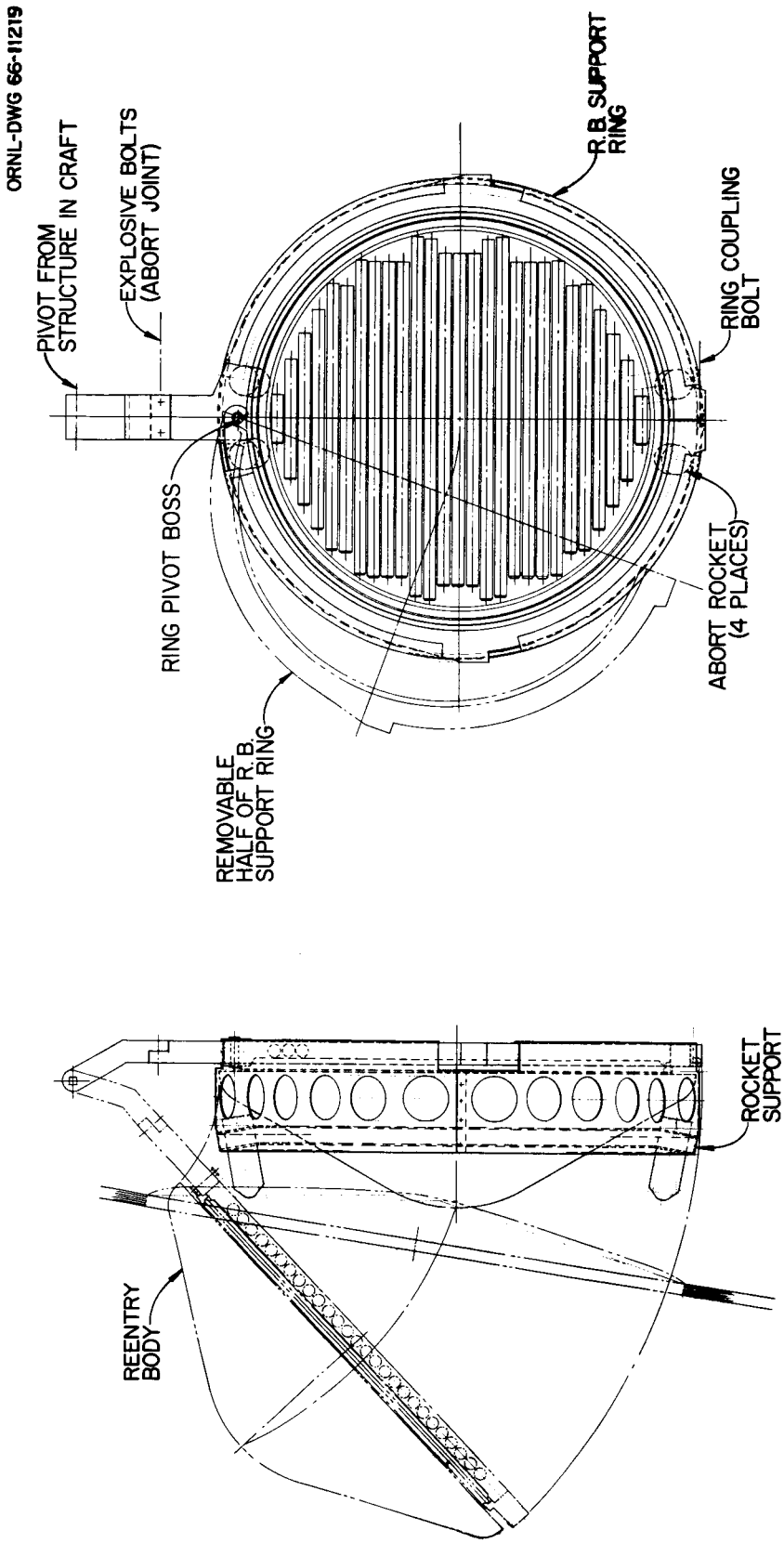

Fig. 5.10. Support Ring and Handling Details for Reentry Body.

An alternative method of inserting the reentry body into the spacecraft is available. The split ring could be preclamped to the reentry body and then positioned so that the explosive-bolt joint could be made. This method would require a different insertion and support tool, but it is a practical means of loading the entire prefueled reentry body.

5.4.4. Capsule Loading

The hatch cover on the SLA must be removed to permit insertion of the fuel capsules into the reentry body attached to the launch vehicle. The reentry body is temporarily pivoted through the opening (shown in Fig. 5.10) by an external mechanism. One-half the split support ring is removed, and the reentry body is held to the other half of the ring with an auxiliary clamp.

Removal of the ring segment exposes the capsule tube holders to the fuel-loading machine. The capsules are inserted into the holders, the end caps are attached, and a crimped seam is provided to secure the capsules. After the ring section is replaced, the auxiliary clamping force is removed, the body is swung back into place in the vehicle, and a tiedown is made to restrain the reentry body during launch. The SLA hatch is secured to complete the loading operation.

5.4.5. Decoupling Method

Dependable and fast metal severance is required for removing any temporary connections or tiedowns, for activating the orbital-recovery scheme, for opening the SLA hatch in the event of an abort, and for jettisoning the abort rockets after orbit is achieved. The controlled-burning explosive hexanitrostilbene (HNS) is specified for these functions. In addition to severance, HNS can supply sufficient thrust to separate the severed pieces. The design of the region containing the compound is shown in Fig. 5.2. The explosive cord is trapped in an unsealed cavity. When the HNS is ignited, it acts as a cutting torch on the member where it is attached. (The slag from the cutting action is caught in a similar cavity to prevent damage to adjacent surfaces.) The combustion gases expand into

the volume formed by the two cavities, and the pressure buildup produces a thrust to eject the severed part.

The ignition source for the HNS is the standard Apollo-initiator (SAI) system with a 99.9% calculated reliability and a confirmed 90% reliability. The detonation specifications are 3.5 amp for 10 msec, but, in actual practice, 5 amp is frequently used. Experience shows that 0.5 msec is all that is required to detonate the explosive.

The lifetime of the explosive and detonator is considered to be at least 2 years in orbit, subject to controlled temperature limits. For HNS the limitations are a short-duration temperature of 350°F and a long-term temperature of 150°F.

At termination of the mission, the HNS explosive can be used to separate the reentry body from the spacecraft. A reentry package that would contain retrorockets, radio beams, etc. could be provided and attached to the support-ring groove for return and recovery of the isotopic heat source if this method of disposal were desired.

5.4.6. Abort Measures

Abort schemes are integrated into the Brayton-cycle heat-source design to assist recovery operations before any fuel-capsule damage occurs. These abort devices are, however, not required to function as mandatory mechanisms to guarantee that no radioisotopes are released. Intrinsic methods are incorporated as a backup means for short periods of time to allow other measures to be taken.

Aborts that occur during the launch phase are handled by abort rockets attached to the reentry-body support ring. These rockets (shown in Fig. 5.8) are capable of delivering 18,000 lb of thrust, which will propel the reentry body 194 ft from the vehicle. The operational sequence is the following: (1) the SLA hatch is blown, (2) the temporary tiedown to keep the reentry body from swinging is severed, (3) the rockets are fired, and, (4) as the rockets pivot the reentry body through the hatch opening, the explosive bolts on the support ring are detonated. The bolts are disconnected last to give the abort rockets enough time to build up sufficient thrust so that the reentry body will not fall inside the SLA. The pivoting

action will also give an upward trajectory, which will increase the distance traveled. As indicated in Fig. 5.8 the abort rockets are mounted within the reentry-body support ring and they are set at an angle so that the exhaust is not directed straight back at the reentry body. This method of mounting was used in order to keep the required diameter of the hatch in the SLA to a minimum. However, if it is feasible to increase the SLA hatch diameter, it may be preferable to attach the abort rockets to the edge of the reentry-body support ring so that the exhaust can be directed straight backward for maximum thrust performance.

In the case of failure of the launch abort scheme, the backup protection is the BeO heat-storage capacity included in the reentry body. The BeO will retard the capsule temperature rise until a mechanical means of dispersing the debris and recovering the reentry body is effected (e.g., during a launch-pad fire). If the launch vehicle fails to obtain orbit and the launch abort scheme also fails, the BeO will retard the temperatures until the launch vehicle falls into water. Immersion in water will cause the fuel capsules to reach an equilibrium temperature approximately 100°F above the ambient water temperature.

After orbit has been established, the SLA, abort rockets, and temporary tiedown holding the reentry body are severed and jettisoned. The normal mode of operation for the heat source–heat exchanger system is activated or the emergency mode of deploying the reentry body is initiated. If the motor-driven deployment mechanism fails, the BeO heat-storage material will sustain the fuel capsules to allow the deployment mechanism to be operated manually. Inability to manually operate the mechanism would require that the explosive HNS on the reentry-body support ring be detonated. This action would sever the reentry body from the system and provide a thrust to separate the pieces in orbit.

5.5. Materials

Component materials for the heat source are divided into two categories: structural and nonstructural. The structural items are fabricated from either aluminum, titanium, stainless steel, or Cb–1% Zr. The nonstructural components are the reentry ablative protection, thermal

insulation, emissivity coating, BeO heat-storage material, LiH shielding, and fuel capsules. The choice of material depends on the operating temperature, compatibility problems, and weight of the strength member.

The ablation protection is a low-density phenolic-nylon ablative coating with a specific weight of 36 lb/ft^3 and thermal conductivity at 100°F of 0.05 Btu-ft/hr·ft^2·°R (see Ref. 38 for additional physical property data). The coating is cemented to the reentry-body structural shell with a flexible bond, RTV-60. This bond has a long-term high-temperature limit of 325°F, which is well above the calculated design value of 53 to 175°F.

Heat losses from the source are minimized by thermally insulating the hot zone with 2 in. of Superinsulation, which is a reflective type. This material is a highly evacuated multiple-layer system of metallic reflectors with ceramic woven spacers, and the composite for this particular application is 1-mil-thick sheets of tantalum and 15-mil mats of quartz fibers with a weave pattern to give 96% voids.

The estimated thermal conductivity of the composite is 2.4×10^{-3} Btu-ft/hr·ft^2·°F with 2000°F on the hot surface and 100°F on the cold surface. This conductivity value for 2 in. of insulation in the reentry body has been used in the calculations of temperature distribution.

One inch of Superinsulation with the same material construction also surrounds the heat exchanger equipment. The two sections of insulation form a labyrinth seal at the reentry body—heat exchanger circumferential junction to provide a completely enclosed insulated volume. The labyrinth seal is a relatively inefficient thermal barrier, but this arrangement is necessary to permit the fuel plate—reentry body assembly to pivot away from the heat exchanger in the emergency heat rejection mode of operation. Tantalum-quartz compatibility problems may exist in the 2000°F range where the system is to operate. However, other ceramic spacers, such as potassium titanate, can be substituted if future experimental work indicates that a compatibility problem does exist.

The radiant heat transfer between the fuel plate and heat exchanger is enhanced by a coating of iron titanate on all surfaces within the insulated volume. The coating has demonstrated a total hemispherical

emissivity when deposited on a Cb–1% Zr alloy tube of greater than 0.8 after 10,000 hr of operation at 1700°F in a vacuum.[39]

The heat-storage capacity of BeO is utilized in the design to exercise transient temperature control. Pie-shaped segments of pressed BeO at 80% of theoretical density are fitted into the spaces between the Cb–1% Zr ribs. From 100 to 300 lb of BeO can be incorporated into the design by changing the thickness of the segments. In the transient temperature analysis, the major physical properties[40] are held constant at 10 Btu-ft/hr·ft^2·°F for the conductivity, 0.5 Btu/lb·°F for the heat capacity, and a total hemispherical emissivity of 0.32. These constants produce a conservative analysis of the temperature retardation of the fuel capsules under transient conditions.

The shielding material is LiH, with a specific weight of 46.8 lb/ft^3, and it is canned in SA 240–TP 304L stainless steel. Other pertinent physical data[40] are not used in this preliminary design, but they would be necessary in a final design. The fuel-capsule materials and fabrication are discussed in Section 3.

The design temperatures of 2000°F for the fuel capsules and 1500°F at the gas outlet restrict the choice of structural materials within the insulated volume. These particular conditions are about at the borderline between a superalloy and a refractory alloy construction, but a refractory alloy was chosen for an extra margin of safety. A Cb–1% Zr alloy was selected, since this material most nearly qualifies as an engineering material among the various refractory alloys. It also has a low specific weight and reasonably good welding and oxidation-resistance characteristics. The master Larson-Miller plot in Fig. 3.16 is used to obtain design stress values for sizing members. The thermal properties used in the temperature analyses are 40 Btu-ft/hr·ft^2·°F and 0.07 Btu/lb·°F for the conductivity and heat capacity, respectively.

The insulating capabilities of Superinsulation are sufficient to permit aluminum to be utilized in the reentry body. The composition and temper selected is 6061-T6 with a minimum yield stress of 32,000 psi from 0 to 210°F. The intrinsic thermal properties are inconsequential in the temperature analyses; however, an iron titanate emissivity coating is used on all radiating surfaces. The specific weight of aluminum was the

dominant factor in its selection over titanium, which is used in the structural support frame. The support framing is fabricated from unalloyed titanium with a minimum yield stress of 60,000 psi from room temperature to 300°F. The thermal properties were disregarded in the preliminary design, but they would have to be considered in a final design. No radiative emissivity coating is specified to increase temperature differentials between the insulation and the frame.

5.6. Stress Analysis

In this preliminary design, an elementary approach of bracketing the stress limits has been used to size the larger and heavier structural members. A series of stringent conditions was applied to the critical items of the components, and the highest stress level calculated determined the dimensions. For this study the determinations were based on (1) a 10-g maximum acceleration force as the launch, abort, or recovery load and (2) an allowable stress level of 90% of the yield stress value. Parts of lesser importance were estimated for dimensional conformity with the remainder of the structure.

Pressure stresses for a 26-psi gas pressure in the heat exchangers were calculated for the tubular shapes by the usual equations. The header stresses were approximated by simplified models of plate and shell solutions.

The metal thicknesses used for heat exchanger tubes and headers were selected for formability rather than stress levels. Thinner material would be adequate for the tubes, since the design criterion is 1% creep in 5 years; however, forming thinner-wall material into complicated geometrical shapes is considered marginal without demonstrated proof. The criterion of 1% creep in 5 years results in an allowable stress at 1500°F of 1500 psi. A comparison of the stress values in Table 5.1 with the 1500-psi allowable value shows that the stresses are below this limit, except those for the inlet headers. The amount of bracing required to reduce the inlet header stresses to the allowable value depends on the temperature-dependent allowable stress, which is higher than the 1500°F value because the inlet temperature is much lower.

Table 5.1. Stresses Due to Gas Pressure

	Stress (psi)
Heat exchanger	
Involute tubes	750
Inlet headers (with internal bracing)	1500
Outlet headers	1000
Heat exchange inlet and outlet	450
Allowable stress for 1% creep in 50,000 hr	1500

5.7. Component Weight Breakdown

The predicted weights of the subassemblies are given in Table 5.2, and a breakdown of the 1300-lb reentry-body weight is given in Table 5.3.

The reentry body is the largest single contributor to the radioisotope heat-source system weight (50%) and the essential parts (fuel, insulation, reentry-body shell, and ablative coating) account for 73% of its total weight. The weights of structural members are closely related to the particular design selected, and changing the design could appreciably alter their total weight.

Table 5.2. Weights of Subassemblies

	Weight (lb)
Reentry body	1300
Abort rockets and support ring	120
Heat exchanger	390
Shield	660
Structure	150
Servos	50
Total	2670
Specific weight, 110 lb/kw(th)	

Table 5.3. Weights of Reentry-Body Components

	Weight (lb)
Fuel	700
Tubes, clips, end caps, etc.	150
Support-plate structure	100
BeO	100
Central bolt	10
Superinsulation	35
Connectors between support-plate structure and reentry-body shell	95
Reentry-body shell	75
Ablative coating	35
Total	1300

Thirty-three per cent of the weight of subassemblies is directly attributable to safety considerations (nuclear radiation shield, launch abort scheme). The combined weight fractions of reentry body and safety features are approximately 83% of the specific weight of 110 lb/kw(th).

5.8. Reentry Characteristics

The safe reentry of the heat source without loss of fuel containment has been stressed in the heat-source design. The values of the important reentry parameters for this design are given in Table 5.4.

The terminal ballistic coefficient of 78 results in an impact velocity of 250 fps and a cratering depth of about 6 in. in soft earth. The center-of-gravity location is slightly behind the conical section, but the separation of center of gravity and center of pressure is about 38 in. The inertial ratio of 1.86 approaches the theoretical value of 2 for a disk, and this high value insures that the reentry body will not oscillate between a spinning and tumbling mode. A 2-in. by 180° righting member segment on the back-side of the reentry body (Fig. 2.1) provides asymmetry

Table 5.4. Reentry-Body Properties

Weight, lb	
With 35-lb ablative coating	1300
After reentry (30 lb lost)	1270
Base diameter, in.	
With ablative coating	63
Structural shell	58
Distance forward of capsule centers to center of gravity, in.	2
Inertial properties	
I_s, spin, slug-ft^2	93.54
I_t, tumble, slug-ft^2	50.00
I_s/I_t	1.87
Terminal ballistic coefficient	78
Hypervelocity ballistic coefficient	40

so that the reentry body does not have a metastable position for reentry in a backward direction. It also assures that the ablative coating is forward so that it functions properly.

The blunted-cone shape for the reentry body was chosen as a result of phase I work, which indicated that this shape would be stable in the forward direction and could be designed to have a sufficiently low frontal impact loading to prevent burial. It is important that the reentry body stabilize in a forward direction before reentry heating becomes significant. The fuel-plate assembly, located at the rear of the reentry shell, is unprotected and could not be expected to remain intact if directly exposed to the airstream.

P. J. Bobbitt of the NASA–Langley Research Center has made preliminary motion and heating calculations[41] to describe the expected reentry behavior of a body corresponding to the phase II design. The hypersonic ballistic coefficient used for the calculations (M/C_DA = 1.645 slugs/ft^2 $\cong$ 53 lb/ft^2) is somewhat higher than that obtained in the final phase II design (W/C_DA = 40 lb/ft^2) which tends to make the heating rate values slightly pessimistic. In the parenthetical expressions above, M is mass in slugs, C_D is drag coefficient, A is drag area, and W is weight in pounds. The

calculations were made for initial tumbling rates of 0, 0.1, 0.2, and 1.0 radian/sec and a reentry angle of 10° at 26,000 fps. Figures 5.11 through 5.14 are plots of the results showing heating rate (Q), equilibrium temperature at the center of the back surface of the fuel plate (TS), and angle of attack (α) versus time and altitude. The data show that the reentry body makes a complete revolution before starting its oscillatory motion only in the case of the 1.0 radian/sec initial tumbling rate and that the heating rate at the time the revolution occurs does not cause any fuel-plate temperature problem. The fuel-plate temperature curves are equilibrium values but do not take into account the thermal conduction along the body, which will cause the actual temperatures to be less than

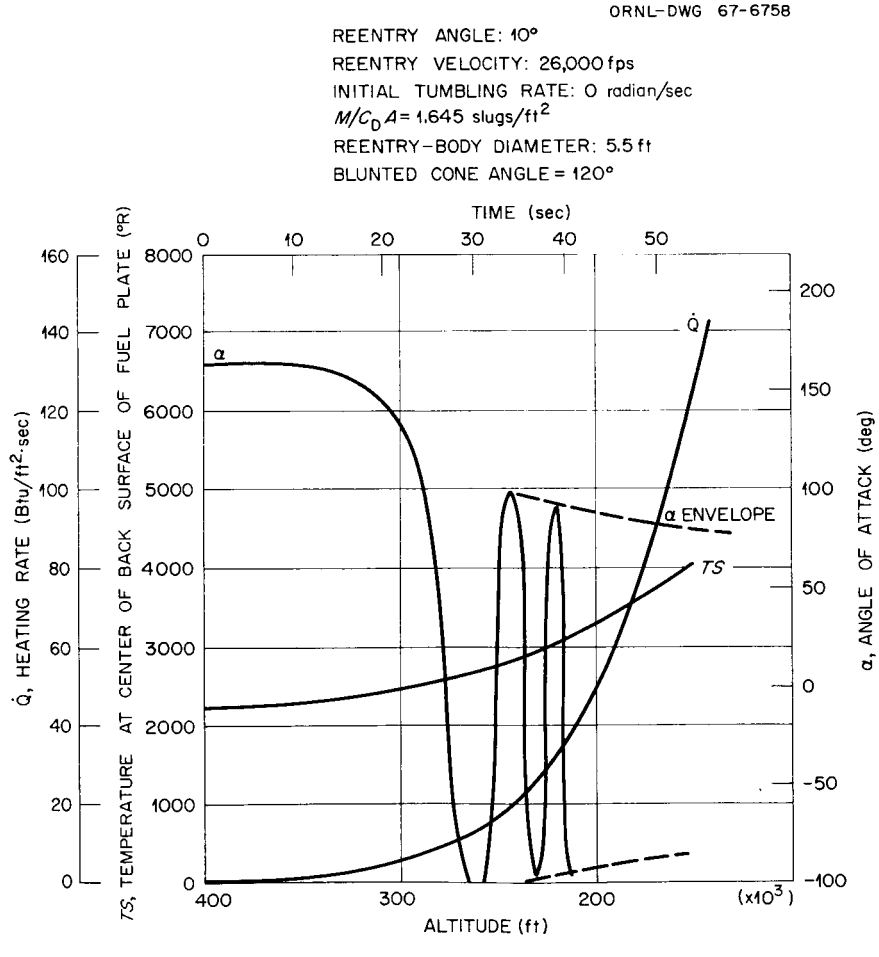

Fig. 5.11. Reentry Behavior for an Initial Tumbling Rate of Zero.

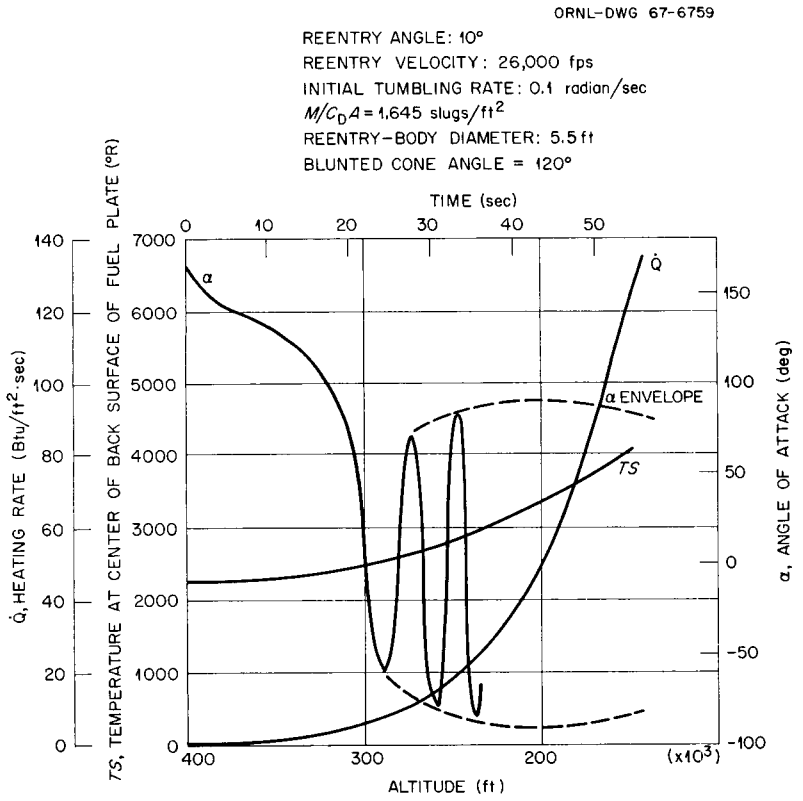

Fig. 5.12. Reentry Behavior for an Initial Tumbling Rate of 0.1 radian/sec.

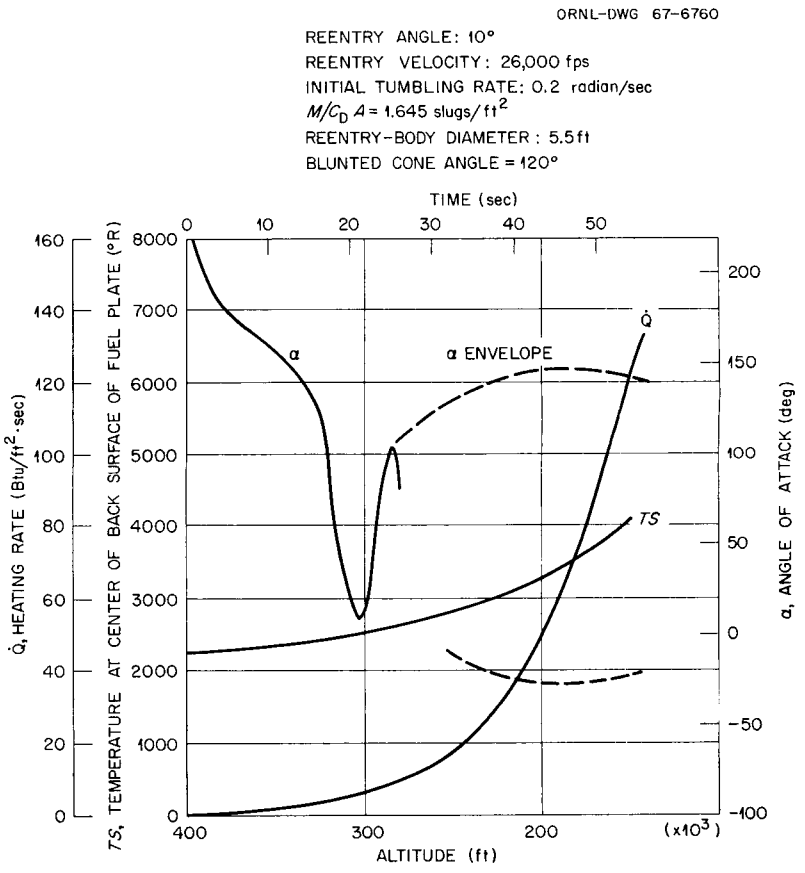

Fig. 5.13. Reentry Behavior for an Initial Tumbling Rate of 0.2 radian/sec.

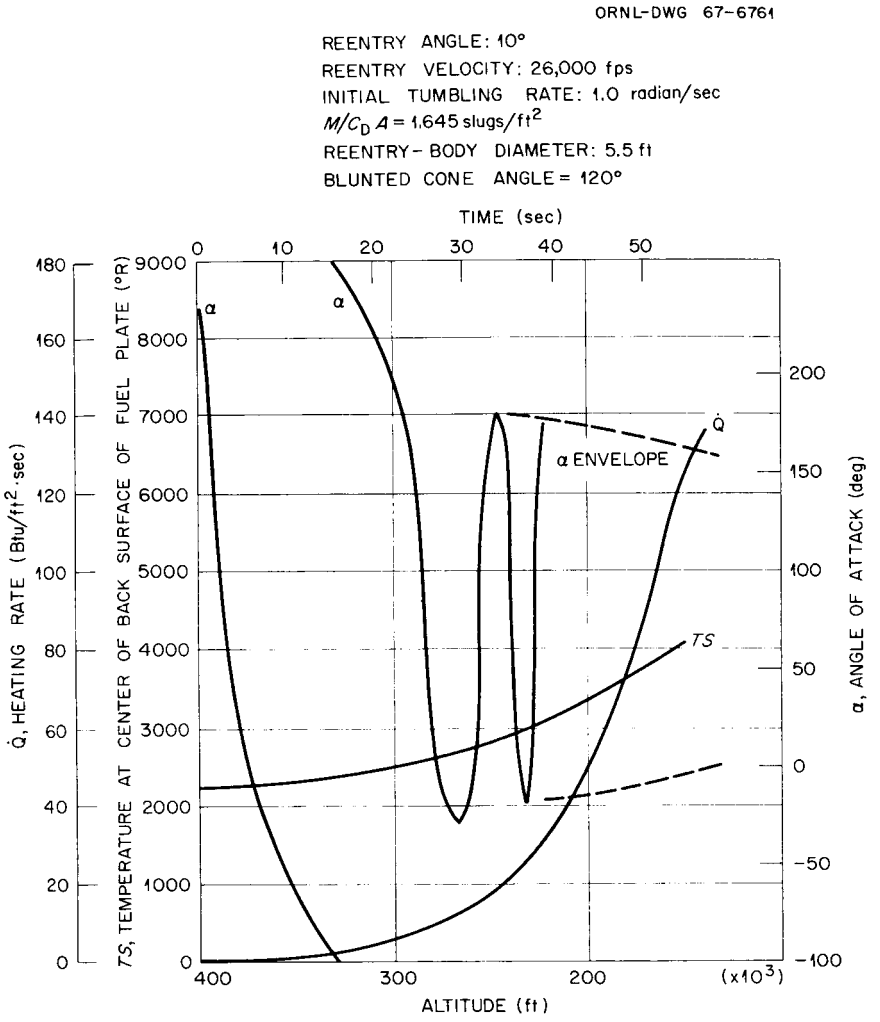

Fig. 5.14. Reentry Behavior for an Initial Tumbling Rate of 1.0 radian/sec.

those shown. Also, the equilibrium values are based on the body being at the angle of attack corresponding to the particular temperature value long enough to reach equilibrium, while in actual practice the body is oscillating and does not reach equilibrium. A reentry angle of 10° is probably pessimistically unrealistic for an earth orbital mission, and angles of 2 to 3° are probably larger than would be expected. At a reentry angle of 2.5°, the maximum heating rate is about one-half that calculated for 10°, and the maximum angle of attack at peak heating is reduced to about 55°. Under these conditions, the peak equilibrium temperature at the center of the base is only about 2700 to 2800°R.

During the initial oscillatory phase of the reentry when the body is at angles of attack between 180° and 60 to 70°, the heating rates at the edge of the base will be higher than those calculated for the center of the base. Additional calculations and experiments are needed to determine whether the ablative coating in this region needs to be thickened beyond the 2.5 in. shown in the phase II design. It may be noted from Figs. 5.11 through 5.14 that the computer runs were terminated while the heating rate curve ($\dot{Q}$) was still following a steep upward slope. However, an extension of the zero tumbling rate case indicated that the maximum $\dot{Q}$ is about 145 $Btu/ft^2 \cdot sec$, which is only slightly above the point where the computer runs were terminated.

The stability of the reentry body in the subsonic terminal phase has not been evaluated but, with the center of gravity so far aft, it is expected that there are some types of initial entry conditions that might lead to tumbling in the terminal phase. Computer studies coupled with tunnel or airplane drop tests are needed to determine whether it will be necessary for subsonic stability to shift the center of gravity of the reentry package forward by dishing the fuel plate in a forward direction, extending the skirt, or adding weight to the nose of the blunted cone.

5.9. Heat Transfer and Flow Analysis

The major portion of the heat transfer evaluations involves radiant exchange of energy, coupled with contributions from conduction. All radiant heat transfer is treated in a general manner, although it is dependent on surface properties, geometry factors, area, and temperatures. All surfaces were considered to have an absorptivity and emissivity of 0.8, which is consistent with an iron titanate coating. The geometry factors were average values rather than integrated values over the surfaces, and the important area was considered to be the prime radiator surface. The temperatures were calculated with these generalized values for a 25 kw(th) heat source seeing an average temperature sink.

The problem was simplified further by assuming infinite planes and a uniform heat flux in order to reduce the calculations to a two-dimensional heat transfer model. Many of the calculations were performed with

the IBM 360 computer by using relaxation techniques; the remainder were made with a desk calculator in a trial-and-error method solution or were direct calculations, whichever was appropriate.

5.9.1. Fuel Capsule

The multilayer capsule construction and tubular holder are depicted schematically in Fig. 5.15 for correlation with the temperature distributions given in Tables 5.5 through 5.9. The tables of constituent temperatures exhibit the circumferential deviations that result from heat removal from only one-half the holder surface (270 to 90°) to various sink temperatures. The temperature distributions are symmetrical about the 0 to 180° diametrical line, and the tables are correspondingly shortened to reflect this.

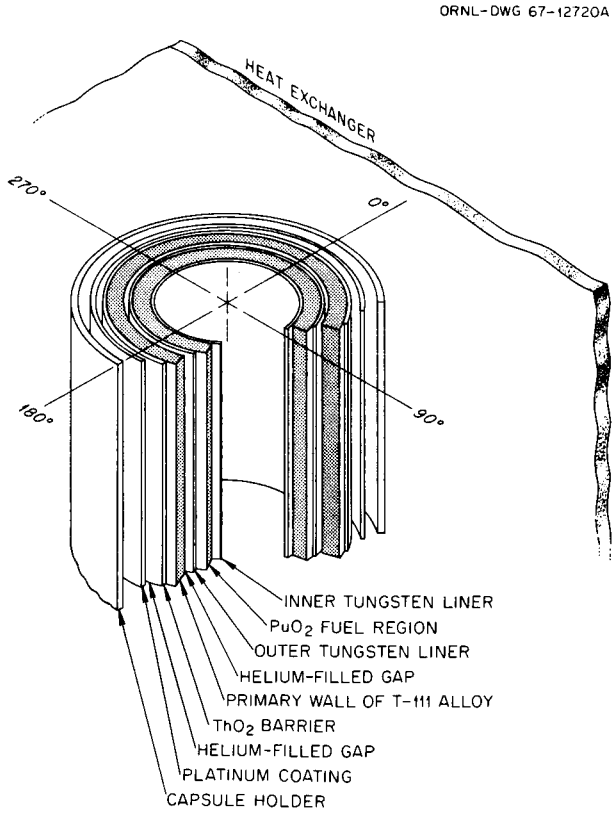

Fig. 5.15. PuO_2 Capsule Components for Temperature Distribution Analysis.

Table 5.5. Capsule Temperature Distribution for Opposing Disks as Radiator and Receiver in a 25-kw Heat Source with a Heat Exchanger Surface Temperature of 1500°F and Heat Removal from One-Half Capsule Holder Surface

Material	Radial Position (in.)	Temperature (°F) at Indicated Angular Position						
		θ = 0°	θ = 30°	θ = 60°	θ = 90°	θ = 120°	θ = 150°	θ = 180°
Inner tungsten liner	0.281	1941	1941	1942	1943	1944	1944	1945
	0.301	1939	1939	1941	1943	1945	1946	1947
PuO_2 fuel region	0.301	1939	1939	1941	1943	1945	1946	1947
	0.381	1916	1917	1920	1924	1928	1930	1931
	0.461	1878	1880	1884	1890	1895	1899	1900
	0.542	1852	1854	1859	1866	1872	1876	1877
Outer tungsten liner	0.542	1852	1854	1859	1866	1872	1876	1877
	0.562	1849	1851	1856	1863	1869	1873	1875
Helium-filled gap	0.562	1849	1851	1856	1863	1869	1873	1875
	0.564	1846	1848	1853	1860	1867	1871	1873
Primary wall of T-111 alloy	0.564	1846	1848	1853	1860	1867	1871	1873
	0.651	1844	1846	1852	1859	1866	1870	1872
	0.737	1840	1842	1849	1858	1865	1869	1871
ThO_2 barrier	0.737	1840	1842	1849	1858	1865	1869	1871
	0.747	1833	1836	1844	1854	1863	1868	1870
Helium-filled gap	0.747	1833	1836	1844	1854	1863	1868	1870
	0.749	1829	1832	1841	1853	1862	1867	1869
Platinum coating	0.749	1829	1832	1841	1853	1862	1867	1869
	0.769	1786	1793	1812	1837	1852	1860	1863
Capsule holder	0.809	1746	1757	1785	1823	1843	1854	1857
	0.871	1745	1756	1784	1823	1843	1854	1857

Table 5.6. Capsule Temperature Distribution for Opposing Disks as Radiator and Receiver in a 25-kw Heat Source with a Heat Exchanger Surface Temperature of 1900°F and Heat Removal from One-Half Capsule Holder Surface

Material	Radial Position (in.)	Temperature (°F) at Indicated Angular Position						
		θ = 0°	θ = 30°	θ = 60°	θ = 90°	θ = 120°	θ = 150°	θ = 180°
Inner tungsten liner	0.281	2232	2233	2234	2235	2235	2236	2236
	0.301	2230	2231	2233	2235	2237	2238	2238
PuO_2 fuel region	0.301	2230	2231	2233	2235	2237	2238	2238
	0.381	2207	2209	2213	2218	2222	2224	2224
	0.461	2169	2172	2178	2184	2190	2193	2194
	0.542	2143	2146	2153	2161	2167	2171	2171
Outer tungsten liner	0.542	2143	2146	2153	2161	2167	2171	2171
	0.562	2140	2143	2150	2158	2165	2168	2169
Helium-filled gap	0.562	2140	2143	2150	2158	2165	2168	2169
	0.564	2136	2140	2147	2155	2162	2166	2167
Primary wall of T-111 alloy	0.564	2136	2140	2147	2155	2162	2166	2167
	0.651	2134	2138	2145	2154	2161	2165	2166
	0.737	2131	2134	2143	2153	2161	2165	2165
ThO_2 barrier	0.737	2131	2134	2143	2153	2161	2165	2165
	0.747	2123	2128	2138	2150	2159	2164	2164
Helium-filled gap	0.747	2123	2128	2138	2150	2159	2164	2164
	0.749	2119	2124	2135	2149	2158	2163	2164
Platinum coating	0.749	2119	2124	2135	2149	2158	2163	2164
	0.769	2084	2092	2111	2137	2151	2158	2159
Capsule holder	0.809	2051	2062	2089	2125	2144	2153	2155
	0.871	2050	2061	2088	2125	2144	2153	2155

Table 5.7. Capsule Temperature Distribution for Opposing Disks as Radiator and Receiver in a 25-kw Heat Source with a Heat Exchanger Surface Temperature of 1800°F and Heat Removal from One-Half Capsule Holder Surface

Material	Radial Position (in.)	Temperature (°F) at Indicated Angular Position						
		θ = 0°	θ = 30°	θ = 60°	θ = 90°	θ = 120°	θ = 150°	θ = 180°
Inner tungsten liner	0.281	2152	2153	2153	2154	2155	2156	2156
	0.301	2150	2151	2153	2155	2157	2159	2159
PuO_2 fuel region	0.301	2150	2151	2153	2155	2157	2159	2159
	0.381	2128	2130	2133	2138	2142	2145	2145
	0.461	2091	2093	2098	2105	2111	2114	2116
	0.542	2065	2068	2074	2081	2088	2092	2093
Outer tungsten liner	0.542	2065	2068	2074	2081	2088	2092	2093
	0.562	2062	2065	2071	2078	2085	2090	2091
Helium-filled gap	0.562	2062	2065	2071	2078	2085	2090	2091
	0.564	2059	2061	2068	2076	2083	2088	2089
Primary wall of T-111 alloy	0.564	2059	2061	2068	2076	2083	2088	2089
	0.651	2057	2060	2066	2075	2082	2087	2088
	0.737	2053	2056	2064	2073	2081	2086	2088
ThO_2 barrier	0.737	2053	2056	2064	2073	2081	2086	2088
	0.747	2046	2049	2058	2070	2079	2085	2086
Helium-filled gap	0.747	2046	2049	2058	2070	2079	2085	2086
	0.749	2042	2046	2056	2069	2078	2084	2086
Platinum coating	0.749	2042	2046	2056	2069	2078	2084	2086
	0.769	2005	2012	2031	2056	2071	2079	2081
Capsule holder	0.809	1970	1980	2007	2044	2064	2074	2076
	0.871	1969	1979	2007	2044	2064	2074	2076

Table 5.8. Capsule Temperature Distribution for Opposing Disks as Radiator and Receiver in a 25-kw Heat Source with a Heat Exchanger Surface Temperature of 1200°F and Heat Removal from One-Half Capsule Holder Surface

Material	Radial Position (in.)	Temperature (°F) at Indicated Angular Position						
		θ = 0°	θ = 30°	θ = 60°	θ = 90°	θ = 120°	θ = 150°	θ = 180°
Inner tungsten liner	0.281	1759	1759	1760	1761	1762	1763	1763
	0.301	1757	1758	1759	1762	1764	1766	1766
PuO_2 fuel region	0.301	1757	1758	1759	1762	1764	1766	1766
	0.381	1736	1737	1741	1745	1749	1752	1753
	0.461	1700	1702	1706	1713	1718	1722	1723
	0.542	1674	1676	1682	1689	1695	1699	1701
Outer tungsten liner	0.542	1674	1676	1682	1689	1695	1699	1701
	0.562	1671	1673	1679	1686	1693	1697	1698
Helium-filled gap	0.562	1671	1673	1679	1686	1693	1697	1698
	0.564	1668	1670	1676	1684	1690	1695	1696
Primary wall of T-111 alloy	0.564	1668	1670	1676	1684	1690	1695	1696
	0.651	1666	1668	1675	1683	1689	1694	1695
	0.737	1662	1665	1672	1681	1689	1693	1695
ThO_2 barrier	0.737	1662	1665	1672	1681	1689	1693	1695
	0.747	1655	1658	1667	1678	1687	1692	1693
Helium-filled gap	0.747	1655	1658	1667	1678	1687	1692	1693
	0.749	1651	1655	1664	1676	1686	1691	1693
Platinum coating	0.749	1651	1655	1664	1676	1686	1691	1693
	0.769	1604	1612	1633	1659	1675	1683	1686
Capsule holder	0.809	1560	1571	1603	1643	1665	1676	1679
	0.871	1558	1570	1602	1642	1665	1676	1679

Table 5.9. Capsule Temperature Distribution for Opposing Disks as Radiator and Receiver in a 25-kw Heat Source with a Heat Exchanger Surface Temperature of 0°F and Heat Removal from One-Half Capsule Holder Surface

Material	Radial Position (in.)	Temperature (°F) at Indicated Angular Position						
		θ = 0°	θ = 30°	θ = 60°	θ = 90°	θ = 120°	θ = 150°	θ = 180°
Inner tungsten liner	0.281	1507	1507	1508	1509	1511	1512	1512
	0.301	1506	1506	1508	1511	1513	1514	1515
PuO_2 fuel region	0.301	1506	1506	1508	1511	1513	1514	1515
	0.381	1485	1486	1490	1494	1498	1501	1502
	0.461	1449	1451	1456	1462	1467	1471	1472
	0.542	1424	1426	1431	1438	1444	1448	1450
Outer tungsten liner	0.542	1424	1426	1431	1438	1444	1448	1450
	0.562	1421	1423	1428	1435	1442	1446	1447
Helium-filled gap	0.562	1421	1423	1428	1435	1442	1446	1447
	0.564	1417	1419	1425	1433	1439	1444	1445
Primary wall of T-111 alloy	0.564	1417	1419	1425	1433	1439	1444	1445
	0.651	1415	1418	1424	1432	1438	1443	1444
	0.737	1412	1414	1421	1430	1437	1442	1444
ThO_2 barrier	0.737	1412	1414	1421	1430	1437	1442	1444
	0.747	1404	1407	1416	1427	1435	1440	1442
Helium-filled gap	0.747	1404	1407	1416	1427	1435	1440	1442
	0.749	1400	1404	1413	1425	1434	1440	1441
Platinum coating	0.749	1400	1404	1413	1425	1434	1440	1441
	0.769	1345	1353	1376	1404	1420	1429	1432
Capsule holder	0.809	1293	1306	1340	1383	1407	1420	1424
	0.871	1291	1305	1340	1383	1407	1420	1424

The primary wall temperature variations are approximately 35°F for all the heat sink temperatures, which reduces the magnitude of the capsule stress analysis by permitting a constant-wall-temperature assumption. The circumferential temperature differential of the tubular capsule holders varies from 125 to 100°F over the heat sink temperature range of 0 to 1900°F. These differentials are sufficient to cause a minor warping of the tubes due to thermal stresses, but they are adequately held to limit warpage.

The maximum fuel capsule surface temperature is plotted in Fig. 5.16 for the heat sink temperature range. The curve has the expected trend at the lower heat sink temperatures (i.e., the heat sink temperature is not important). As would be anticipated, the higher temperatures follow an approximately linear relationship.

5.9.2. Heat Exchanger

Analysis of the heat exchanger tubing for pressure loss and heat transfer utilizes the expressions developed from basic assumptions.[1]

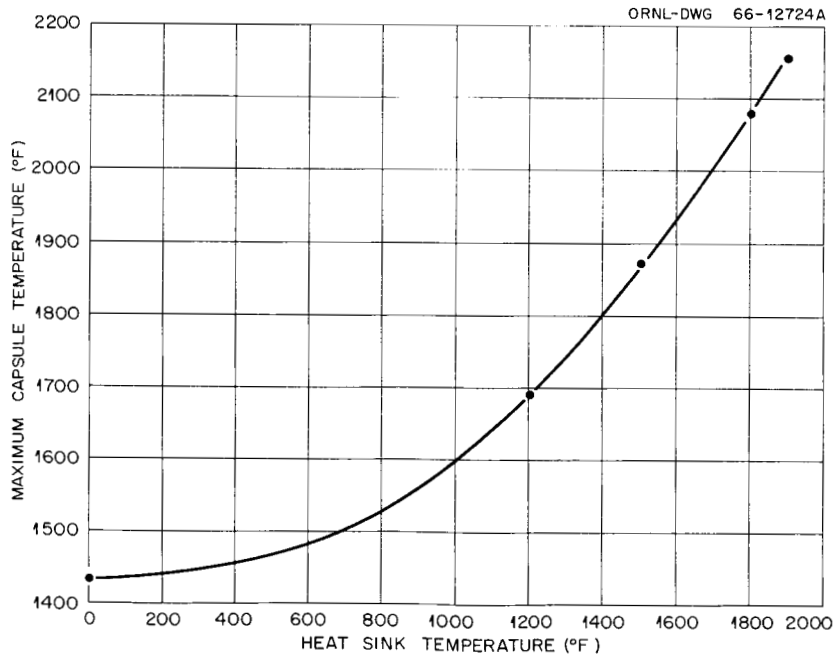

Fig. 5.16. Maximum Capsule Surface Temperature for Opposing Disks as Radiator and Receiver in a 25-kw Heat Source.

Simple modifications of mass flow rate and Prandtl number are required to convert from argon to the helium-xenon mixture. The tubing lengths were established when the decision was made to have approximately equal opposing disks for the radiator-receiver.

The resultant pressure drops are numerically evaluated with additional corrections for the involute curvature[42] and equivalent lengths of straight tube for the bends. The inlet and exit losses are restricted to one-half the theoretical maximum combined value to remain within the guideline of 3% $\Delta P/P$. This restriction requires that the inlets and exits be contoured, which is possible in the design.

The heat transfer coefficient is approximately 300 Btu/hr·ft^2·°F for either coolant in its respective tube size. The physical properties of argon are standard values; the ones for the helium-xenon mixture are calculated values[43] based on the mole fractions and constituent properties.

The circumferential temperature distribution of the heat exchanger tubing was estimated to be one-half that calculated for the fuel-capsule holders. This estimate is based on radiation energy transfer from parallel flat plates with a nonabsorbing medium between them. No conduction is assumed in the maximum deviation of about 50°F and the average value of about 25°F.

5.9.3. Operating Temperatures

The gas enters the heat exchanger at 1089°F and exits at 1500°F in the normal operating mode. The average gas temperature is 1294°F, the gas film drop is 300°F, and the average wall temperature variation is 25°F. These additions make the average sink temperature 1619°F, and the average capsule (determined from Fig. 5.16) will have a maximum surface temperature of approximately 1940°F. The capsules transferring heat to the exit gas temperature could have a maximum surface temperature of 2100°F for a uniform heat flux. The radiator-receiver surfaces are actually separated by 5 in. to permit a nonuniform heat flux so that an almost flat temperature profile will exist over the radiator and receiver surfaces.

The launch pad and orbital emergency mode cooling will see a constant low sink temperature. The sink temperature is immaterial, since it has

little effect on the maximum capsule surface temperature of approximately 1450°F for these essentially uniform heat flux conditions.

The temperatures of the various parts of the reentry body are summarized in Fig. 5.17. The significant temperatures here are those in the area of the HNS and the RTV-60 ablative adhesive; however, these temperatures are well within the limits imposed for both short- and long-term operating temperatures.

ORNL-DWG 66-12719

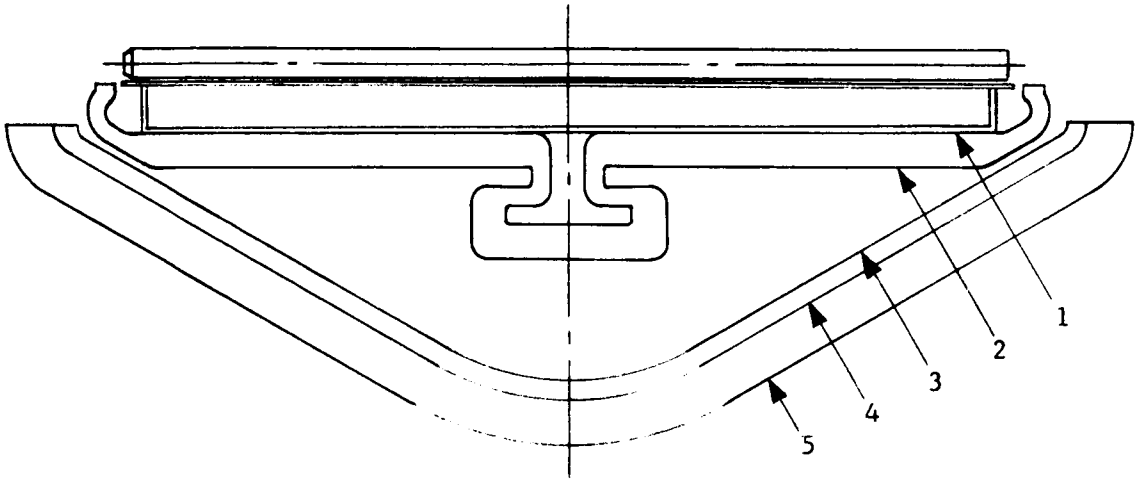

Material	Location	Temperature (°F)		
		Normal Mode of Operation	Emergency Mode of Operation	Launch-Pad Operation
Fuel assembly	1	1735	1150	1400
Insulation	2	154	104	266
Reentry-body structure	3	121	77	189
	4	92	53	175
Reentry-body ablative coating	5	17	5	130
Heat sink		−20	−20	100

Fig. 5.17. Reentry-Body Temperature Distribution.

The temperatures of the insulation surrounding the heat exchangers are 1800°F on the hot surface and 100°F on the cold side during normal orbital operating conditions. These temperatures are 1450 and 150°F, respectively, on the launch pad.

The heat losses from the insulated volume during normal operating conditions in orbit are 50 Btu/hr·ft^2 for the heat exchanger insulation surface and 20 Btu/hr·ft^2 for the recovery vehicle surface. The respective values are reduced approximately one-third during operation on the launch pad. Corresponding heat losses from the labyrinth seal formed by the two insulated subassemblies were also estimated, and the total heat losses are given in Table 5.10 for 3% pressure drop. Composite values show a 4% heat loss in the normal orbital operating condition and a 2% heat loss in the launch-pad operating condition.

The transient temperature behavior of the fuel capsules is an important consideration in the design, and BeO was included to retard the temperature rise by providing a heat sink. An analysis of the system was made for submersion in debris from a launch-pad fire, but this can also be interpreted for launch pad to orbit or from normal to emergency-mode orbital operation.

The major assumption is an insulated system above 2000°F. In the fire environment the capsules receive energy until their temperatures reach 2000°F. In the other interpretations, the initial 3 to 4 min that correspond to the fire immersion are ignored. A correction could be made for initial capsule temperatures below 2000°F, but it is not important in these interpretations.

Table 5.10. Heat Losses from Labyrinth Seal

	Heat Loss (kw)	
	From Crack	From Insulation
During orbit	0.4	0.6
During launch	0.1	0.4

In Fig. 5.18, the maximum fuel temperature, the capsule surface temperature, and the BeO temperature are plotted as a function of time with 100 lb of BeO present. The graph is terminated when the platinum protective coat reaches its melting temperature. In the fire environment, this point is reached at 66 min, which meets the design guideline of a 1-hr submersion in a 2000°F fire.

An interpretation for a 30-min insertion into an earth orbit reveals that the fuel capsules reach a tolerable maximum surface temperature of approximately 2600°F. Another interpretation for deployment of the reentry body to change from the normal to the emergency mode of operation

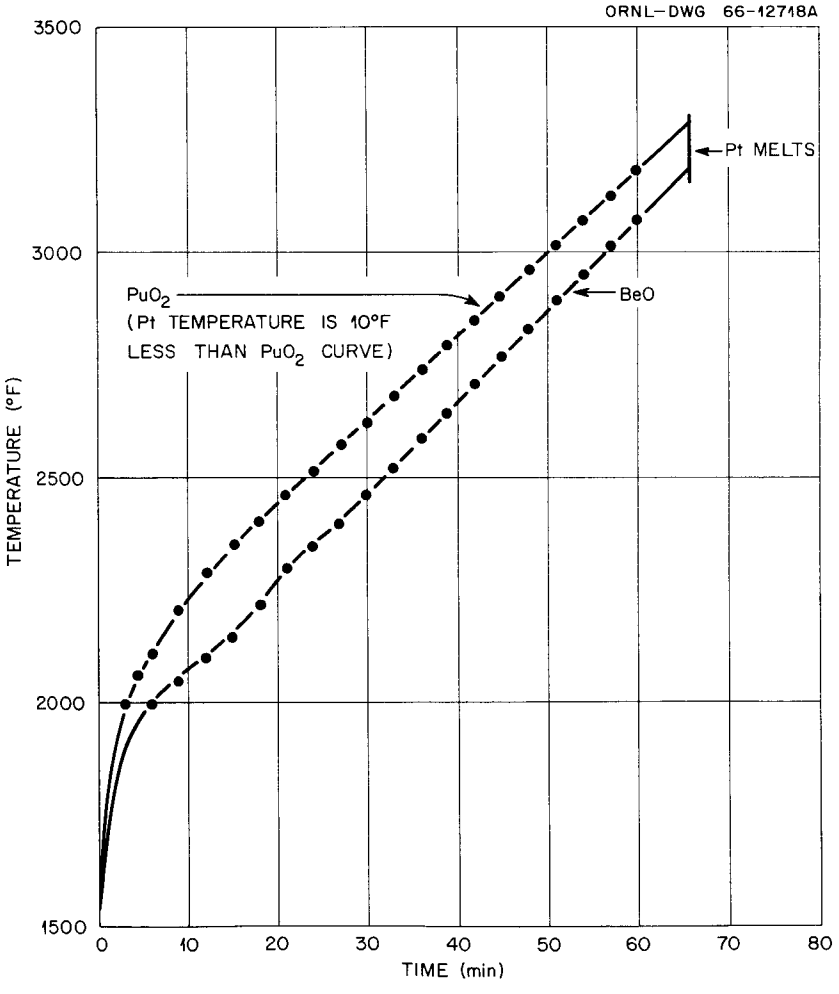

Fig. 5.18. Launch-Pad Fire Temperature for the BeO Heat Sink, Fuel, and Capsule Surface.

can be made which shows that a relatively slow movement will not raise the maximum capsule surface temperature appreciably.

The reentry body is designed to accept up to 300 lb of BeO if it is desired to increase the heat capacity for greater temperature retardation. For 300 lb, the terminal ballistic coefficient would be 90 and the impact velocity would be 280 fps; for 100 lb of BeO, these values are 78 and 250 fps, respectively. The added penalty may be necessary if a time lag is required before the SLA is opened after orbit is achieved.

6. LOGISTICS OF FUELING

6.1. Capsule Fueling Facility Requirements

The primary requirements in the design of a capsule fueling facility are that (1) the radioactive material must be completely contained at all times, (2) the radiation exposure to personnel must be limited to standard operating limits as imposed by the AEC or, in some cases, the state licensing agencies, and (3) the radioisotope fuel must be maintained in a subcritical form at all times. Since the plutonium fuel emits alpha, neutron, and gamma radiation, remote-handling facilities provide the most practical and least hazardous method of containment.

Fig. 6.1 shows a basic facility that would be capable of encapsulating 25 kw(th) of $^{238}PuO_2$ fuel in a two-month period. It is assumed that the $^{238}PuO_2$ microspheres would be prepared at some other location and shipped to this facility for encapsulation. The facility consists of seven shielded cells (1 through 7 in Fig. 6.1) equipped for remote operations, a normal operating gallery for personnel, offices, a flame-spray area, a final inspection area for the unfueled capsules, and storage areas for miscellaneous parts, tools, etc. A restricted work area in back of the cells can accommodate both lift trucks and personnel for loading and unloading carriers into the cell bank and for removing waste from the cell-block area. This restricted area is also an access area for direct maintenance of the cells.

Each of the seven cells is equipped with a $ZnBr_2$ shielding window, which provides shielding equivalent to that of a 2-ft-thick normal concrete wall. A pair of master-slave manipulators is installed in each cell facing the operating gallery. A sealed intercell conveyor connects all cells so that the fuel and capsules can be transferred from cell to cell remotely. A waste load-out facility (located in the rear of the middle of the cell block) allows waste from the cell-block area to be loaded directly into a shielded carrier-loading station for removal.

Two feet of standard concrete (density, 2.3 g/cm^3) is provided for shielding on the front and top of the cells. The inside of the cell is

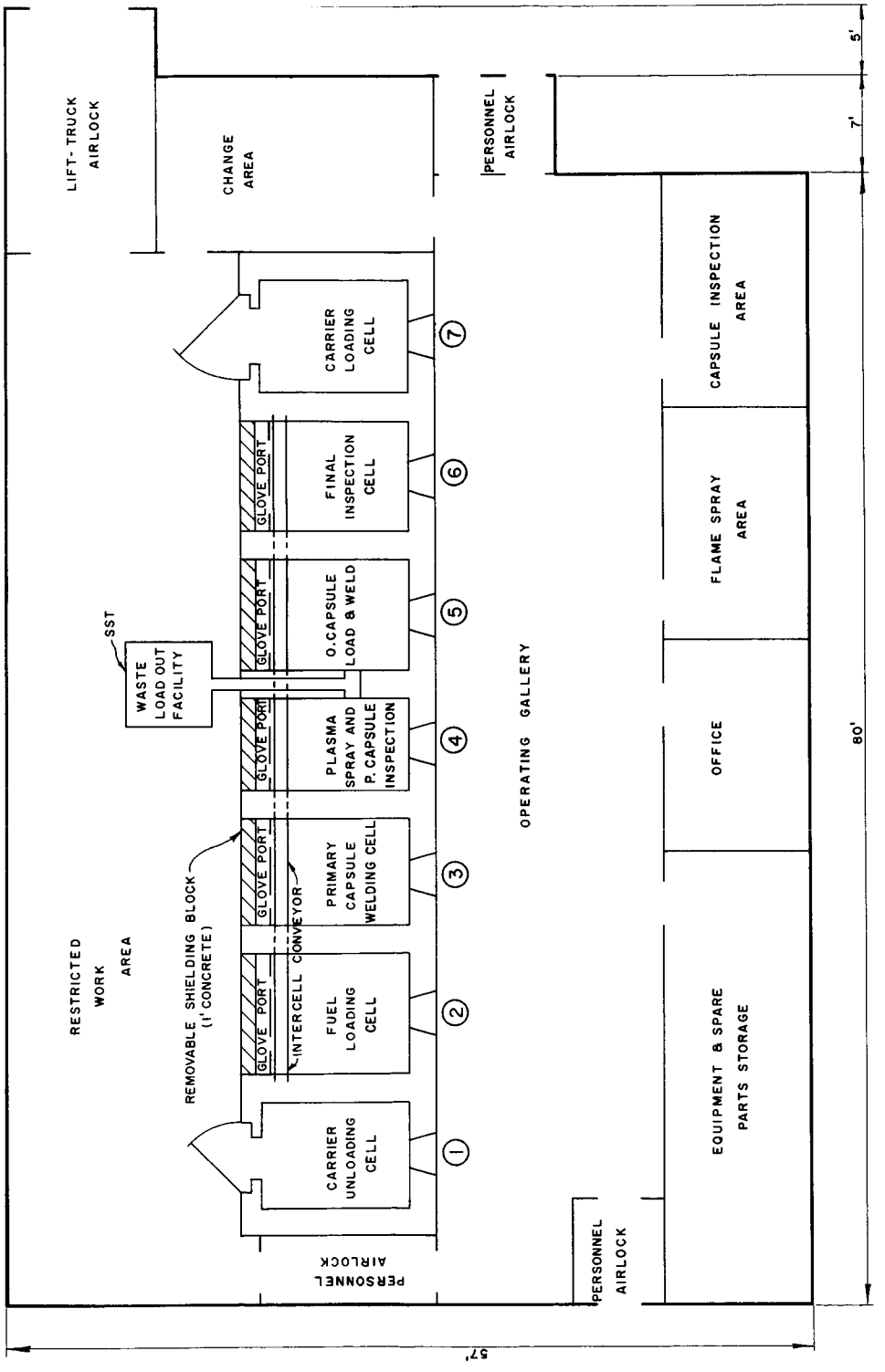

Fig. 6.1. Basic Facility Required for $^{238}PuO_2$ Encapsulation for 25 kw(th) Brayton-Cycle System.

lined with stainless steel to facilitate decontamination. The two carrier-loading and -unloading cells (1 and 7 in Fig. 6.1) are similar to the others except for the backs of the cells. These two outer cells have a permanent shielding wall in the rear with a shielded door that can be opened to permit direct access for carrier installation and removal. All cells are 14 ft high and 10 ft deep; however, only 8 ft of the depth in the inner cells is usable for remote operations. Cell widths vary from 6 to 9 ft.

This cell design combines the advantages of remote cell operation with the advantages of direct maintenance by utilizing glove ports and the load-out facility in the rear of the cell. During the fuel encapsulation period, or other periods of peak radiation levels, a removable 1-ft-thick concrete shielding wall is located at the rear of the five inner cells to provide additional radiation protection. If equipment malfunction should occur and direct access is required, the fuel and capsules would be removed from the cell through the intercell conveyor, the cell would be decontaminated to a low level, and the shielding wall in the rear would be removed so that access to the cell could be made through the glove ports. Capsules and other small objects would be passed into the cells in this manner.

All operations are carried out under at least double containment to insure that there will be no spread of contamination to the surroundings. After fuel is removed from the shipping container, the cells provide the first line of containment, and they are maintained at a slightly negative pressure relative to the building itself. Air flow is only in one direction — toward the cells. Since the fuel will be in the microsphere form (shown by Mound Laboratory to contain the activity well, with very little smearable activity detectable), a second containment glove box within the cell, which is a common practice with alpha-radiation-emitting materials, is not considered necessary. The building, which is the second line of containment, is maintained at a slightly negative pressure relative to the outside atmosphere. Air locks are located on all building entrances.

For normal operation in a remote cell, the radiation level should be maintained at less than 1 mrem/hr on the operating front of the cell

or, in case of a maximum source of radiation for a short period of time, at approximately 3.0 mrem/hr. The basic operating plan for this facility is based on the maximum amount of fuel in a cell at one time being limited to ten capsules per cell or approximately 2830 g of ^{238}Pu. However, the radiation shielding is based on a value that is double this "normal" limit, or 20 capsules (5660 g of ^{238}Pu), since delays might occur during processing that would result in a buildup of material in one particular cell. The only exception to the ten-capsule limitation will be in the carrier loading and unloading cells (1 and 7 of Fig. 6.1), which will handle up to 40 capsules at one time. Extra shielding will be provided in the equipment for these cells to limit the total radiation dose rates to the 1- to 3-mrem/hr values.

Since the plutonium fuel emits alpha, gamma, and neutron radiation, all three types of radiation have to be considered. All cells will have alpha-type sealing to prevent the release of activity to other cells or to the building itself. The shielding requirements are based on a total of less than 1 mrem/hr from fast neutrons, gamma radiation from decay and fission of ^{238}Pu, and capture gamma radiation in the shielding material. For the maximum dose rates, it was assumed that the source is a point source with a minimum separation of 1 m between the source and the person receiving the dose. For two cases, the fuel in bulk microsphere form and the fuel in encapsulated form with a maximum concentration of 5660 g ^{238}Pu (20 fueled capsules), the total unshielded dose rates 1 m from the source are 396 and 38 mrem/hr, respectively. The shielding provided by the capsules themselves reduces the total dose rate from the encapsulated fuel. For both these cases, 2 ft of ordinary concrete will reduce the radiation level to less than 1 mrem/hr.

Since the rear of the cell bank is a restricted area and only relatively short exposure periods are permitted, higher dose rates can be tolerated in this area. If maintenance work with the glove ports at the rear of the cell was required and the fuel was already loaded into the capsules, the capsules could easily be removed to another cell before starting the maintenance operation. If the fuel was not encapsulated, the cell could be decontaminated before the shielding wall was removed.

It is expected that contamination in the cell could be reduced to acceptable radiation levels with a minimum amount of decontamination. Even if 1 kg of microsphere fuel were present, the total dose rate at the face of the glove port from a source 1 m away would be only 70 mrem/hr, which is low enough for regulated short-time-exposure work.

As noted previously, the five inner cells will have to be maintained under an inert-gas atmosphere to insure that the refractory metal components of the capsule assemblies are not damaged by reactions at elevated temperatures with air and associated impurities. From an operational standpoint, it will probably be best to also operate the cells at each end of the bank under an inert-gas atmosphere, although they can be operated in an air atmosphere if airlocks are installed between them and the adjoining cells. Either helium or argon can be used for the inert gas; however, the purification system used would depend upon the choice made. In the case of argon, the gas from the cells would be circulated through a dryer and then through a series of chemical reactors containing reactive metals; for example, uranium, copper, or titanium chips and chemical sorbtion agents. With helium, a more satisfactory arrangement consists of circulating the gas through a chemical dryer and then through a liquid-helium-cooled trap to freeze out contaminants. With either system, it is possible to maintain impurity levels in the 5 ppm or lower range. The inert-gas system will operate at about 2 in. H_2O below atmospheric pressure for contamination containment protection in the event a leak develops in one of the cells or the piping. When the cells are not in use for capsule-fueling operations, the inert-gas system can be shut down and the cells valved into a regular cell ventilation system to maintain them under negative pressure.

The building housing the cells will be kept at a slightly negative pressure with respect to the outside (~0.5 in. H_2O below atmospheric) by means of local exhaust fans. All air exhausted from the building will pass through absolute (CWS-type) filters before discharge to the atmosphere through a stack.

In addition to the ventilation services, each cell will be equipped with the necessary electrical, cooling water, and radioactive drain services.

6.2. Capsule Fueling and Inspection Procedure

The bulk fuel shipments will be unloaded into cell 1 (see Fig. 6.1), the Brayton-cycle fuel capsules will be assembled and inspected in cells 2 through 6, and the fueled capsules will be reloaded into the same shipping containers in cell 7 for shipment to the launch site. Each cell will be equipped to provide inert-gas atmospheres, and special cooling-station facilities will be located in each cell to prevent overheating of the fuel or capsules during assembly.

The flow diagram for the capsule assembly is shown in Fig. 6.2, and the procedural steps (by cell) are described in Sections 6.2.1 through 6.2.7.

6.2.1. Cell 1 – Carrier Unloading Cell

1. Unload carrier inner container into recirculating water tank.
2. Unload bulk fuel capsules as required.
3. Inspect capsules.
4. Assay capsules with calorimeter.

The fuel is shipped to the site in four carriers (described in Sect. 6.3) designed to meet all ICC and AEC shipping requirements. Each carrier handles approximately 16 kg of $^{238}PuO_2$ microspheres contained in eight Hastelloy X capsules (~1.5 in. in diameter and 10 in. in length) positioned in an inner container. When the carrier is received at the fuel encapsulation facility, it is placed in the limited access area back of cell 1. The inner container is lifted from the shipping carrier and placed in cell 1 in a recirculating-water tank that provides both shielding and cooling for the fuel.

The bulk fuel capsules are removed, inspected for shipping damage, assayed by means of a calorimeter to determine the quantity of fuel in each capsule, and loaded back into the container. As needed, the fuel capsules are removed and transferred to the fuel loading cell (cell 2) by the intercell conveyor. Processing of two bulk fuel capsules per day is required to maintain the two-month facility schedule.

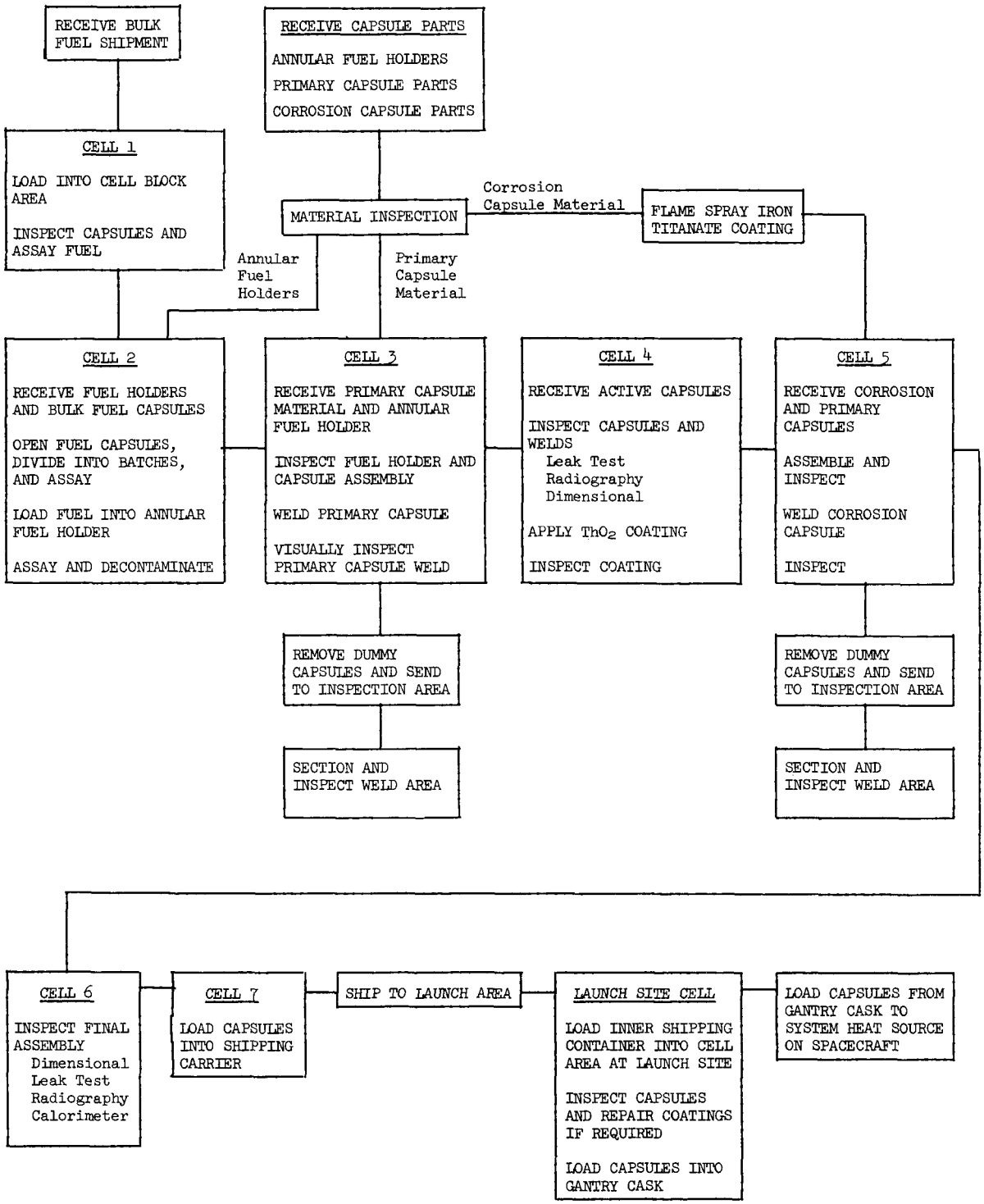

Fig. 6.2. Flow Diagram for $^{238}PuO_2$ Capsule Assembly.

6.2.2. Cell 2 – Fuel Loading Cell

1. Open bulk fuel capsule.
2. Separate microspheres into batches by weight and size measurement.
3. Check wattage output of each batch by calorimeter.
4. Load fuel into inner tungsten annular fuel holder (vibrating compaction).
5. Press fit annular fuel-holder cap into place.
6. Check wattage output of filled annular fuel holder.
7. Decontaminate outside of fuel holder.

When the two bulk fuel capsules are received in cell 2, they are opened by a remotely operated tube cutter, and the microspheres are separated into different sizes. After a predetermined microsphere size blending, which will result in the required packing at 80% of theoretical density, the fuel is separated by weight measurement into ten portions, with each containing 157 w of fuel. To check the weight measurements, each portion is assayed by a calorimeter to verify its 157-w thermal output before it is loaded into the inner tungsten fuel holder and packed (by means of a vibratory compactor). The annular fuel-holder cap is then press fitted into the top of the holder by means of a special remotely operated clamping device. After the fuel has been loaded, the wattage output of the holder is checked by calorimeter measurements to determine whether any losses occurred during the fueling operation. After all the above steps have been completed for ten fuel holders, each holder is visually checked, decontaminated on the outside, and placed in a special cooling block (to prevent excessive heating of the fuel in the tungsten holders) for transfer to the primary capsule loading and welding cell (cell 3).

6.2.3. Cell 3 – Primary Loading and Welding Cell

1. Check dimensions of annular tungsten fuel holder.
2. Load fuel holder with spacers into bottom half of primary capsule.
3. Check dimensional clearance at top of fuel holder.

4. Load primary capsule bottom into remote welder.
5. Insert top of primary capsule.
6. Weld joint with remote electron-beam welder.
7. Visually check weld area.

Before the annular holders are transferred from cell 2, ten primary capsule assemblies and two dummy capsule assemblies, which have been checked in the inspection area outside the cell block and determined to be within dimensional tolerances, are loaded into the cell through the glove ports in the rear of the cell. When the annular fuel holders are received, they are also checked with go—no-go gages to determine whether they are still within dimensional tolerances. A fuel holder, together with top and bottom spacers, is then placed in the bottom section of a primary capsule. The clearance between the top of the spacer and the edge of the capsule bottom is dimensionally checked to insure that there is sufficient clearance to allow the primary capsule top, with its lip, to seat properly on the bottom section for welding purposes.

The assembled primary capsule section (bottom) is then loaded into a remotely operated electron-beam welder, the primary capsule top is inserted into the capsule, and the welder is sealed. The welding system is evacuated to 10^{-4} to 10^{-5} torr, and the capsule is sealed under vacuum by a full-penetration electron-beam weld. Inert atmospheres and cooling blocks will be used to maintain the temperature of the capsules at levels that will prevent damage.

After each capsule has been welded, the weld area is visually checked for defects (e.g., excessive thickness, visible pinhole leaks). Before and after each set of ten active capsules is welded, a dummy capsule simulating the active capsules is welded, removed from the cell, sectioned, and examined to determine that satisfactory full-penetration welds are being achieved. When ten active capsules have been successfully welded, they are transferred to the weld inspection and plasma spray cell (cell 4).

6.2.4. Cell 4 — Weld Inspection and Plasma Spray Cell

1. Leak test primary capsule weld.
2. Check weld area.

3. Dimensionally check primary capsule.
4. Load capsule into plasma spray apparatus.
5. Apply ThO_2 coating on primary capsule.
6. Dimensionally check coating.

Additional quality control methods are employed in cell 4 as a further check on the capsules. Each active capsule is helium mass-spectrometer leak tested to insure that it is completely sealed. It is anticipated that either ultrasonic or radiographic weld inspection may be a quality control requirement. Finally, the primary capsules are checked dimensionally by go–no-go gages to verify that they are still within dimensional tolerances. After the primary capsules have successfully passed all the inspections, a 10-mil coating of ThO_2 is applied to the outer surface of each capsule by remote flame-spraying techniques. Capsules are then inspected and dimensionally checked with go–no-go gages to insure the evenness of the ThO_2 coating. During the time the capsules are not being inspected or coated, they are maintained at low temperature by means of cooling blocks. The processed capsules are removed to cell 5.

6.2.5. Cell 5 – Corrosion-Resistant Capsule Loading and Welding Cell

1. Load primary capsule into corrosion-resistant capsule bottom.
2. Dimensionally check capsule.
3. Load corrosion-resistant capsule bottom into remote TIG (tungsten inert gas) welder.
4. Insert corrosion-resistant capsule top.
5. TIG weld platinum corrosion-resistant capsule joint.
6. Visually inspect weld.

As in cell 3, the platinum outer corrosion-resistant capsules will be placed in the cell through the cell glove ports before the primary capsules are transferred into the cell. These corrosion-resistant capsules already have a 2-mil coating of iron titanate on the outside surfaces, except for the immediate weld joint area.

The welding procedure is the same as the one used for the primary capsule, except that a TIG welding process is used instead of the electron-beam welding process. After each capsule is welded, the weld area is visually inspected for imperfections. As in cell 3, dummy capsules

are welded before and after each set of active capsules for a quality control check. Completed active capsules are transferred to the final inspection cell (cell 6).

6.2.6. Cell 6 – Final Inspection Cell

1. Dimensionally check final capsule.
2. Helium leak test final weld area.
3. Make final calorimeter check.

Capsules are helium leak tested to determine that a leak-tight weld was made on the platinum outer capsule. Each assembly is dimensionally checked with go–no-go gages, and the thermal output is measured by a calorimeter. After all quality-control inspections have been made, the capsules are removed to the carrier loading cell (cell 7).

6.2.7. Cell 7 – Carrier Loading Cell

1. Perform shelf-life quality-control test.
2. Leak test capsule.
3. Load capsules into shipping carrier (each carrier will handle 40 capsules).
4. Remove shipping carrier from cell.
5. Insert in large shipping container for shipment to launch site.

Each batch of ten completely assembled and inspected capsules transferred to this cell is given a shelf-life test (several days) and again helium leak tested to determine whether aging had any effect. After this test the capsules are loaded into the inner shipping container, which is stored in a recirculating water bath until it is fully loaded (maximum capsule loading, 40 capsules). When loading has been completed, the inner container is removed from the cell and inserted into the large shipping container (located at the rear of the cell), and the carrier is then shipped to the launch-site fuel-handling facility.

6.2.8. Launch-Site Fuel-Handling Facility

As each shipping container is received at the launch site, it is placed in a cell equipped for remote operations, and the inner container is removed. The capsules are removed and inspected for any shipping

damage. Facilities in the cell will include helium leak test equipment and a flame-spraying device for touching up the iron titanate outer coating if this is necessary. After the final inspection, the capsules are loaded into a gantry carrier, transferred to the launch site, and inserted into the heat-source holder in the Brayton-cycle system of the spacecraft.

6.3. Shipping Cask Design

6.3.1. Regulations Governing Carrier Design

A special shipping container will be required to handle the transfer of bulk fuel to the encapsulation facility and to ship the fueled capsules to the launch site. The specific AEC and ICC regulations governing such shipments are outlined in AEC Manual Chapter 0529; Chapter 10, Part 71, of the Code of Federal Regulations (10 CFR 71);[44] and ICC Tariff No. 15 (Ref. 2).[45] Subpart C of 10 CFR 71 provides the general standards that must be incorporated in the design of a shipping container. The specific standards that would be applicable to a container for shipping large quantities of ^{238}Pu fuel are included in the following paragraphs:

71.31 General Standards for all Packaging

71.32 Structural Standards for Large Quantity Packaging

71.33 Criticality Standards for Fissile Material Packages

71.34 Evaluation of a Single Package

71.35 Standards for Normal Conditions of Transport for a Single Package

71.36 Standards for Hypothetical Accident Conditions for a Single Package

71.40 Specific Standards for a Fissile Class III Shipment.

(See the Appendix for a reprint of specified paragraphs.)

6.3.2. Proposed Carrier Design

Figure 6.3 shows a shipping container design that will meet all AEC and ICC requirements for shipping large quantities of ^{238}Pu, either as bulk fuel or as fabricated capsules. This carrier has a loaded weight of approximately 6000 lb and will handle a maximum of 40 fueled capsules

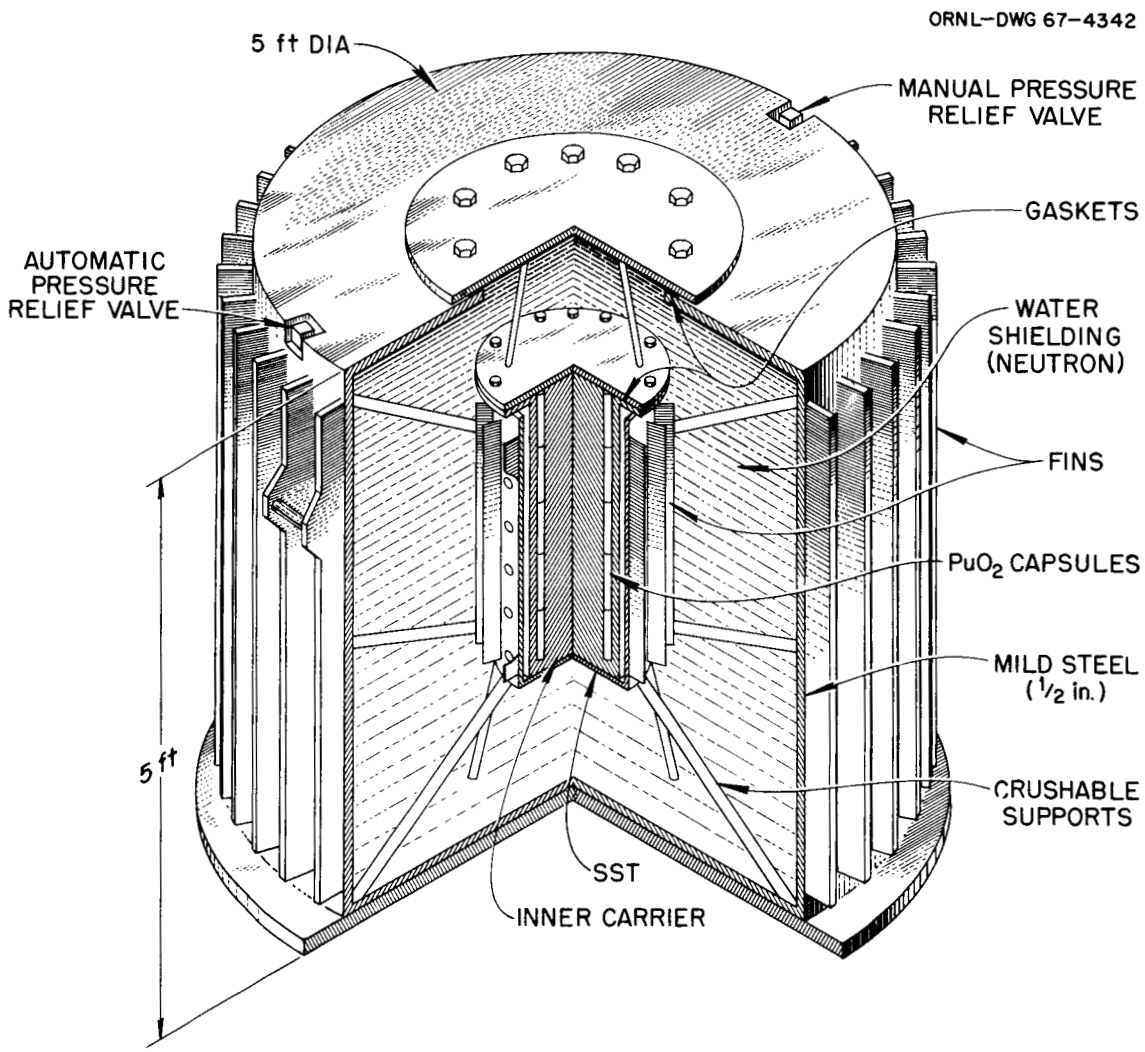

Fig. 6.3. Shipping Carrier for Bulk Shipment of PuO_2 Microspheres and Fueled PuO_2 Capsules.

or about 6 kw(th) of bulk fuel per shipment. Four carriers of this type will be required to handle the 24.5 kw(th) source material required for the Brayton-cycle heat source. The carrier is 5 ft in diameter and 5 ft in length and consists of two parts: an outer carrier of 1/2-in.-thick mild steel, which provides neutron shielding during shipment by being water filled, and an inner container that is easily removed and can be utilized for loading and unloading capsules and bulk fuel containers in the cell areas at the various sites.

The inner container is a solid stainless steel body (~12 in. in diameter and 32 in. in length) with a gasketed flange at the top to prevent water in-leakage. Eight holes, 31 in. deep, are drilled 1/2 in. from the outer circumference. These holes provide space for up to 40 capsules or 8 bulk fuel capsules per shipment. When loaded into the larger shipping carrier, the inner fuel-capsule holder will rest in a stainless steel framework that has several small holes to provide water circulation around the holder. Angle-iron framing is used to hold the center section in place and is considered to be an energy-absorbing crushable member in case of an accidental impact. The neutron shielding for this carrier is provided by the 2 ft of water. The gamma shielding is provided by the steel supporting structure on both the inner and the outer containers.

In general the shipping container was analyzed by the method outlined by Shappert.[46] The carrier is heat limited rather than radiation limited. Only 6 in. of water is required to reduce the radiation dose to the ICC specifications — 200 mr/hr at any accessible surface area or 10 mr/hr at 1 m; however, the diameter required to lower the surface temperature of the carrier to less than 180°F with 100°F ambient air is 5 ft. Fins are utilized on both the outer surface and the inner container to provide an additional heat transfer area. Using the additional water shielding, the dose rate at the surface of the carrier will be 2 mr/hr and at about 3 ft, 0.3 mr/hr, which is well below ICC requirements.

Under normal shipping conditions, the carrier will meet all the outlined structural requirements (§71.31 through 71.36 of 10 CFR 71). With a surface temperature of 180°F, the maximum expected temperature of the water in the shield is approximately 200°F, and the maximum temperature at the center of the carrier will not exceed 800°F, which is well below the critical point for capsules or carrier components.

Under the hypothetical accident conditions outlined in §71.36, the carrier would remain essentially intact but would probably break a weld seam. This could result in loss of the water. Even if this should occur, the temperature at the center of the carrier would not exceed 1300°F during the "fire condition," which was considered to be the most adverse. With the loss of the water shielding, the total dose rate at 3 ft would

be 20 mr/hr, which is still well below the 1000 mr/hr allowed in the regulations.

The ^{238}Pu will remain subcritical under all conditions specified in the regulations (§71.33 and 71.40) for normal shipment and in case of a shipping accident. None of the specified situations will result in the release of the fuel from either the Brayton-cycle capsules or the bulk-fuel Hastelloy capsules, and without release of fuel, the fissile material will remain subcritical under all conditions.

6.4. Gantry Fueling Fixture

Fueling of the heat source can be accomplished either by transporting individual fuel capsules or groups of capsules to the fuel plate in the reentry body after it has been installed aboard the launch vehicle, or the entire fueling can be done in a shielded cell located near the launch pad and the reentry body—fuel plate assembly transported to the launch vehicle and attached as a unit to the reentry-body support ring. Fueling of the fuel plate assembly prior to installation aboard the spacecraft has the advantages of minimizing interference with other launch-pad operations and probably also would result in the shortest time period during which radioisotopes were aboard the spacecraft prior to launch. However, because of its large dimensions and high temperature after fueling, the reentry-body shell—fuel plate assembly would have to be transported in a large inert-gas-filled and -cooled container in order to prevent damage to the components.

Fueling with groups of capsules after the reentry-body shell—fuel plate assembly has been installed aboard the spacecraft can be carried out with less bulky equipment, although auxiliary cooling will still be required during transport of small groups of capsules to the launch pad, since the surface temperature of a single capsule is about 1200°F (Sect. 5) at this time. Figure 6.4 is a conceptual drawing of a fueling fixture for loading up to eight capsules at one time. A number of capsules corresponding to the number that will fit into one tube in the fuel plate are loaded into the transfer-loading cask in a handling cell located at the launch site. The transfer-loading cask is mounted on a transport dolly

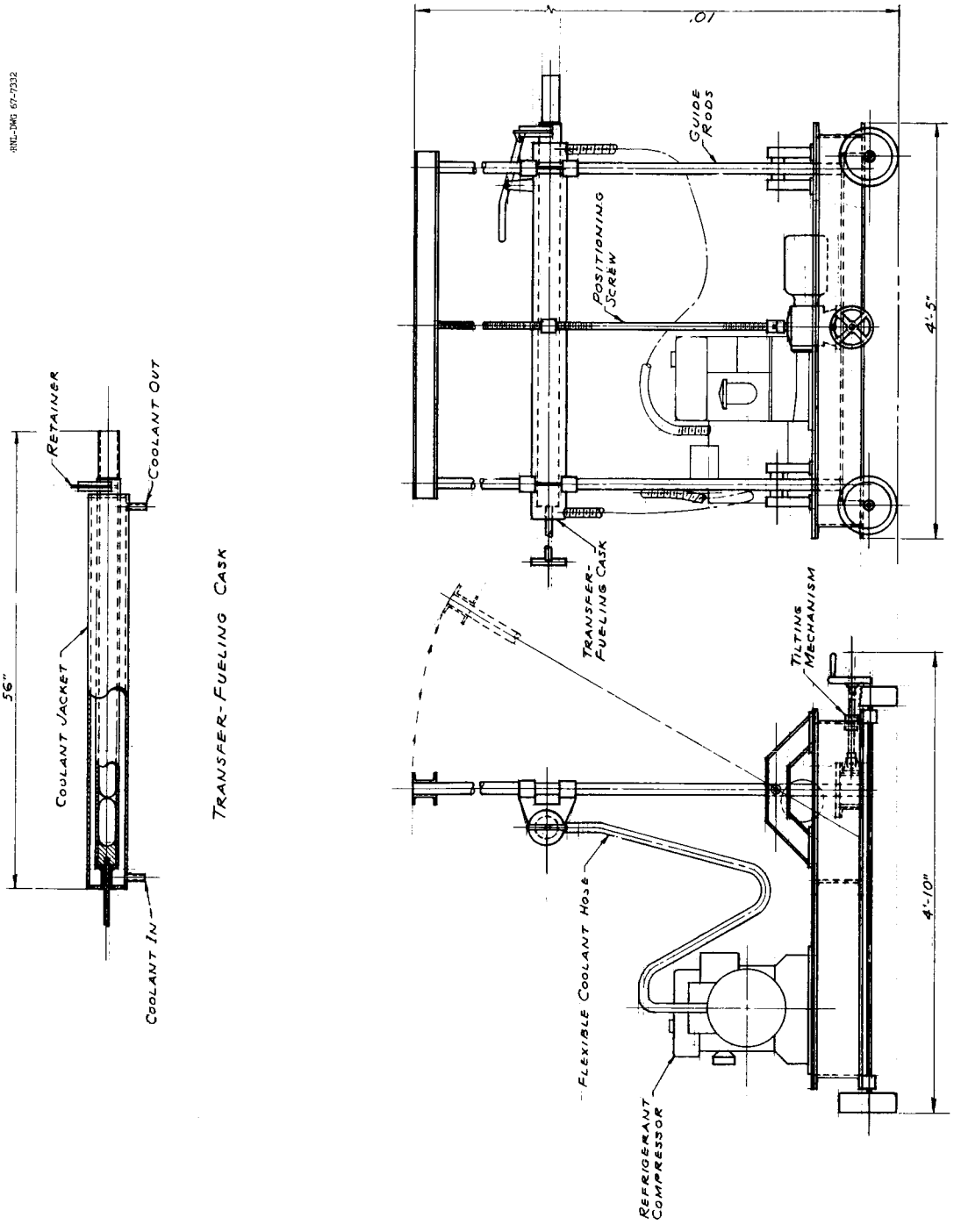

Fig. 6.4. Gantry Fueling Fixture.

along with a motor-driven refrigerant compressor, which feeds coolant through the cask. When the dolly is positioned for loading, the cask is brought to the elevation of the fuel-plate tube to be loaded by a motor-driven positioning screw. In the loading position, the reentry body–fuel plate assembly will be swung out at an angle from the side of the launch vehicle (Sect. 5, Fig. 5.10), so a tilt mechanism is provided to align the extension on the end of the transfer-fueling cask with the end of the fuel-plate tube to be loaded. When the end extension and fuel-plate tube are mated, the capsules are slid into the tube by a manually operated push rod.

A more complete definition of the expected prelaunch operational countdown is necessary before a decision can be made as to the best method of fueling. Fortunately, as noted in Section 4, only minimal shielding, if any, is needed during the loading operations. However, the temperature of the capsules and fuel plate is an important problem during fueling. If launch-pad operations require that the fuel not be put aboard until quite close to launch (<8 hr), it will probably be necessary to design a loading fixture that can install the prefueled reentry body–fuel plate assembly as a unit. In either case, it will be necessary to keep an inert-gas purge around the loaded fuel plate to prevent damage to the emissive coating and Cb–1% Zr alloy.

7. RESEARCH AND DEVELOPMENT REQUIREMENTS

The research and development requirements are related to the validity of specific assumptions made in connection with some of the data used in the preliminary design of the heat source. As already pointed out, the design makes considerable use of what is judged to be near-future technology, and efforts are necessary to progress to a usable technology. It is recognized that all the design data could be further refined, but this discussion is, for the most part, limited to research and development and design data changes that could lead to significant revisions in the heat-source design. What is formulated is not an overall development plan but, rather, an identification of those design assumptions known to require further investigation.

The significant problems are in the fields of materials and aerodynamics and not in areas of nuclear physics, such as shielding or criticality. The materials problems are present because only a small body of short-time data exists that covers the properties of T-111 alloy, the main structural alloy for the multilayer fuel capsule, and there are also very few data on the compatibility of the many materials, including the fuel, which are used in construction of the capsule. In allowing for possible loss under extreme emergency conditions, the capsules are designed as well as possible for hundreds of years of life in air, earth, or seawater. It is hoped that a reasonable estimate of the value of the chosen concept has been provided by applying available data, but investigations in the problem areas would provide the basis for a greater degree of confidence.

The performance of the reentry vehicle in the passive extreme-emergency reentry mode is based on a combination of data from experiments with other vehicles and aerodynamic calculations. Further investigations must be conducted to better evaluate its integrity during reentry heating, its terminal velocity, its landing attitude, and methods to prevent deformation of the fuel capsules.

Specific recommendations for research and development are the following.

1. Plutonium Fuel Form. In the preliminary design, PuO is the designated form of the ^{238}Pu fuel. At the operating temperature of the capsule it could well be that the stable form of the fuel has less oxygen than PuO_2; for example, a mixture of PuO_2 and Pu_2O_3. If this were the case, the microspheres might be partly disintegrated by loss of oxygen over a long period of time to produce a fine powder, which could migrate from the vented tungsten annular holder to the T-111 alloy, with which it might not be compatible. The oxygen evolved would react with the refractory metal capsule materials. It is therefore important to determine the stable form of the oxide so that this form can be utilized for loading the capsules.

2. Bulk Density of Fuel. The volume and weight of the isotope heat source is extremely sensitive to the bulk density of the fuel form. In the preliminary design, the fuel was assumed to be PuO_2 at 80% of its theoretical density, a bulk value which has been attained at ORNL with packed microspheres produced by the sol-gel process. Research and development must not only be oriented toward producing a stable fuel form but also one that provides an acceptable density of plutonium.

3. Primary Capsule Strength. The primary structural material for the capsule is a new alloy, T-111. Large research and development programs are in progress on this material and other closely related tantalum alloys. Currently there is only a small amount of data on its mechanical strength, and these data were obtained from simple uniaxial constant-stress constant-temperature short-term experiments. The longest experiment has been 10,000 hr (Sect. 3).

These meager data have been used to design capsules for five years of service with varying temperature and internal gas pressure and for impact resistance during an emergency landing. The capsules also comply, insofar as we can calculate, with a guideline of ten half-life containment under all credible accident conditions; for example, loss due to burial of individual capsules in earth or immersion of the entire reentry vehicle in seawater. If buried in earth, a capsule would be subject to creep due to helium pressure for approximately 50 years before cooling to a temperature below the creep range for the alloy.

If the creep rate in service is too high, there is a possibility that the protective platinum cladding may be unduly thinned or ruptured. Yield of the capsule in an emergency impact could lead to rupture of the T-111 alloy or to a rupture of the platinum cladding. Creep greater than expected over a period of years in a lost capsule could also lead to rupture. Although Section 3 shows that reasonable methods have been devised to conduct the preliminary design work, it also states that additional and long-term data are necessary to confirm and improve the usefulness of such methods.

Data must be acquired to check the applicability of the life-fraction summation assumption and modified Larson-Miller parameter that has been used and to evaluate the need for any revisions required because of time-hardening, strain-hardening, or other effects that could lead to significant changes from the postulated behavior of the alloy. Preliminary plans can be made for a data-acquisition program for obtaining sufficient information to design capsules with a specified reliability, but the programming should be modified from time to time on the basis of analyses of the significance of the results.

These mechanical property investigations would include temperature and stress cycling and biaxial stressing of the alloy. An indication of how long to test can be obtained from examination of the data on T-111 and other alloys (Sect. 3) and an analysis of the T-111 alloy results as they are obtained. However, it is advisable that in addition to such statistically programmed testing, some ultra long-term testing, such as 50-year tests, should be commenced. The early behavior of the specimens, in perhaps five years, and their eventual behavior would help settle the kinds of materials questions that have always been moot.

In the presently designed capsule the weld closure is made in 175-mil material. To date only a few welding experiments have been conducted on T-111 alloy, and these have been on thinner samples. An adequate welding procedure for the capsule must be developed.

4. Thoria Diffusion Barrier. Research and development must be conducted to demonstrate a method for maintaining an intact thorium layer between the T-111 alloy and the platinum outer layer during both normal service and emergency conditions.

5. Platinum Strength. It must be determined that the layer of platinum, which protects the T-111 alloy from oxidation by air or corrosion by seawater under emergency conditions, is sufficiently ductile to withstand the impact on landing without rupture.

6. Heat Transfer. The volume and weight of the heat source are quite sensitive to the emissivity of the iron titanate surfaces. Research is necessary to determine whether the high values for emissivity used in the preliminary design can be retained for a year of normal operation in vacuum.

Another uncertainty involving heat transfer is whether Superinsulation has enough strength in compression to provide the entire support for the fuel plate, as is the case in the preliminary design. Penetration of the heat insulation with supplemental supports could lead to deterioration of the bond between the aluminum and the phenolic resin serving as the ablative material on the reentry body because of higher temperatures that would result from the higher heat losses through the reentry body.

7. Reentry-Body Performance. The aerodynamics of fins or fences used to provide turn around for the reentry body are not well known. The back-side heating, hypersonic drag coefficient, subsonic drag coefficient, and cratering calculations are not as suspect, but they are so important to the design concept that further verification must be obtained. The subsonic stability and therefore the landing attitude is open to some question, and further experimental and computer studies are required.

Research must also provide assurance that the reentry body, fuel-plate assembly, and capsules have the ability to absorb sufficient energy to protect the capsules from the impact of an emergency landing. The calculations in Section 3 are made on the basis that this is the case, and experimental verification of the calculated performance is required.

8. Materials Compatibility. As described in the phase I report, compatibility of the fuel with the tungsten liner is based on calculations of free-energy changes occurring in reactions between pure compounds, rather than on any experience with actual impure fuels under service conditions. Experiments on fuel-liner compatibility must be conducted. It is also necessary to check the compatibility of the T-111 alloy with both tungsten and the thoria diffusion barrier.

Data on the stability of platinum in air and seawater provide the means for making some of the less uncertain extrapolations to ultra-long periods of time. The stability of platinum if buried in some types of soils is open to serious question, however, and must be investigated. As described in the phase I report, there are no orderly data on platinum stability in soil, but many materials that are known to react with platinum (e.g., nitrates, certain hydroxides, sulfur) are found in soils.

REFERENCES

1. R. A. Robinson et al., Brayton-Cycle Radioisotope Heat Source Design Study, Phase I (Conceptual Design) Report, USAEC Report ORNL-TM-1691, NASA CR-72090, Oak Ridge National Laboratory, December 1966.
2. R. R. Rotelli, Design Data Book — Study of Multipurpose Mission Module, Report D2-90648, Boeing Airplane Company, October 1965.
3. A. B. Leaman, Non Contaminating Separation Systems for Spacecraft, Proceedings of 1st Aerospace Mechanisms Symposium, University of Santa Clara, California, May 19–20, 1966.
4. Naval Ordnance Laboratory, Investigation of High and Low Temperature Resistant Explosive Devices, Report T-32602 (NASA CR-65542).
5. Mound Laboratory Isotopic Power Fuels Programs: July–September 1966, USAEC Report MLM-1362, Mound Laboratory, October 1966. (Classified)
6. G. R. Grove et al., Plutonium-238 Isotopic Power Sources: A Summary Report, USAEC Report MLM-1270, Mound Laboratory, August 1965. (Classified)
7. Mound Laboratory, Plutonium-238 Fuel Data Sheets, Nov. 15, 1965 (rev. 3, July 15, 1966). (Classified)
8. A. L. Lotts, Oak Ridge National Laboratory, personal communication.
9. R. W. Buckman and R. C. Goodspeed, Development of Dispersion Strengthened Tantalum Base Alloy, Eighth Quarterly Progress Report NASA CR-54935, Westinghouse Electric Corporation, Astronuclear Laboratory, November 1965.
10. K. W. Haff, Oak Ridge National Laboratory, personal communication.
11. J. P. Nichols and D. R. Winkler, A Program for Calculating Optimum Dimensions of Alpha Radioisotope Capsules Exposed to Varying Stress and Temperature, USAEC Report ORNL-TM-1735, NASA CR-72172, Oak Ridge National Laboratory, April 1967.
12. E. L. Robinson, Trans. ASME, 74(5): 778–781 (July 1952).
13. F. R. Larson and J. Miller, Trans. ASME, 74(5): 765–775 (July 1952).
14. E. C. Larke and N. P. Inglis, A Critical Examination of Some Methods of Analyzing and Extrapolating Stress-Rupture Data, pp. 6-33 to 6-47 in Joint International Conference on Creep, Institute of Mechanical Engineers, 1963.
15. C. R. Kennedy, pp. 44–45 in Metals and Ceramics Div. Ann. Progr. Rept. May 31, 1962, USAEC Report ORNL-3313, Oak Ridge National Laboratory, August 1962.
16. H. E. McCoy, pp. 122–123 in Metals and Ceramics Div. Ann. Progr. Rept. June 30, 1965, USAEC Report ORNL-3870, Oak Ridge National Laboratory, November 1965.

17. H. E. McCoy, Creep Rupture Properties of the Tantalum-Base Alloy T-222, USAEC Report ORNL-TM-1576, Oak Ridge National Laboratory, September 1966.

18. R. L. Stephenson, Oak Ridge National Laboratory, unpublished data.

19. J. C. Sawyer and E. A. Steigerwald, Generation of Long Time Creep Data on Refractory Alloys at Elevated Temperature, 11th Quarterly Report, NASA CR-54973, TRW Equipment Laboratory, March 1966.

20. J. C. Sawyer and E. A. Steigerwald, Generation of Long Time Creep Data on Refractory Alloys at Elevated Temperature, 14th Quarterly Report, NASA CR-72185, TRW Equipment Laboratory, January 1967.

21. Westinghouse Electric Corporation, T-111, Tantalum Base Alloy Refractory Metal, Special Technical Data 52-365, March 1963.

22. E. S. Bartlett and F. F. Schmidt, Review of Recent Developments — Columbium and Tantalum, Defense Metals Information Center, January 10, 1964. (Preliminary information from Westinghouse Electric Corporation under U.S. Navy contract.)

23. Fansteel Metallurgical Corporation, Fansteel-222, A Tantalum-Base Alloy.

24. W. F. Simons and J. A. Van Echo, The Elevated Temperature Properties of Stainless Steels, American Society for Testing and Materials, 1965.

25. R. W. Swindeman, The Mechanical Properties of INOR-8, USAEC Report ORNL-2780, Oak Ridge National Laboratory, January 1961.

26. J. T. Venard, Tensile and Creep Properties of INOR-8 for the Molten Salt Reactor Experiment, USAEC Report ORNL-TM-1017, Oak Ridge National Laboratory, February 1965.

27. H. E. McCoy, Creep Properties of the Nb—1% Ar Alloy, USAEC Report ORNL-TM-905, Oak Ridge National Laboratory, August 1964.

28. Pratt and Whitney Aircraft, Creep Rupture Data for Cb—1 Zr Alloy, USAEC Report CNLM-4267, September 1962.

29. D. H. Stoddard and E. L. Albenesius, Radiation Properties of $^{238}PuO_2$ Produced for Isotopic Power Generators, USAEC Report DP-984, Savannah River Laboratory, July 1965.

30. E. K. Hyde, Fission Phenomena, in The Nuclear Properties of the Heavy Elements, Vol. III, Prentice Hall, New York, 1964.

31. V. A. Druin, V. P. Perelygin, and G. I. Khlebnikov, Spontaneous Fission Periods of Np^{237}, Pu^{238}, and Pu^{242}, Zhur. Eksptl'. i Teoret. Fiz., 40: 1296—1298 (1961).

32. E. D. Arnold, Neutron Sources, in IAEA Engineering Compendium on Radiation Shielding, Springer-Verlag, Vienna (to be published).

33. E. D. Arnold, Radiation Hazards of Recycled ^{233}U-Thorium, p. 253 in Proceedings of the Thorium Fuel Cycle Symposium, Gatlinburg, Tennessee, December 5—7, 1962, USAEC Report TID-7650, Book I, Division of Technical Information Extension.

34. J. P. McBride, Oak Ridge National Laboratory, unpublished data (December 1966).

35. C. W. Craven, Jr., Oak Ridge National Laboratory, unpublished data (December 1966).

36. Excerpts from North American Aviation Report SID 62-821-2 transmitted by NASA–Lewis Research Center (September 1966).

37. E. D. Arnold and B. F. Maskewitz, SDC, A Shielding Design Calculation Code for Fuel Handling Facilities, USAEC Report ORNL-3041, Oak Ridge National Laboratory, March 1966.

38. G. R. Wilson, Thermophysical Properties of Six Charring Ablators from 140° to 700°K and Two Chars from 800° to 3000°K, Report NASA-TND 2991, October 1965.

39. Pratt and Whitney Aircraft, Determination of the Emissivity of Material, Report PWA-2750, NASA CR 54891, Dec. 20, 1965.

40. Pratt and Whitney Aircraft, Data Book on Physical Properties of Materials, Report CNLM 2393, Mar. 15, 1960, rev. June 15, 1960.

41. Letter from Charles J. Donlan, NASA Langley Research Center, to Donald W. Burton, Mar. 31, 1967.

42. W. M. Rohsenow and H. Choi, Heat, Mass, and Momentum Transfer, Prentice-Hall, New York, 1961.

43. R. B. Bird, W. E. Stewart, and E. N. Lightfoot, Transport Phenomena, Wiley, New York, 1960.

44. Code of Federal Regulations, Title 10, Part 71, Packaging of Radioactive Material for Transport; see Federal Register, Rules and Regulations, July 22, 1966, pp. 9941–9949.

45. T. C. George, Supplement No. 7 to Tariff No. 15, Interstate Commerce Commission Regulation for Transporting Explosives and Other Dangerous Articles by Land and Water in Rail Freight Service and by Motor Vehicle (Highway) and Water Including Specifications for Shipping Containers, New York, June 10, 1966.

46. L. B. Shappert, A Guide to the Design of Shipping Casks for the Transportation of Radioactive Material, USAEC Report ORNL-TM-681, Oak Ridge National Laboratory, April 1965.

Appendix

PARAGRAPHS OF CHAPTER 10, PART 71, OF THE CODE OF FEDERAL REGULATIONS APPLICABLE TO SHIPPING LARGE QUANTITIES OF ^{238}Pu FUEL

§71.31 General standards for all packaging.

(a) Packaging shall be of such materials and construction that there will be no significant chemical, galvanic, or other reaction among the packaging components, or between the packaging components and the package contents.

(b) Packaging shall be equipped with a positive closure which will prevent inadvertent opening.

(c) Lifting devices:

(1) If there is a system of lifting devices which is a structural part of the package, the system shall be capable of supporting three times the weight of the loaded package without generating stress in any material of the packaging in excess of its yield strength.

(2) If there is a system of lifting devices which is a structural part only of the lid, the system shall be capable of supporting three times the weight of the lid and any attachments without generating stress in any material of the lid in excess of its yield strength.

(3) If there is a structural part of the package which could be employed to lift the package and which does not comply with subparagraph (1) of this paragraph, the part shall be securely covered or locked during transport in such a manner as to prevent its use for that purpose.

(4) Each lifting device which is a structural part of the package shall be so designed that failure of the device under excessive load would not impair the containment or shielding properties of the package.

(d) Tie-down devices:

(1) If there is a system of tie-down devices which is a structural part of the package, the system shall be capable of withstanding, without generating stress in any material of the package in excess of its yield strength, a static force applied to the center of gravity of the package having a vertical component of two times the weight of the package with its contents, a horizontal component along the direction in which the vehicle travels of 10 times the weight of the package with its contents, and a horizontal component in the transverse direction of 5 times the weight of the package with its contents.

(2) If there is a structural part of the package which could be employed to tie the package down and which does not comply with subparagraph (1) of this paragraph, the part shall be securely covered or locked during transport in such a manner as to prevent its use for that purpose.

(3) Each tie-down device which is a structural part of the package shall be so designed that failure of the device under excessive load would not impair the ability of the package to meet other requirements of this subpart.

§71.32 Structural standards for large quantity packaging.

Packaging used to ship a large quantity of licensed material, as defined in §71.4(f), shall be designed and constructed in compliance with the structural standards of this section. Standards different from those specified in this section may be approved by the Commission if the controls proposed to be exercised by the shipper are demonstrated to be adequate to assure the safety of the shipment.

(a) Load resistance. Regarded as a simple beam supported at its ends along any major axis, packaging shall be capable of withstanding a static load, normal to and uniformly distributed along its length, equal to 5 times its fully loaded weight, without generating stress in any material of the packaging in excess of its yield strength.

(b) External pressure. Packaging shall be adequate to assure that the containment vessel will suffer no loss of contents if subjected to an external pressure of 25 pounds per square inch gauge.

§71.33 Criticality standards for fissile material packages.

(a) A package used for the shipment of fissile material shall be so designed and constructed and its contents so limited that it would be subcritical if it is assumed that water leaks into the containment vessel, and:

(1) Water moderation of the contents occurs to the most reactive credible extent consistent with the chemical and physical form of the contents; and

(2) The containment vessel is fully reflected on all sides by water.

(b) A package used for the shipment of fissile material shall be so designed and constructed and its contents so limited that it would be subcritical if it is assumed that any contents of the package which are liquid during normal transport leak out of the containment vessel, and that the fissile material is then:

(1) In the most reactive credible configuration consistent with the chemical and physical form of the material;

(2) Moderated by water outside of the containment vessel to the most reactive credible extent; and

(3) Fully reflected on all sides by water.

(c) The Commission may approve exceptions to the requirements of this section where the containment vessel incorporates special design features which would preclude leakage of liquids in spite of any single packaging error and appropriate measures are taken before each shipment to verify the leak tightness of each containment vessel.

§71.34 Evaluation of a single package.

(a) The effect of the transport environment on the safety of any single package of radioactive material shall be evaluated as follows:

(1) The ability of a package to withstand conditions likely to occur in normal transport shall be assessed by subjecting a sample package or scale model, by test or other assessment, to the normal conditions of transport as specified in §71.35; and

(2) The effect on a package of conditions likely to occur in an accident shall be assessed by subjecting a sample package or scale model, by test or other assessment, to the hypothetical accident conditions as specified in §71.36.

(b) Taking into account controls to be exercised by the shipper, the Commission may permit the shipment to be evaluated together with or without the transporting vehicle, for the purpose of one or more tests.

(c) Normal conditions of transport and hypothetical accident condition different from those specified in §71.35 and §71.36 may be approved by the Commission if the controls proposed to be exercised by the shipper are demonstrated to be adequate to assure the safety of the shipment.

§71.35 Standards for normal conditions of transport for a single package.

(a) A package used for the shipment of fissile material or a large quantity of licensed material, as defined in §71.4(f), shall be so designed and constructed and its contents so limited that under the normal conditions of transport specified in Appendix A of this part:

(1) There will be no release of radioactive material from the containment vessel;

(2) The effectiveness of the packaging will not be substantially reduced;

(3) There will be no mixture of gases or vapors in the package which could, through any credible increase of pressure or an explosion, significantly reduce the effectiveness of the package;

(4) Radioactive contamination of the liquid or gaseous primary coolant will not exceed 10^{-7} curies of activity of Group I radionuclides per milliliter, 5×10^{-6} curies of activity of Group II radionuclides per milliliter 3×10^{-4} curies of activity of Group III and Group IV radionuclides per milliliter; and

(5) There will be no loss of coolant.

(b) A package used for the shipment of fissile material shall be so designed and constructed and its contents so limited that under the normal conditions of transport specified in Appendix A of this part:

(1) The package will be subcritical;

(2) The geometric form of the package contents would not be substantially altered;

(3) There will be no leakage of water into the containment vessel. This requirement need not be met if, in the evaluation of undamaged packages under §71.38(a), §71.39(a) (1), or §71.40(a), it has been assumed that moderation is present to such an extent as to cause maximum reactivity consistent with the chemical and physical form of the material; and

(4) There will be no substantial reduction in the effectiveness of the packaging, including.

(i) Reduction by more than 5 percent, in the total effective volume of the packaging on which nuclear safety is assessed;

(ii) Reduction by more than 5 percent in the effective spacing on which nuclear safety is assessed, between the center of the containment vessel and the outer surface of the packaging; or

(iii) Occurrence of any aperture in the outer surface of the packaging large enough to permit the entry of a 4-inch cube.

(c) A package used for the shipment of a large quantity of licensed material, as defined in §71.4(f), shall be so designed and constructed and its contents so limited that under the normal conditions of transport specified in Appendix A of this part, the containment vessel would not be vented directly to the atmosphere.

§71.36 Standards for hypothetical accident conditions for a single package.

(a) A package used for the shipment of a large quantity of licensed material, as defined in §71.4(f), or for the shipment of fissile material when the package will contain more than 0.001 curie of Group I radionuclides, 0.05 curie of Group II radionuclides, 3 curies of Group III radionuclides, 20 curies of Group IV and Group V radionuclides and radionuclides in special form, or 1,000 curies of Group VI radionuclides shall be so designed and constructed and its contents so limited that if subjected to the hypothetical accident conditions specified in Appendix B of this part as the Free Drop, Puncture, Thermal, and Water Immersion conditions, in the sequence listed in Appendix B, it will meet the following conditions:

(1) The reduction of shielding would not be sufficient to increase the external radiation dose rate to more than 1,000 milliroentgens per hour or equivalent at 3 feet from the external surface of the package.

(2) No radioactive material would be released from the package except for gases and contaminated coolant containing total radioactivity exceeding neither:

(i) 0.1 percent of the total radioactivity of the package contents; nor

(ii) 0.01 curie of Group I radionuclides, 0.5 curie of Group II radionuclides, and 10 curies of Group III and Group IV radionuclides, except that for inert gases, the limit is 1,000 curies.

A package need not satisfy the requirements of this paragraph if it contains only low specific activity material as defined in §71.4(g), and is transported on a motor vehicle, railroad car, aircraft, inland water craft, or hold or deck of a seagoing vessel assigned for the sole use of the licensee.

(b) A package used for the shipment of fissile material shall be so designed and constructed and its contents so limited that if subjected to the hypothetical accident conditions specified in Appendix B of this part as the Free Drop, Puncture, Thermal, and Water Immersion conditions, in the sequence listed in Appendix B, the package would be subcritical. In determining whether this standard is satisfied, it shall be assumed that:

(1) The fissile material is in the most reactive credible configuration consistent with the damaged condition of the package and the chemical and physical form of the contents;

(2) Water moderation occurs to the most reactive credible extent consistent with the damaged condition of the package and the chemical and physical form of the contents; and

(3) There is reflection by water on all sides and as close as is consistent with the damaged condition of the package.

§71.40 Specific standards for a Fissile Class III shipment.

A package for Fissile Class III shipment shall be so designed and constructed and its contents so limited, and the number of packages in a Fissile Class III shipment shall be so limited, that:

(a) The undamaged shipment would be subcritical with an identical shipment in contact with it and with the two shipments closely reflected on all sides by water; and

(b) The shipment would be subcritical if each package were subjected to the hypothetical accident conditions specified in Appendix B of this part as the Free Drop, Thermal, and Water Immersion conditions, in the sequence listed in Appendix B, with close reflection by water on all sides of the array and with the packages in the most reactive arrangement and with the most reactive degree of interspersed hydrogenous moderation which would be credible considering the controls to be exercised over the shipment. The condition of the package shall be assumed to be as described in §71.37. Hypothetical accident conditions different from those specified in this paragraph may be approved by the Commission if the controls proposed to be exercised by the shipper are demonstrated to be adequate to assure the safety of the shipment.

. . . . . .

Appendix B — Hypothetical Accident Conditions

The following hypothetical accident conditions are to be applied sequentially, in the order indicated, to determine their cumulative effect on a package or array of packages.

1. Free Drop — A free drop through a distance of 30 feet onto a flat essentially unyielding horizontal surface, striking the surface in a position for which maximum damage is expected.

2. Puncture — A free drop through a distance of 40 inches striking, in a position for which maximum damage is expected, the top end of a vertical cylindrical mild steel bar mounted on an essentially unyielding horizontal surface. The bar shall be 6 inches in diameter, with the top horizontal and its edge rounded to a radius of not more than one-quarter inch, and of such a length as to cause maximum damage to the package, but not less than 8 inches long. The long axis of the bar shall be normal to the package surface.

3. Thermal — Exposure for 30 minutes within a source of radiant heat having a temperature of 1,475°F. and an emissivity coefficient of 0.9, or equivalent. For calculational purposes, it shall be assumed that the package has an absorption coefficient of 0.8. The package shall not be cooled artificially until after the 30 minute test period has expired and the temperature at the center of the package has begun to fall.

4. Water Immersion — Immersion in water for 24 hours to a depth of at least 3 feet.